UNCLASSIFIED
Security Classification

AD 743903

DOCUMENT CONTROL DATA - R & D

Security classification of title, body of abstract and indexing annotation must be entered when the overall report is classified)

1. ORIGINATING ACTIVITY *(Corporate author)*
Naval Ordnance Laboratory

2a. REPORT SECURITY CLASSIFICATION
Unclassified

2b. GROUP

3. REPORT TITLE
Experimental Investigations of a Fin Protuberance Partially Immersed in a Turbulent Boundary Layer at Mach 5

4. DESCRIPTIVE NOTES *(Type of report and inclusive dates)*

5. AUTHOR(S) *(First name, middle initial, last name)*
Allen E. Winkelmann

6. REPORT DATE	7a. TOTAL NO. OF PAGES	7b. NO. OF REFS
21 January 1972	77	18

8a. CONTRACT OR GRANT NO.	9a. ORIGINATOR'S REPORT NUMBER(S)
b. PROJECT NO. A32320C/WF20-322-205	NOLTR 72-33
c.	9b. OTHER REPORT NO(S) *(Any other numbers that may be assigned this report)*
d.	

10. DISTRIBUTION STATEMENT
Approved for public release; distribution unlimited

11. SUPPLEMENTARY NOTES	12. SPONSORING MILITARY ACTIVITY
	Naval Air Systems Command Washington, D.C.

13. ABSTRACT

Various flow visualization results are presented for cylindrically blunted, unswept and 60-degree swept fins with and without small clearance gaps, partially immersed in a turbulent boundary layer ($\delta \approx$ 2.6 inches). In addition, pressure and heat transfer measurements were obtained on the flat plate upon which the fin was mounted. These experiments were completed in the U.S. Naval Ordnance Laboratory Boundary Layer Channel at a nominal Mach number of 5 and nominal free-stream Reynolds numbers of 2.8×10^6 and 7.4×10^6. Oil smear, azobenzene and Schlieren flow visualization tests showed the complex interaction flow fields which exist around the fin-flat plate combination. Pressure measurements showed large peak pressures to occur in regions of high heat transfer. Complementary heat transfer measurements indicated heating rates on the flat plate with fin to be up to six times the rate on an undisturbed flat plate. Tests showed that when a spacer was placed underneath the fin to provide a clearance gap of only 20 percent of the flat plate boundary layer thickness, the major boundary layer interaction was produced by the spacer itself.

DD FORM 1 NOV 68 1473 (PAGE 1)

S/N 0101-807-6801

UNCLASSIFIED
Security Classification

14 KEY WORDS	LINK A		LINK B		LINK C	
	ROLE	WT	ROLE	WT	ROLE	WT
Fin-Flat Plate						
Protuberances						
Separated Flow						
Wing-Body Interference						
Flow Visualization						
Heat Transfer						
Pressure Distributions						
Boundary Layer Interactions						

EXPERIMENTAL INVESTIGATIONS OF A FIN PROTUBERANCE PARTIALLY IMMERSED IN A TURBULENT BOUNDARY LAYER AT MACH 5

Prepared by

Allen E. Winkelmann

ABSTRACT: Various flow visualization results are presented for cylindrically blunted, unswept and 60-degree swept fins with and without small clearance gaps, partially immersed in a turbulent boundary layer ($\delta \approx 2.6$ inches). In addition, pressure and heat transfer measurements were obtained on the flat plate upon which the fin was mounted. These experiments were completed in the U.S. Naval Ordnance Laboratory Boundary Layer Channel at a nominal Mach number of 5 and nominal free-stream Reynolds numbers of 2.8×10^6 and 7.4×10^6. Oil smear, azobenzene and Schlieren flow visualization tests showed the complex interaction flow fields which exist around the fin-flat plate combination. Pressure measurements showed large peak pressures to occur in regions of high heat transfer. Complementary heat transfer measurements indicated heating rates on the flat plate with fin to be up to six times the rates on an undisturbed flat plate. Tests showed that when a spacer was placed underneath the fin to provide a clearance gap of only 20 percent of the flat plate boundary layer thickness, the major boundary layer interaction was produced by the spacer itself.

Naval Ordnance Laboratory
Silver Spring, Maryland

NOLTR 72-33 21 January 1972

EXPERIMENTAL INVESTIGATIONS OF A FIN PROTUBERANCE PARTIALLY IMMERSED IN A TURBULENT BOUNDARY LAYER AT MACH 5

In this report, flow visualization results are presented for cylindrically blunt unswept and 60-degree swept fins partially immersed in a 2.6-inch-thick turbulent boundary layer developed on a flat plate. In addition, detail pressure measurements were obtained on the flat plate in the vicinity of the fin. Heat transfer measurements indicated peak heating rates on the flat plate up to six times the rates on an undisturbed flat plate.

This work was performed under the support of the Naval Air Systems Command, Airtask Number A32320C/WF20-322-205 with W.C. Volz as project monitor. The author wishes to acknowledge the helpful advice of personnel of Divisions 313 and 312 in the completion of the experimental work. In addition, special acknowledgement is made of the excellent photographic work done by personnel of the Wind Tunnel Photographic Group.

ROBERT WILLIAMSON II
Captain, USN

L. H. Schindel
L. H. SCHINDEL
By direction

CONTENTS

	Page
INTRODUCTION	1
EXPERIMENTAL APPARATUS	2
Test Facility	2
Models and Instrumentation	3
Supersonic Tunnel No. 2 Fin-Flat Plate Model	3
Fin-Flat Plate Model for the Channel	4
Fin-Flat Plate Pressure Model for the Channel	4
Pressure Data Acquisition and Recording	5
Heat Transfer Gage	6
EXPERIMENTAL TECHNIQUES AND PROCEDURE	7
Flow Visualization Studies	7
Oil Smear Tests	7
Azobenzene Studies	8
Schlieren Tests	8
Flat Plate Surface Pressure Tests	8
Heat Transfer Tests	9
Summary of Nominal Test Conditions	9
RESULTS AND DISCUSSION	10
Tunnel No. 2 Flow Visualization Tests	10
Surface Pressure Measurements on the Boundary Layer Channel Flat Plate Model	12
Heat Transfer Measurements	15
Boundary Layer Channel Flow Visualization Studies	19
Oil Smear Tests	19
Azobenzene Movies	25
Schlieren Photographs from the Boundary Layer Channel	27
Boundary Layer Surveys in the Boundary Layer Channel.	30
Discussion of the Results	30
SUMMARY	31
REFERENCES	33

CONTENTS (Con't)

ILLUSTRATIONS

Figure	Title
1	Typical Missile Fin-Body Geometry
2	Possible Flow-Field Model of the Interaction Produced By A Fin Protuberance
3	NOL Supersonic Tunnel No. 2 With Fin-Flat Plate Model
4	NOL Boundary Layer Channel With Fin-Flat Plate Model
5	Plan Views of Fin Models on Bakelite Flat Plate
6	Fin-Flat Plate Pressure Model
7	Static Pressure Tap Locations on Flat Plate
8	Heated Differential Heat Transfer Gage
9	Oil Smear Test in Supersonic Tunnel No. 2
10	Schlieren Photograph of Unswept Fin in Supersonic Tunnel No. 2
11	Schlieren Photograph of 60° Swept Fin in Supersonic Tunnel No. 2
12a	Flat Plate Pressure Distribution Produced by an Unswept Fin
12b	Unswept Fin with 0.125-Inch Clearance Gap
12c	Unswept Fin with 0.25-Inch Clearance Gap
12d	Unswept Fin with 0.50-Inch Clearance Gap
13	Flat Plate Pressure Distribution for Varying Clearance Gaps of an Unswept Fin
14	Pressure Distribution on Flat Plate Around Leading Edge of Fin
15	Oil Smear Photograph of Region Around Leading Edge of Fin (Reference 5)

CONTENTS (Con't)

Figure	Title
16a	Flat Plate Pressure Distribution Produced by a 60° Swept Fin
16b	60° Swept Fin with 0.125-Inch Clearance Gap
16c	60° Swept Fin with 0.25-Inch Clearance Gap
16d	60° Swept Fin with 0.50-Inch Clearance Gap
17	Flat Plate Pressure Distribution for Varying Clearance Gaps on a 60° Swept Fin
18	Azobenzene Pattern Showing Region of High Heat Transfer Produced by a Blunt Unswept Fin (Reference 5)
19	Typical Data Obtained From Heated Differential Heat Transfer Gage
20	Heat Transfer Data in Region Ahead of an Unswept Fin
21	Recovery Factors in Region Ahead of an Unswept Fin
22a	Oil Pattern on the Flat Plate for an Unswept Fin
22b	Enlarged View - Upstream of Unswept Fin
22c	Enlarged View - Downstream of Unswept Fin
23a	Unswept Fin with 0.075-Inch Clearance Gap
23b	Enlarged View - Fin with 0.075-Inch Clearance Gap
24	Unswept Fin with 0.125-Inch Clearance Gap
25	Unswept Fin with 0.25-Inch Clearance Gap
26a	Unswept Fin with 0.50-Inch Clearance Gap
26b	Enlarged View - Fin with 0.50-Inch Clearance Gap
27a	Oil Smear Pattern on the Flat Plate for a 60° Swept Fin
27b	Enlarged View - 60° Swept Fin
28	60° Swept Fin with 0.125-Inch Clearance Gap
29a	60° Swept Fin with 0.50-Inch Clearance Gap

CONTENTS (Con't)

Figure	Title
29b	Enlarged View - 60° Swept Fin with 0.50-Inch Clearance Gap
30a	Oil Patterns on an Unswept Fin
30b	Oil Pattern on an Unswept Fin with an 0.125" Clearance Gap Obtained During Test
30c	Oil Pattern on an Unswept Fin
31a	Oil Patterns on a 60° Swept Fin - Obtained During Test
31b	60° Swept Fin with 0.125" Clearance Gap
31c	60° Swept Fin with 0.50" Clearance Gap
32a	Azobenzene Movies of an Unswept Fin
32b	Azobenzene Moviews of an Unswept Fin with a 0.125-Inch Clearance Gap
33a	Schlieren Photographs of the Flow Field Upstream of a Cylindrically Blunt Fin (M_∞ = 4.93 Re_∞/ft = 7.4x10^6)
33b	Fin with 0.25-Inch Clearance Gap
33c	Fin with 0.50-Inch Clearance Gap
34a	Schlieren Photographs of the Flow Field Upstream of a 60° Swept, Cylindrically Blunt Fin
34b	Fin with 0.50-Inch Clearance Gap
35	Composite of Schlieren Photographs of the Regions Upstream and Downstream of an Unswept Fin
36	Boundary-Layer Surveys (Reference 5)

TABLES

Number	Title
1	Nominal Test Conditions
2	Boundary Layer Survey Results

NOMENCLATURE

d	=	diameter of leading edge of fin
h	=	heat transfer coefficient $[BTU/_{ft^2 sec°R}]$
h_o	=	heat transfer coefficient on a flat plate
M_∞	=	free-stream Mach number
P	=	pressure
P_o	=	supply pressure
P_∞	=	free-stream pressure (flat plate static)
r	=	recovery factor on a flat plate
Re_∞/ft	=	free-stream Reynolds number per foot
t	=	duration of test in minutes
T_o	=	supply temperature
T_w	=	wall temperature
T_{aw}	=	adiabatic wall temperature
X	=	distance on flat plate along the fin centerline
θ	=	momentum thickness of boundary layer
δ	=	boundary layer thickness
δ^*	=	displacement thickness of boundary layer

INTRODUCTION

In high-speed flight, regions of high heat transfer and extensive flow separation are produced by conventional missile control surfaces. A typical configuration of a fin-type control surface on a missile is shown in Figure 1. The boundary layer on the aft section of a missile is generally turbulent and can be several inches thick. The shock structure of the fin interacts with this boundary layer to produce large regions of separated flow and localized regions of high heat transfer. Canard-type surfaces mounted near the front of the missile may in addition, experience heating problems associated with the impingement of the missile nose bow shock. Besides the conventional missile control surfaces, other structural features (such as shroud struts, external piping, etc.) of a missile or high-speed aircraft experience similar interaction problems.

A comprehensive survey of past research done on these aerodynamic interaction problems was recently presented by Korkegi (reference 1). Extensive literature surveys and reviews of past studies of aerothermodynamic interaction problems have been compiled by Ryan (reference 2) and Cramer (reference 3). In addition, a number of studies of aerodynamic interference problems was presented in the proceedings of a recent AGARD meeting (reference 4).

One of the studies presented in reference 4 was an experimental program conducted at NOL aimed at defining more clearly the flow-field model of the interaction produced by a fin-type protuberance partially immersed in the turbulent boundary layer of a missile. A more detailed account of that study is presented in reference 5. From a series of flow visualization studies completed in reference 5, the flow-field model in Figure 2, was proposed for the

interaction produced by a blunt unswept fin. Oil smear tests were used to determine the surface shear directions. These tests indicated a number of vortex systems to exist in the fin-flat plate interaction region. In particular, the horseshoe vortex pair and the wake vortices were believed responsible for producing regions of high heat transfer which were determined by a number of surface sublimator (azobenzene) tests. Schlieren and shadowgraph studies were used to construct the shock wave structure. All of the experiments conducted in reference 5 were completed using a very basic model consisting of a cylindrically blunted unswept fin and a flat-plate mounted on the NOL Boundary Layer Channel. This configuration included the more important geometrical variations which characterize a typical missile fin design (Figure 1). Test conditions in the channel were limited to a nominal Mach number of 5 and two free-stream Reynolds numbers per foot of 2.8×10^6 and 7.4×10^6.

The present report gives results from the second phase of this experimental study. Since actual missile designs utilize highly swept maneuverable fins with clearance gaps (Figure 1), a series of additional flow visualization tests were conducted to study the effect of these geometries. A review of the flow visualization results from the first phase of work (reference 5) indicated that the maximum shear and heat transfer rates on the flat plate were occurring along the centerline of the fin. This prompted a series of experiments in which surface pressure measurements were obtained on the flat plate along the fin centerline. In addition heat transfer measurements were made on the flat plate just ahead of the fin in the region containing the "stagnation line" shown in Figure 2.

EXPERIMENTAL APPARATUS

A. Test Facilities

The first series of experiments to be discussed in this report were completed in the NOL Supersonic Tunnel No. 2. This open-jet

blowdown facility was fitted with its Mach 5 nozzle for the present tests (Figure 3). The tunnel operates on a compressed air bottlefield with the air preheated by a steam heater and exhausted into a compressor driven vacuum system.

The remaining experimental program was completed in the NOL Boundary Layer Channel (BLC) (reference 6). This channel utilizes a flexible plate and flat test plate (13x10 inches) to form the two opposite walls of a two-dimensional supersonic nozzle (Figure 4). The present tests were completed with a nominal Mach number setting of 5 and a zero pressure gradient. The flat test plate was water cooled (T_w = 80°F). The Channel is operated on the same tunnel network as Supersonic Tunnel No. 2 except the air is heated by a propane fired heater. The relatively thick (δ = 2.6 inches) turbulent boundary layer developed on the flat plate was utilized in the present study. Plate glass windows (3x13 inches) mounted in the doors allowed Schlieren and shadowgraph photographs to be taken of the developed boundary layer.

B. Models and Instrumentation

1. Supersonic Tunnel No. 2 Fin-Flat Plate Model

An aluminum flat plate (0.5x22x24 inches) was added on as an extension to the bottom contoured nozzle wall of the Mach 5 nozzle block (Figure 3). The thick turbulent boundary layer developed on the nozzle wall then continued on over the flat plate which spanned the open jet area between the nozzle and the diffuser. The plate was 4 inches wider on both sides of the nozzle (nozzle width = 16 inches) to aid in maintaining nearly 2-D flow without the use of Schlieren-impairing side plates. The black bakelite fin was mounted 8 inches downstream of the flat plate nozzle block juncture. At this location, the weak shock formed at the juncture did not pass through the region of interest in the Schlieren photographs.

2. Fin-Flat Plate Model for the Channel

To provide an insulating surface for flow visualization studies a black Bakelite flat plate with dimensions 0.25x13x39 inches was mounted on the channel test plate (Figure 4). A steel five-degree ramp was added to the front of the plate to minimize interference effects. At a station 84 inches from the nozzle throat, a cylindrically blunted, unyawed fin was mounted. For previous tests in which this model was used (reference 5) a 2.0-inch diameter yawing plug was located in the Bakelite flat plate. Two different mounting holes in the plug allowed a 1.0-inch translation of the fin along the flat plate as well as providing a port for instrumentation leads. At a location upstream of the fin, a 1.0-inch diameter hole was cut in the Bakelite flat plate to allow installation of a heat transfer gage (Figure 5). The mismatch of the plugs and surrounding flat plate was generally less than 0.0005 inch.

The two black Bakelite fins used in this study are also shown in Figure 5. Spaces of various thicknesses (0.075, 0.125, 0.25, 0.50 inch) were used to study the effect of small clearance gaps beneath the fins. The initial flow visualization studies used spacers which were 0.75 inch in length. Later pressure tests were made with spacers 1.63 inches in length.

3. Fin-Flat Plate Pressure Model for the Channel

To obtain detail surface pressure measurements on the flat plate along the centerline of the fin, a model was constructed in which the fin could be "driven" a short distance along the flat plate centerline (Figure 6). A fin drive mechanism was mounted under the Boundary Layer Channel side wall and the fins were bolted to it through an instrumentation port in the wall (Figure 4). This allowed a limited number of pressure taps to "probe" in detail the flat plate surface pressure distribution. The stainless steel flat plate of the model was identical in size to the Bakelite flat plate and had 28 pressure taps distributed along the centerline of the fin

(Figure 7). Eight taps were concentrated in an area near the leading edge of the fin where flow visualization studies show the maximum flat plate heating rates and the existence of a region of very high shear and a "stagnation line" (reference 5). Since previous studies (reference 7) had indicated rather large pressure gradients just upstream of the fin, these eight pressure taps were relatively small with an I.D. of 0.019 inch. The fin could be translated 0.55 inch which was more than sufficient to allow each tap to "probe" the 0.5-inch pressure profile it was designed to. A slide potentiometer mounted independent of the motor drive allowed a digital read out of the location of the fin (Figure 6).

The black Bakelite fins used with the Bakelite flat plate were also used on the pressure model. To allow the necessary translation while providing a pressure seal, the clearance gap spacers used with the pressure model were longer than the spacers used in the initial flow visualization studies.

4. Pressure Data Acquisition and Recording

To reduce running times of the tests, pressure data were recorded on two data recording systems; the NOL PADRE (reference 6), a card punch recording system, and the NOL DARE IV, a ten-channel tape recording system. Sixteen of the pressure taps were fed into eight scanning value units which were recorded on PADRE. The twelve remaining taps were fed into a multiple pressure bank, each with its own pressure transducer. Three of these twelve transducers were connected to PADRE and the remaining nine to DARE IV. Pressures were read on 1 and 5 psia Staham transducers (Figure 7). Critical pressure taps were monitored on plotters (P vs x) during a run to assure that data were taken after all the taps had properly responded. The axial location of the fin via the slide potenimeter was recorded on DARE IV. Supply conditions were only recorded on PADRE, but both systems were "tied" together by a number coding system and

simultaneous taking of data. The pressure transducers were calibrated by means of a conventional mercury manometer.

5. Heat Transfer Gage

Since the Channel is a closed jet, long test duration tunnel, a "steady state" means to measure heat transfer rates was required. The gage used in the present studies consisted of an RdF Micro-Foil Heat Gage mounted onto a Minco button heater and this unit in turn potted into a phenolic plug (Figure 8). The RdF gage uses a differential thermocouple junction to measure the temperature difference across a 0.007-inch thick wafer of Nomex. Since the Nomex wafer was so thin, the assumption can be made that a one-dimensional heat flux occurs across the wafer. Hence the output from the differential element is related through a calibration to the heat flux across the foil gage. A thermocouple adjacent to the differential element measures the absolute temperature on the front surface of the foil. The foil gage was bonded with high-temperature epoxies to the surface of the button heater which could be driven to various temperatures by means of a voltage regulator. A thermocouple was welded to the back side of the heater to monitor the heater temperature (in addition to the foil thermocouple) and prevent the temperature from exceeding the maximum operating limit of 400°F. The phenolic plug was mounted in the 1.0 inch diameter holes provided for it in the Bakelite flat plate (Figure 5). In this location the differential thermocouple could be positioned in the suspected region of highest heat transfer on the flat plate (reference 5). The relatively large size of the gage posed two problems to be discussed in more detail later in this report: (1) the square differential thermocouple measured approximately 0.0625 inch on a side which meant that any readings were an average along the diagonal, (2) the thermocouple to monitor the foil temperature was located behind and to one side of the differential thermocouple (Figure 8).

During a test, the heater was driven over a temperature range from about 100°F to 400°F. The thermocouple on the foil gage was constantly monitored with a Leeds Northrop standard temperature unit while the thermocouple on the backside of the gage was monitored with a Mini-mite standard source. The output from the differential thermocouple junction was recorded in microvolts on a Bristol recorder which has a full-scale reading of one millivolt. A calibration provided with the RdF gage allowed a conversion to heat transfer rate, q [BTU/hr.ft^2]. Plotting q versus temperature yielded a nearly linear curve. The slope of a straight line faired through the data was then used to determine a heat transfer coefficient.

EXPERIMENTAL TECHNIQUES AND PROCEDURE

A. Flow Visualization Studies

1. Oil Smear Tests

An indication of surface shear directions on the model was obtained by using an oil smear technique. The proportions of the oil mixture were:

1 tsp. 100 centistokes silicone oil
1 tsp. titanium dioxide powder
5 drops oleic acid

This mixture was applied with a paper wiper towel to obtain a bold smear pattern perpendicular to the free-stream flow. This pattern was easily identified in regions of low shear where the pattern remained essentially undisturbed throughout a test. For tests conducted in the Boundary Layer Channel, the model was removed after the tests to be photographed. However, photographs had to be obtained during the test in Tunnel No. 2 since shutdown turbulence otherwise distroyed the oil smear patterns.

2. Azobenzene Studies

To provide qualitative information on the location of regions of high shear/high heat transfer, tests were conducted with the Bakelite model coated with an orange surface subliming compound (azobenzene). Azobenzene crystals were mixed seven percent by weight with a petroleum ether carrier and applied with a paint sprayer at a supply pressure of 25 psia. Motion pictures were obtained of the patterns on the model which developed with time during the test.

3. Schlieren Tests

Schlieren photographs were obtained in Tunnel No. 2 using the single pass Schlieren optical system of that facility. Photographs were obtained with a constant light source (exposure 20 milliseconds) and with a spark source (exposure 3 microseconds).

A temporary bench-type setup was used to obtain Schlieren photographs in the Boundary Layer Channel. A spark source (exposure 3 microseconds) was used to obtain photographs of the apparent unsteady shock system developed upstream of the fin protuberance. Motion pictures using the 3 microsecond spark source and a filming rate of 100 frames/second were obtained to show the unsteadiness of this shock structure.

B. Flat Plate Surface Pressure Tests

With the pressure model it was possible to "probe" the centerline pressure distribution on the flat plate. The pressure taps just upstream of the leading edge of the fin or clearance spacers were monitored on plotters since it was expected that large pressure gradients would occur in these regions. The fin was driven a short distance at a time (generally 0.05 inch) and then stopped to allow the pressure taps to fully respond before any data was taken. In

regions of pressure peaks, it was possible to locate the peak merely by driving the fin back and forth and observing the output on the plotters.

C. Heat Transfer Tests

The location of the heated differential heat transfer gage allowed measurements to be obtained on the flat plate in a small region just upstream of the unswept fin. The fin was positioned by means of set screws underneath and the two mounting holes (Figure 5) such that the differential thermocouple junction of the gage could be located at various distances from the leading edge of the fin. During a test the button heater was driven to a certain temperature (generally from 100°F to 400°F) and the differential junction output was monitored on a Bristol recorder until the reading was nearly constant or slowly changing. Data were then taken by simultaneously reading the foil temperature and marking the point on the differential junction output record. Then the heater was driven to a new temperature 10 to 15°F higher and a new set of data was taken. The first data points of each run were made with no power to the heater button and indicated a heat flow into the gage. After the maximum attainable temperature of each run was reached, the gage was allowed to cool back down and a few additional data points were taken as a check of repeatibility.

D. Summary of Nominal Test Conditions

The nominal test conditions for the Boundary Layer Channel and Tunnel No. 2 are summarized below. It should be noted that the supply temperature for test condition 2 in the Boundary Layer Channel was incorrectly specified in reference 5 and is correctly listed in the table below.

TABLE 1

NOMINAL TEST CONDITIONS

Facility/Condition	P_o (psia)	T_o (°F)	M_∞	Re_∞/ft
BLC/1	75	302	4.88	2.8×10^6
BLC/2	150	166	4.93	7.4×10^6
Tunnel No. 2	150	200	5.07	6.7×10^6

RESULTS AND DISCUSSION

A. Tunnel No. 2 Flow Visualization Tests

Several runs were made in Tunnel No. 2 in an attempt to obtain higher quality Schlieren photographs than were originally obtained in the first phase of work in the Boundary Layer Channel (reference 5). To check the two-dimensionality of the flow on the flat plate, one test was conducted using the oil smear technique with the aluminum flat plate painted black for better contrast. A photograph taken during the test (Figure 9) shows the flow patterns as found in the earlier tests in the Boundary Layer Channel. Initial or primary flow separation upstream of the fin is apparent as the sharp oil ridge developed on the flat plate. A more subtle line marks the point of so-called secondary separation. A region of very high shear is indicated on the flat plate immediately upstream of the leading edge of the fin as well as on the very bottom leading edge of the fin (by the fact that nearly all of the oil has been swept away). This region was shown in reference 5 to experience the maximum heating on the flat plate. The regions of oil accumulation on the fin within the boundary layer (the edge of which is indicated in Figure 9) is associated with vortices which exist in the fin-flat

plate corner region (Figure 2). A turning or straightening of the wake is also apparent and the patterns developed in the wake are associated with wake recompression shocks and vortices. The flow appears to be quite two-dimensional over the central part of the plate but it is obviously subject to wash-out effects on the edges of the plate where some of the original oil smear patterns still remain.

Schlieren photographs of the fins mounted on the flat plate are shown in Figures 10 and 11. These were obtained with a constant light source (20 millisecond exposure) and the Schlieren knife edge parallel to the flat plate. The boundary layer on the flat plate ($\delta \approx 1.8$ inches) is apparent as the lighter band above the flat plate. The bow shock on the unswept fin is seen to interact with a separation shock developed off the point of primary flow separation (indicated in Figure 10 from the oil patterns developed in Figure 9). The so-called lambda shock structure produced in this region is apparently very complex and unsteady. This unsteadiness was apparent in the spark Schlieren photographs since each photo taken randomly during the test was somewhat different. In the constant light Schlieren of Figure 10, the unsteadiness has caused a rather diffuse lambda shock structure. The Schlieren photographs also show the complex flow field present at the top edge of the fin. The various density gradients could be identified with expansion fans and trailing vortices which emanate from the edge of the fin. The diagonal gradient which slopes upward to the left in the photos is the disturbance produced by the flat plate - nozzle block juncture. Despite the fact that the tunnel No. 2 Schlieren system was of higher optical quality than the original Boundary Layer Channel setup (reference 5), the spark Schlieren photographs obtained in Tunnel No. 2 showed less detail than those from the Boundary Layer Channel. This lack of detail is attributed to light integration effects - since the Tunnel No. 2 system had to "look through" a two-foot wide turbulent boundary layer as well as the expansion fans developed off the ends of the nozzle block.

B. Surface Pressure Measurements on the Boundary Layer Channel Flat Plate

Detailed surface pressure measurements were obtained on the flat plate along the fin centerline. Both the swept and unswept fins were tested with and without clearance gaps. The results of these measurements are presented in the normalized form of P/P_∞, where P_∞ is the undisturbed flat plate static pressure. For any particular run, the pressures measured by the two most forward taps (Figure 7, taps No. 1 and 2) were found to be equal to P_∞ and these were used to normalize the data. A number of oil smear tests were completed prior to the pressure tests, but the discussion of these and comparisons with the pressure data will be deferred to a later section. In most regions, the number of data points was sufficient to plot a smooth pressure profile. In regions of very large pressure gradients, the local pressure taps were monitored on pen plotters and the region was virtually probed for the peak pressure. The data from one pressure tap (no. 24, Figure 7) in the wake region were not usable because of difficulties with the recording channel. Since the adjacent pressure profile was relatively smooth this region was merely faired in. Moreover, the fin was driven 0.536 inch during the run and this provided a certain data overlap.

Figure 12a shows the pressure distribution found on the flat plate alone and with the unswept fin in place. The pressure distribution just upstream of the fin displays a very sharp pressure gradient. This has been observed by previous investigations of this type of aerodynamic interaction problem (e.g. references 7 - 12). The present data indicate that an increased Reynolds number produces an increase in the peak pressure and a slight shift of the peak toward the fin. This peak pressure is known to coincide with the region of maximum heat transfer on the flat plate (reference 5). In interpreting the following pressure data, pressure peaks can generally be associated with regions of high heat transfer, and pressure lows with low heat transfer and separated flow. It is

apparent that the higher Reynolds number flow produces a different pressure profile ahead of this peak and delays the initial pressure rise to flow separation. The dip in the profile after the initial pressure rise is characteristic of the higher Reynolds number data but is nearly nonexistent in the lower Reynolds number profile. The pressure distributions in the wake are not as strongly Reynolds number dependent and the wake pressure appears to be relaxing toward $P/P_\infty = 1$ at large X/d.

Figures 12b, 12c and 12d show the pressure distributions obtained on the flat plate for the unswept fin with various clearance gaps. As for the fin with no clearance gap, a definite Reynolds number dependency is indicated in various portions of these data. In all cases, the initial pressure rise to separation is delayed for the higher Reynolds number data. In addition, the higher Reynolds number data possess both the relative maximum and minimum pressures wherever they may occur along the model. The most apparent feature in comparing these figures is the change of the pressure distribution as the clearance gap is increased. This is clearly seen in Figure 13 where the pressure distribution for various clearance gaps has been superposed for the high Reynolds number case. The initial pressure rise profile is seen to move toward the leading edge of the fin as the gap is increased. The peak pressure observed near the leading edge decreases and at the same time an increasing pressure peak is observed just ahead of the clearance spacer. As the gap increases to 0.5 inch, the clearance spacer itself begins to produce a peak pressure distribution comparable to the unswept fin with no gap. If the gap were increased beyond 0.5 inch, the shape of the pressure distribution would eventually be the same as for the fin with no gap. It is of interest to note that a clearance spacer of only 20 percent of the boundary layer thickness has already begun to look like a blunt protuberance of its own. The pressure distributions observed ahead of the smaller clearance spacers are unlike that ahead of the fin in Figure 12a and are somewhat similar to that produced by a two-dimensional corner or step. As the gap is

increased from 0.25 to 0.50 inch, the separation plateau appears to have disappeared. This change in profile indicates a possible change in the flow field model in going from the fin with no gap to the fin with a 0.50-inch gap. The pressure distributions in the wake also undergo rather substantial changes as the gap is increased. The profiles for all the gaps follow that of the no-gap case in the region downstream of the trailing edge of the fin. Just behind the clearance spacer a rather large pressure is attained which subsequently decreases to a lower pressure just downstream of the trailing edge. With the presence of the relatively large pressure developed immediately behind the spacer, one can expect a region of relatively high heat transfer to exist there.

In the region just upstream of the unswept fin, six pressure taps were located off centerline. The pressures measured in this region are shown in Figure 14 for the high Reynolds number case. The three profiles closest to the centerline end abruptly merely because the pressure taps become covered at some point as the fin is translated over the flat plate. The sketched insert indicates the type of "pressure surface" which exists in the region just upstream of the fin. A rearward shift in the pressure peak is apparent as well as a decrease of this peak as one goes off the centerline. Since the location of peak pressures can be correlated to peak heating rates (reference 13), this implies that the heating rate is maximum on centerline and decreases off centerline. The location of these pressure profiles are superposed on an oil smear photograph obtained from reference 5 (Figure 15). The location of the peak pressures on each survey line is indicated by the open circles which show that the pressure peaks coincide with the "Stagnation line." The open circles are scaled to represent the 0.019-inch diameter pressure taps used in this region. This helps to demonstrate that finite-sized pressure taps really measure an average pressure over their inlet area. In this sense then, the peak pressure is probably slightly higher than measured (judging from the pressure profiles, perhaps at most 2 percent higher).

The pressure distributions obtained for the 60-degree swept fin are presented in Figures 16A to 16D. The pressure data for the swept fins indicate a Reynolds number dependency very similar to that of the unswept fin. In comparing the data for the swept and unswept fins with no gap, it is apparent that sweeping a fin will greatly reduce the pressure distribution produced in the interaction region about the fin. This in turn means that a swept fin will produce less flow separation and less interaction heating on the flat plate. The relative changes produced by the clearance spacers are seen in Figure 17 where the data for the high Reynolds number case has been superposed. It is apparent that the swept leading edge has substantially reduced the peak pressure (and hence peak heating) that occurs on the flat plate just upstream of the fin. However with the introduction of the clearance gap, large pressure peaks are observed just ahead of the clearance spacer. Eventually, the pressure distribution ahead of the 0.5-inch spacer is virtually the same shape as for the unswept fin with no gap. The pressure underneath the fin from the leading edge to the clearance spacer is characteristic of a separation pressure plateau. An oblique shock wave off the tip of the fin apparently interacts with the flow on the flat plate and produces a shock induced separation as indicated by the pressure bump for the 0.125-inch gap. The pressure profiles in the wake region are similar in shape to the case of the unswept fin, but the maximum wake pressure is barely over 1.0.

C. Heat Transfer Measurements

The heat transfer measurements made in this study were confined to the region on the flat plate just upstream of the unswept fin with no gap. Azobenzene studies made previously (reference 5) indicated the highest heating to occur in a crescent shaped region just upstream of the fin (Figure 18).

The raw data from the heat transfer gage consisted of output from the differential thermocouple junction and the temperature of

the adjacent thermocouple. After the differential output was converted by use of a calibration chart supplied with the gage, a plot of heat transfer rate, q, versus gage temperature T was obtained. A typical plot is shown in Figure 19 in which the leading edge of the fin was 0.122 inch from the center of the differential thermocouple. As indicated in Figure 19, a straight line is drawn through the data and the slope is then related to a heat transfer coefficient, h. Because a certain nonlinearity was apparent in the data, the straight line was generally based on the points nearer the "adiabatic wall" temperature where the differential output indicated no heat transfer through the surface of the gage.

The first several tests were conducted with no fin in place so as to measure the heat transfer coefficient, h_o, for the flat plate alone. Then a series of tests were conducted in which the fin was translated to various positions relative to the differential thermocouple. The size and position of the differential element relative to the fin at one particular location is shown by the white square in Figure 18. From each test conducted, a particular h was found from a plot similar to Figure 19. The results of these tests are presented in Figure 20 where the absolute values of h_o are also given. Superposed on this figure are the pressures measured in this region. From these data a peak heating rate is measured at a point slightly upstream of the pressure peak. The probable cause of this anomaly will be discussed subsequently. The peak heating rates are in the range of values which have been measured previously by Burbank, et. al. (reference 11) in the region immediately upstream of a right circular cylinder mounted on a flat plate. An apparent Reynolds number effect is evident in the present data, but this effect must be interpreted in light of the thermal boundary layer history effects to be discussed below.

Attempts have been made in the past to correlate the measured peak heating rates to the measured peak pressures in various aerodynamic interaction problems by a relation of the form $h/h_o=(P/P_\infty)^{0.85}$

(reference 13). As to be discussed below, the present peak heat transfer data arenot considered to be of sufficient accuracy to provide a good test of this correlation. Yet from looking at the data in Figure 20, a one-to-one correlation does a fair job of fitting the data over the region just ahead of the fin. From this, the missile designer could get a relatively good estimate of heating rates in this region strictly by measuring the pressure distribution. It should be cautioned, however, that there are apparent Reynolds number and Mach number effects (references 7 and 11). Moreover, this probably applies only near the fin's leading edge since the heating rates in the wake region, for example, range perhaps as high as h/h_o = 2 to 3 (based on measurements in the wake of a cylinder (reference 11) and qualitative observations of azobenzene results) while pressures range only as high as P/P_∞ = 1.5 (Figure 12a). It is of interest to note that the wake pressure normalized by the base pressure ($P/P_\infty \approx 0.6$) is about 2.5.

Since the heat transfer gage could be heated to a point where a zero heat flux was measured through the gage, an adiabatic wall temperature could be measured on the flat plate. Results of these measurements were used to calculate a local recovery factor, r, at points ahead of the fin. These recovery factors as well as the normalized form r/r_o (r_o from flat plate alone measurements) are presented in Figure 21. Again a peak is observed slightly ahead of the pressure peak and an apparent Reynolds number effect is evident. Of major concern in these results is the low values of recovery factor measured on the flat plate alone. Some recent studies in the boundary layer channel by Voisinet, et. al. (reference 14) have indicated that the upstream temperature of the side wall and throat of the channel has a significant thermal boundary layer history effect on the measured recovery factor. In the present tests, the throat was water cooled to approximately 100°F and the side wall temperature was held at approximately 80°F. In addition, a portion of the Boundary Layer Channel side wall was covered with the Bakelite flat plate (Figure 4) that probably attained temperatures comparable

to the adiabatic wall temperature measured on the flat plate (Figure 21). From the conclusions reached in reference 14, the relatively cool throat creates a boundary layer on the channel side wall which is temperature deficient. This effect becomes more severe as the total temperature is increased and the throat temperature is held constant. This trend is apparent in Figure 21. However, the presentation of the data in the form of h/h_o and r/r_o should help to offset the problems encountered in the present measurements. The results of the present tests point out the importance of having information on the thermal boundary layer history on actual missile designs.

Several additional questions may arise concerning the correctness of these measurements. Firstly, the calibration used to convert the raw data was supplied by RdF and as such was strictly for the micro foil gage itself. The composite gage was not recalibrated after fabrication so the question remains whether the RdF calibration still applied. However, considering the way that the gage was put together, this probably was not a serious source of error.

A more serious problem occurred because of the relatively large size of the gage. The square differential element was 0.0625 inch on a side and so really sensed an average heat flow over the length of the diagonal. The size of the gage is indicated in Figure 20 by the line drawn through each data point. Probably the most serious shortcoming of these measurements was the fact that the surface temperature of the gage was actually being monitored at a location behind and to the side of the differential element (Figure 8). Closer examination of the location of the differential element with respect to the surface thermocouple indicated the following: when the differential element was located on the stagnation line (Figure 15), the surface thermocouple was behind the stagnation line. When the differential element was slightly ahead of the stagnation line, the surface thermocouple was on the stagnation line. Obviously in the region of large gradients in the

heating rate in which the gage was used, there would be significant variations in surface temperature between the differential element and the surface thermocouple. This was apparently one factor which produced a shift in the peak heating rates. The problems mentioned here are also likely responsible for the nonlinearity of the data such as those present in Figure 19.

One of the purposes of using this gage in the present study was to check the feasibility of using it for heat transfer measurements in a "steady state" wind tunnel facility. While the data obtained certainly does indicate peak heating rates do occur in the vicinity of maximum pressure measurements, the present results must be used with the above limitations in mind. At this point it appears that the heated differential gage could be subminiaturized with perhaps the surface temperature being monitored directly from the differential element itself. In this sense then, it appears that this type of gage could be put to valuable use in future studies.

D. Boundary Layer Channel Flow Visualization Studies

1. Oil Smear Tests of Fins with Small Clearance Gaps

Information concerning surface shear directions and locations of flow separation was obtained from a series of oil smear tests. The thickness of the oil and any oil build-up was small compared to the boundary layer thickness and was considered to have negligible effects on the flow field. Oil smear tests of the flat plate alone indicated that the plugs in the plate had no adverse effects on the developed patterns (reference 5).

In the present study a series of oil smear tests were made in which small clearance gaps (small compared to the 2.6-inch thick flat plate boundary layer) were introduced under the fins. Figure 22a is a photograph of the pattern developed on the flat plate for the unswept fin with no gap. The fin has been removed for

photographic purposes but its location during the run is obvious. Detailed measurements can be extracted from the photograph by merely scaling with the dimensions given in Figure 5. While most of the oil smear photographs were obtained after the channel was shut down, no basic changes occurred during shutdown except some oil splattering and the collapse of oil buildups.

The test shown in Figure 22a was conducted at test condition 2 ($Re_\infty/ft = 7.4x10^6$) while the remainder of the oil tests in this study were conducted at test condition 1 ($Re_\infty/ft = 2.8x10^6$). However, as found in reference 5, the development of the patterns was weakly Reynolds number dependent in this study. In Figure 22a, the oil is seen to have accumulated in ridges which form the boundaries between the various interaction regions. While at times it may seem more correct to refer to these ridges as "interaction lines," this report will conform to the usual terminology of "separation lines." Regions of high shear are apparent where the oil has been nearly swept away. The primary separation line corresponds to the point of initial flow separation upstream of the fin. The standoff distance of the "primary separation" oil ridge has been indicated in the figure. This flow separation is initiated by the adverse pressure gradient set up by the fin bow shock-flat plate boundary layer interaction. A portion of the bow shock trace calculated from blast wave theory is indicated in Figure 22a, but this shock trace does not necessarily coincide with any of the patterns developed on the plate. The secondary separation line also is produced as a result of the bow shock wave interaction. These interaction regions feature recirculating/reversed flow as can be inferred from the surface shear directions. A model based in part on these flow patterns was described in Figure 2. The separated regions noted in the wake are attributed to interactions produced by the wake recompression shocks. An enlargement of the regions immediately upstream and downstream of the fin are shown in Figures 22b and 22c. The detailed "herringbone" patterns seen in the photographs suggest the presence of a counter-rotating "horseshoe" vortex system to form around the

front of the fin (Figure 2). Similar patterns suggest the presence of vortex systems in the fin-flat plate corner region and in the wake. A small portion of the original oil smear is still visible in the separated region in the wake. A sort of "source point" or "nodal point of attachment" is apparent immediately upstream of the secondary separation line. A more complete discussion of this oil smear test as well as comparisons with azobenzene photographs can be found in reference 5.

Also indicated in Figures 22b and 22c are the pressure profiles measured on the flat plate along the centerline of the fin (Figure 12a). The peak pressure is seen to occur in the region of high shear just ahead of the fin. The secondary separation line is associated with the dip in the pressure profile while the peak in the initial pressure rise occurs near to the "nodal point of attachment." It is apparent that the initial pressure rise to separation starts upstream of the primary separation oil ridge. In the wake region, the low base pressure corresponds to the oil pooling at the rear of the fin. The relatively larger pressures downstream of the fin are associated with the high shear produced by the vortex systems.

Figures 23 to 26 show the oil patterns for the same conditions except that a clearance gap has been introduced under the unswept fin. The loss in clarity from Figure 22 is attributed in part to the lower shear forces at test condition 1 and in part to the thicker application of the oil mixture in the remaining tests. The initial tests using the 0.075-inch clearance gaps were plagued with various problems such as misalignment of the gap spacer (Figure 24) and oil splattering during channel shut down (Figure 25). After design and fabrication of the flat plate pressure model, larger (1.63 inches) spaces locked in alignment to the fin became available. The yawing plug was glued to the flat plate to cure the latter problem and a final oil smear test was conducted using the 0.50-inch spacer. The oil pattern of this test is shown in Figures 26a and 26b. Despite

the problems encountered during these tests, the results have been included in this report to be interpreted with the above limitations in mind.

For the unswept fin, the basic regions of flow separation noted for the fin with no gap (Figure 22a) are seen to exist in nearly the same relative positions as the gap size is increased. The "primary separation line" is seen to move downstream as the gap is increased. This was previously noted in the pressure data of Figure 13. An enlarged view of Figure 23a indicates the very complex flow structure which develops when even a small gap is placed under the fin (Figure 23b). While a "stagnation line" is still apparent at the location of the fin leading edge, a new type of reversed flow pattern has developed just ahead of the spacer. The oil smear patterns ahead of the spacer look very much like the patterns observed ahead of the 2-D step. A similar type of pattern was also observed ahead of the other sized spacers and the pressure profiles appeared to be different than the profiles obtained ahead of the fin with no gap (figure 13).

Increasing the gap size produced a rather noticeable change of the flow field in the wake region of the fin. This was also noted in the pressure data of Figure 13. A superposition of the pressure data on Figure 26a clearly indicates how regions of varying shear flow shown by the oil smears correspond to the variation in the pressure distribution. An enlarged view of the oil pattern produced with the 0.5-inch spacer is shown in Figure 26b. Again the type of flow structure apparent in Figure 23b is to be observed here. Now however, it appears that a "stagnation line" has developed just ahead of the spacer.

The oil patterns for the 60-degree swept fin indicate a much smaller region of flow separation when compared to the unswept fin (Figure 27a). Regions of high shear (which implies high heat transfer) still exist in the region of the leading edge as well as in the

wake region. Enlargements of these regions in Figure 27b show the complex flow in these areas. A type of "stagnation line" is still weakly visible ahead of the fin. The wake region appears much like that of the unswept fin. A superposition of the pressure data shows the correspondence between the pressure profiles and the patterns observed in the oil. When a 0.125-inch spacer was placed below the fin, the intensity of the regions of high shear were reduced (Figure 28). With the 0.125-inch spacer a problem was encountered when the surrounding Bakelite plate raised off the Channel side wall and left the bolted down yaw plug somewhat lower. This produced the regions of separated flow visible on the plug as a region of undisturbed original oil smears. This problem was solved when the larger 0.5-inch spacer was used under the fin.

The oil patterns for the 0.5-inch gap under the 60-degree swept fin indicate a rather large change in the flow field as the spacer is increased (Figure 29a). Unlike the unswept fin where the basic pattern ahead of the fin still remains at a 0.5-inch gap, the 60-degree swept fin displays a totally new pattern. The region nearer the leading edge indicates a very subtle oil pattern associated with the pressure plateau. Now the clearance spacer has taken on an oil pattern nearly identical to that of the unswept fin with no gap. Clearly visible in the enlarged view (Figure 29b) are the primary and secondary separation and the "stagnation line." The pressure distribution in this region is also virtually identical to the case of the unswept fin with no gap. A region of relatively high shear (high heat transfer) must exist below the fin behind the clearance spacer since the pressure has a local maximum in this region and the oil patterns are indicative of high shear forces. The downstream wake is reduced quite substantially from the case of no clearance gap.

The oil smear patterns developed on the unswept fin for this sequence of tests are shown in Figures 30a - c. For the case of no clearance gap the "herringbone" patterns appearing on the fin further indicate that a vortex system is operating in the fin-flat plate

corner region (see Figure 2). The characteristic "hump" observed in the oil patterns may be due to the interaction of this corner vortex system and the previously mentioned "horseshoe" system which forms around the leading edge of the fin. No oil accumulation exists on the first fin merely because a much lighter oil coat was originally put on the fin prior to the run. When spacers were introduced below the fin, the patterns shifted rearward. The small region of upward flow noted to exist (reference 5) at the base of the leading edge of the fin with no gap, virtually disappears as the gap size is increased. This region of upward flow was thought to be associated with the horseshoe vortex pair which exists around the leading edge of the fin (Figure 2). As the gap is increased, the effect of this horseshoe vortex on the leading edge of the fin virtually disappears. The so-called parting line of the corner vortex pair still remains quite visible in the case of the 0.5-inch spacer. The other patterns observed on the fins are far too complex to describe in detail here.

With the photograph of the fin and 0.125-inch spacer obtained during the test, it is possible to see the detail otherwise lost during tunnel shutdown. The superposed pressure distribution corresponds very clearly with every oil pattern observed on the flat plate. Since the oil tests were conducted using a shorter clearance spacer than the pressure tests, a portion of the pressure distribution under the fin was shifted so as to match up with the spacer. The large pressure dip after the first pressure peak is apparently associated with the "hairpin" region of separation noted below the fin.

The final oil smear photographs show the patterns developed on the swept fin for the present tests (Figures 31a - c). Again the photograph obtained during the test shows the fine detail which the oil smear tests are able to bring out. The patterns developed on the fins indicate a very complex series of vortex systems to exist in the fin-flat plate corner region.

2. Azobenzene Movies

Several tests were made in which a movie camera recorded the patterns which developed on the azobenzene coated Bakelite model. Figures 32a and 32b show select frames of the movie for an unswept fin with and without a 0.125-inch gap. The time in minutes into the run, after the establishment of steady conditions, is given below each photo. Because of difficulties with the timing light on the camera, these values of time are approximate and are intended to be interpreted only in a relative sense. Moreover, the two tests shown in Figure 32 cannot be accurately compared on the time basis given. The rather shallow viewing angle dictated by the small windows did not allow a good view of the flat plate and only a view of the lower portion of the fin. As the patterns develop, the yawing lug and the instrumentational holes in the flat plate become quite visible. In particular, the circular instrumental hole should not be confused with the crescent pattern which eventually develops on the flat plate just ahead of the leading edge of the fin.

From the sequence of photographs the regions of high heat transfer can be identified where the azobenzene disappeared the quickest. The leading edge of the fin which experiences stagnation point heating develops first. This pattern is followed shortly by the development of a region on the flat plate just upstream of the leading edge of the fin (Figure 32a, $t = 0.2$). As the test progresses, this pattern near the leading edge takes on a crescent shape (CR) ($t = 0.7$). Photographs of this pattern are shown in true perspective in Figure 18. Eventually the entire region near the leading edge looses all of the azobenzene coating. Later in the run the lines identified in the oil smear photographs as primary separation (PS) and secondary separation (SS) become visible. The patterns developed in the wake region clearly indicate the rather large heating rates along the centerline and the region of flow separation (FS) noted in the oil smear photographs (Figure 22a). Also apparent later in the run are regions of high heating (HH) on the flat plate which extend

downstream along the fin. At about the same time that the crescent region develops on the flat plate, a small region at the bottom of the leading edge of the fin begins to develop (t = 0.7). This pattern eventually develops along the bottom front edge of the fin. The regions of high shear and adjacent separated flow on the side of the fin are associated with the vortices which are present in the fin-flat plate corner region.

Of interest in the photographs of Figure 32a is the way in which the azobenzene pattern develops on the leading edge of the fin. As one proceeds downward into the boundary layer, the azobenzene loss decreases and this implies a decrease in heating rates. A region is indicated in the photo at t = 0.2 which, according to oil smear and Schlieren tests of reference 5, has some type of vortex sheet impingement produced by the separation shock interacting with the bow shock of the fin. The triple point of this shock interaction is toward the bottom of the region indicated. Yet, the azobenzene photographs do not seem to indicate any large local heating rates other than the smooth transition from the stagnation point heating rates of the fin. Experiments of fins on plates have in the past indicated rather large heating rates to occur in this region (e.g. references 11 and 16). However, pressure and heat transfer measurements presented in reference 11 indicate that this fin heating problem is a function of fin thickness to boundary layer thickness, as well as the usual Reynolds and Mach number parameters. For the present study, the governing parameters are such as not to predict a region of high heat transfer on the fin due to the lambda shock interaction.

When a 0.125-inch spacer was placed under the fin and the above test repeated, a series of photographs at the same test duration were obtained and are shown in Figure 32b. As for the case of the fin in Figure 32a, a small crescent region develops on the flat plate near the fins leading edge shortly after the fin leading edge pattern begins to develop. At time t = 0.8, a pattern begins

to develop at the leading edge of the clearance spacer. The patterns on the plate and fin develop as before and regions noted in the oil smear photographs of Figures 24 and 30b can be identified. In particular the "hairpin" region (HP) of flow separation noted in the oil smear photograph is apparent under the forward part of the fin (t = 2.2). Regions of high heating are noted under the rearward part of the fin (t = 3.4) and these are associated with high levels of pressure measured in this region (Figure 12b).

Several other runs were made using the 60-degree swept fin, but light reflection and over-exposure problems produced movies with very little contrast, and not of sufficient quality to reproduce for this report. The observed patterns developed far more slowly than on the unswept fin and of course indicated that heating rates produced by the swept fin are much lower than the unswept fin. However, the wake region of the swept fin developed rather quickly and this implied wake heating rates comparable to the unswept fin's wake. When a 0.125-inch spacer was placed under the fin, the heating in the wake was decreased rather substantially. However, a region of high heating was noted at the front edge of the clearance spacer, just as for the case of the unswept fin in Figure 32b.

3. Schlieren Photographs from the Boundary Layer Channel

To obtain information on the lambda shock interaction produced by a fin protuberance, a series of Schlieren photographs were obtained of the flow fields about several of the fin geometries used in this study. All Schlieren photographs were obtained at test condition 2 and with the knife edge parallel to the flat plate.

Since it was known that the lambda shock structure upstream of the fin was unsteady, Schlieren motion pictures were taken at 100 frames/sec and exposure of 3 microseconds. These motion pictures clearly showed the unsteadiness. Unfortunately, the quality of the motion pictures did not permit reproduction in this report. Because

of the relatively slow filming rate, the pictures did not portray a changing pattern, but rather were a sequence of photos, each one different from the other. The frequency of the shock oscillations was of course much faster than the filming rate and probably was on the order of several thousand cycles per second.

Since the individual frames of the movies were random anyhow, a series of plate photographs were merely taken at a 3-microsecond exposure. Several of these photographs have been placed together in the following figures to give an indication of the flow unsteadiness. Where appropriate, the location of various features found in the oil smear tests have been indicated on the photographs. The edge of the boundary layer has been indicated in each figure.

The first series of photographs were obtained of the unswept fin and are shown in Figure 33. Various density gradients visible in these photographs have been indicated in the figure. Apparent in these photographs is the unsteadiness of the complex lambda shock structure produced upstream of the fin. The shock structure is apparently far more involved than depicted in Figure 2. As indicated in reference 17, the particular type of shock interaction may involve vortex sheets, expansion fans or jets which could account for the patterns observed in the oil smear photographs. Despite the apparent unsteadiness of the shock structure, the oil patterns developed on the model were very sharp and well defined. Primary separation is indicated by two arrows; the left being the point where the pressure data first begins to indicate an increase (test condition 2) the right as the location of the oil ridge (test condition 1). The parting band was observed in tests of reference 5 and is apparently the location the impingement of a vortex sheet or jet produced at the triple point. The photographs appear to show a number of oblique shock waves emanating from the primary separation region.

Figure 33b shows the shock structure developed ahead of and below the fin with the 0.25-inch gap. The intensity of the lambda shock structure has been reduced from the previous case of no clearance gap. It appears that a type of shock reflection occurs from the flat plate. There is not sufficient detail to determine any shock structure just upstream of the clearance spacer. From observing the many single frames of the movies, it appears that the shock knee pulses back and forth underneath the fin.

Figure 33c shows the Schlieren photographs obtained when a 0.5-inch clearance spacer was placed under the unswept fin. In addition to the appearance of a reflected-like shock, several other density gradients are apparent below the fin. These gradients are likely shock waves which are reflecting back and forth between the fin and flat plate. This structure is likely unstable as the shock structure for Figure 32. It might be imagined that these reflected shocks pulse back and forth underneath the fin. On the other hand, the oil patterns developed on the flat plate were quite sharp and clearly defined.

The photographs of the 60-degree swept fin also suggest the shock wave unsteadiness and what may appear to be the existence of muliple oblique shocks in the interaction region (Figure 34a). When a 0.5-inch clearance was placed under the fin (Figure 34b), a pattern developed ahead of the clearance spacer which began to look like the patterns seen ahead of the unswept fin of Figure 33a. Also visible off the tip of the leading edge of the fin is a very weak oblique shock wave.

Finally, several Schlieren photographs were taken of the wake region of the unswept fin with no clearance gap. Figure 35 shows a composite photograph with the flow field both upstream and downstream of the fin. The wake region shows several lines which are density gradients produced by the fin-flat plate interaction. When linearly extrapolated, they appear to originate at the bottom of the leading

edge of the fin. When compared to the oil smear photographs in Figure 30a, it appears that these gradients could possibly be associated with vortices shed from the fin-flat plate corner region.

E. Boundary Layer Surveys in the Boundary Layer Channel

Boundary layer surveys were obtained in the first phase of work and were reported in reference 5. For completeness these results are repeated in this report. Table 2 summarizes these surveys taken on the Bakelite flat-plate model. In addition, data obtained by Lee, et. al. (reference 18) are included which also list the boundary layer momentum thicknesses and displacement thicknesses for the two test conditions. Figure 36 shows the static pressure and Mach number distribution through the boundary layer for test condition 1.

F. Discussion of the Results

From the results presented in this report, the designer can get a qualitative feel for the heating rates and extent of flow separation to be expected on configurations with blunted swept and unswept fin-type protuberances. In addition, the results indicate the flow field structure to be expected on missile control fins which have clearance gaps to allow for movement of the fin.

The flow visualization results have indicated the complex and somewhat unsteady flow field which is present in the fin-flat plate interaction regions. These results qualitatively indicate regions of high shear and high heat transfer to exist on various portions of the model. In particular, the region on the flat plate both upstream and downstream of the unswept fin experiences large heating rates. The 60-degree swept fin has lower heating rates ahead of the fin, but the wake region still has rates comparable to the unswept fin. When a spacer is placed under the fin to provide a clearance gap, regions of flow separation and high heating began to occur in the vicinity of the spacer itself. For a clearance gap of only 20

percent of the flat plate boundary layer thickness, the major boundary layer interaction is produced by the clearance spacer. For missile designs in which the fin is supported by the yawing lug (Figure 1) more than this distance of the body, the yawing lug will produce the major interaction heating problems on the body. Hence, even though a missile may have a highly swept fin, the yawing lug (generally just a circular shaft) will produce heating rates on the missile body comparable to those of a right circular cylinder. A possible remedy to this problem would be to put a diamond shaped fairing around the lug which would greatly reduce the interaction problem.

The pressure surveys obtained in this report support the above conclusions. The heat transfer measurements indicate heating rates up to six times the undisturbed flat plate values in the region just upstream of the unswept fin. From the present data, the heating rates ahead of the fin could be estimated on a one-to-one basis with the measured pressure distribution.

SUMMARY

Various flow visualization results are presented for cylindrically blunted, unswept and 60-degree swept fins with and without small clearance gaps, partially immersed in a turbulent boundary layer ($\delta \approx 2.6$ inches). In addition, pressure and heat transfer measurements were obtained on the flat plate upon which the fin was mounted. These experiments were completed in the Naval Ordnance Laboratory Boundary Layer Channel at a nominal Mach number of 5 and nominal free-stream Reynolds numbers of 2.8×10^6 and 7.4×10^6. Oil smear, azobenzene and Schlieren flow visualization tests showed the complex interaction flow fields which exist around the fin-flat plate combination. Pressure measurements showed large peak pressures to occur in regions of high heat transfer. Complementary heat transfer measurements indicated heating rates on the flat plate with fin to be up to six times the rate on an undisturbed flat plate. Tests

showed that when a spacer was placed underneath the fin to provide a clearance gap of only 20 percent of the flat plate boundary layer thickness, the major boundary layer interaction was produced by the spacer itself.

REFERENCES

1. Korkegi, R.H., "Survey of Viscous Interactions Associated with High Mach Number Flight," AIAA Journal, Vol. 9, No. 5, May 1971

2. Ryan, B.M., "Summary of the Aerothermodynamic Interference Literature," NWC TN 4061-160, April 1969

3. Cramer, R.H., "Status of Wing Body Interference Research at Hypersonic Speeds," APL/JHU Memo BBA-RC-69

4. AGARD Conference Proceedings No. 71 on Aerodynamic Interference, AGARD-CP-71-71, January 1971

5. Winkelmann, Allen E., "Flow Visualization Studies of a Fin Protuberance Partially Immersed in a Turbulent Boundary Layer at Mach 5," NOLTR 70-93, 20 May 1970

6. Lee, R.E., Yanta, W.J., Leonas, A.C. and Carner, J.W., "The NOL Boundary Layer Channel," NOLTR 66-185, 7 November 1966

7. Price, E.A., Jr. and Stallings, R.L., Jr., "Investigation of Turbulent Separated Flows in the Vicinity of Fin-Type Protuberances at Supersonic Mach Numbers," NASA TN D-3804, February 1967

8. Jones, Robert A., "Heat Transfer and Pressure Investigation of a Fin-Plate Interference Model at a Mach Number of 6," NASA TN D-2[illegible], July 1964

9. Uselton, James C., "Fin Shock/Boundary-Layer Interaction Tests on a Flat Plate with Blunted Fins at M_∞ = 3 and 5," AEDC-TR-67-113, June 1967

10. Lucas, Ernest J., "Investigation of Blunt Fin-Induced Flow Separation Design on a Flat Plate at Mach Numbers of 2.5 to 4.0," AEDC-TR-70-265, January 1971

11. Fairbank, P.B., Newlander, R.A. and Collins, I.K., "Heat Transfer and Pressure Measurements on a Flat-Plate Surface and Heat Transfer Measurements on Attached Protuberances in a Supersonic Turbulent Boundary Layer at Mach Numbers of 2.65, 3.51 and 4.44," NASA TN D-1372, December 1962

12. Young, F.L., Kaufman, L.G. and Korkegi, R.H., "Experimental Investigation of Interactions Between Blunt Fin Shock Waves and Adjacent Boundary Layers at Mach Numbers 3 and 5," Aerospace Research Laboratories Report, ARL 68-0214, December 1968

13. Markarian, F.C., "Heat Transfer in Shock Wave-Boundary Layer Interaction Regions," NWC TP 4485, November 1968

14. Voisinet, Robert L.P., Lee, Roland E., Yanta, William J., "An Experimental Study of the Compressible Turbulent Boundary Layer with an Adverse Pressure Gradient," presented at the AGARD Specialist Meeting on Turbulent Shear Flows, London, England, September 13-15, 1971

15. Thomas, J.P., "Flow Investigations About a Fin Plate Model at a Mach Number of 11.26," Aerospace Research Laboratories Report, ARL 67-0188, September 1967

16. Hiers, R.S. and Loubsky, W.J., "Effects of Shock Wave Impingement on the Heat Transfer on a Cylindrical Leading Edge," NASA TN D-3859, February 1967

17. Edney, B.E., "Effects of Shock Impingement on the Heat Transfer Around Blunt Bodies," AIAA Journal, Vol. 6, No. 1, January 1968

18. Lee, R.E., Yanta, W.J., and Leonas, A.C., "Velocity Profile, Skin-Friction Balance and Heat Transfer Measurements of the Turbulent Boundary Layer at Mach 5 and Zero-Pressure Gradient," NOLTR 69-196, 16 June 1969

TABLE 2

BOUNDARY LAYER SURVEY RESULTS

Survey	P_o (psia)	T_o (°F)	T_w/T_{aw}	M_∞	Re_∞/ft	δ (in.)	δ^* (in.)	θ (in.)
Reference 5	75	302	- *	4.88	2.8×10^6	2.60	-	-
	150	166	-	4.93	7.4×10^6	2.50	-	-
Reference 19	75	302	0.83	4.79	2.8×10^6	2.57	0.8239	0.1157
	150	236	0.96	4.93	7.4×10^6	2.49	0.7946	0.09119

*The temperature distribution along the Channel test plate and on the model flat plate were not measured. However, the test plate was water-cooled at approximately 80°F. Hence, the Bakelite model plate was assumed to have approached T_w/T_{aw} values comparable to those of Reference 18. T_{aw} = adiabatic wall temperature.

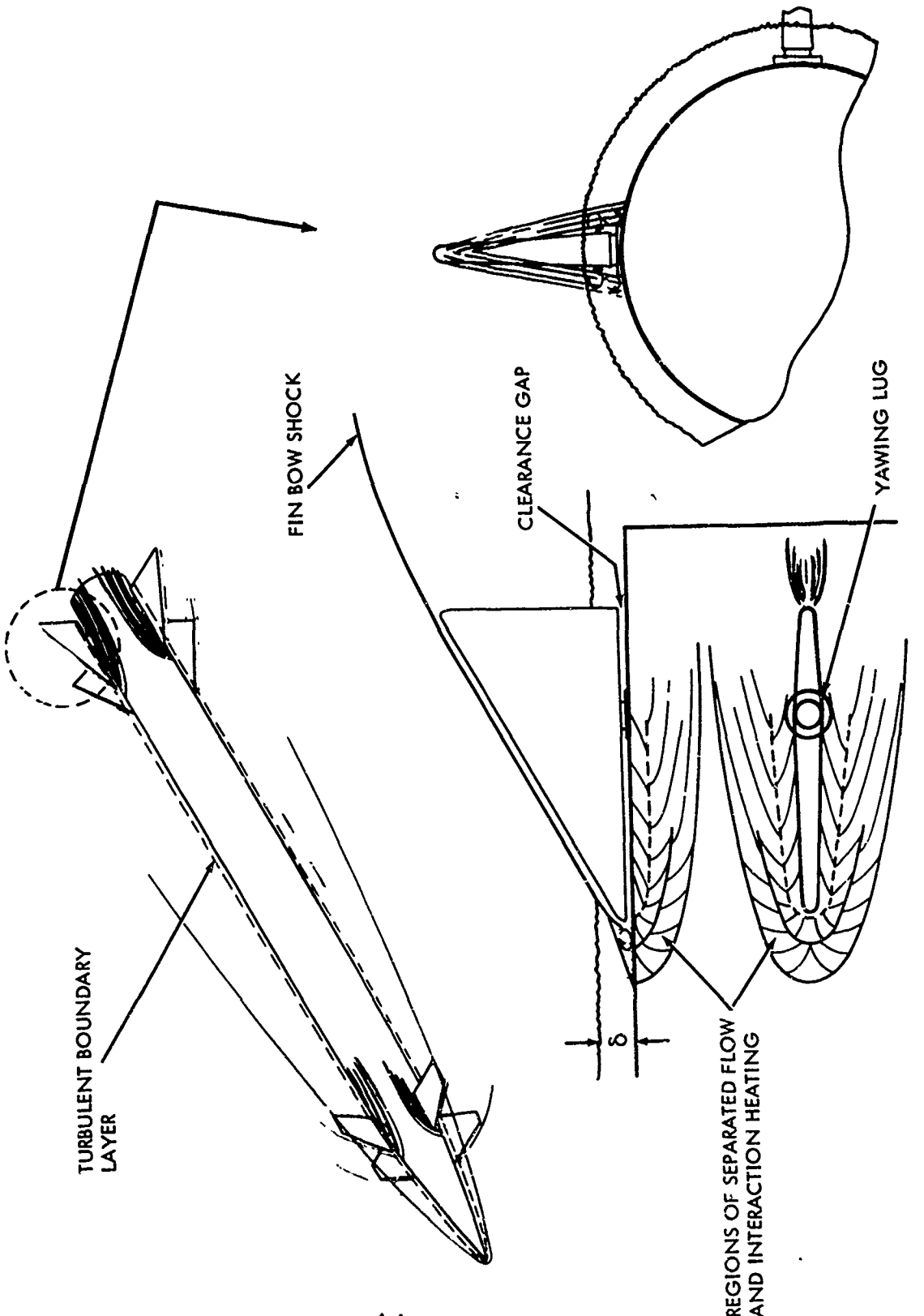

FIG. 1 TYPICAL MISSILE FIN-BODY GEOMETRY

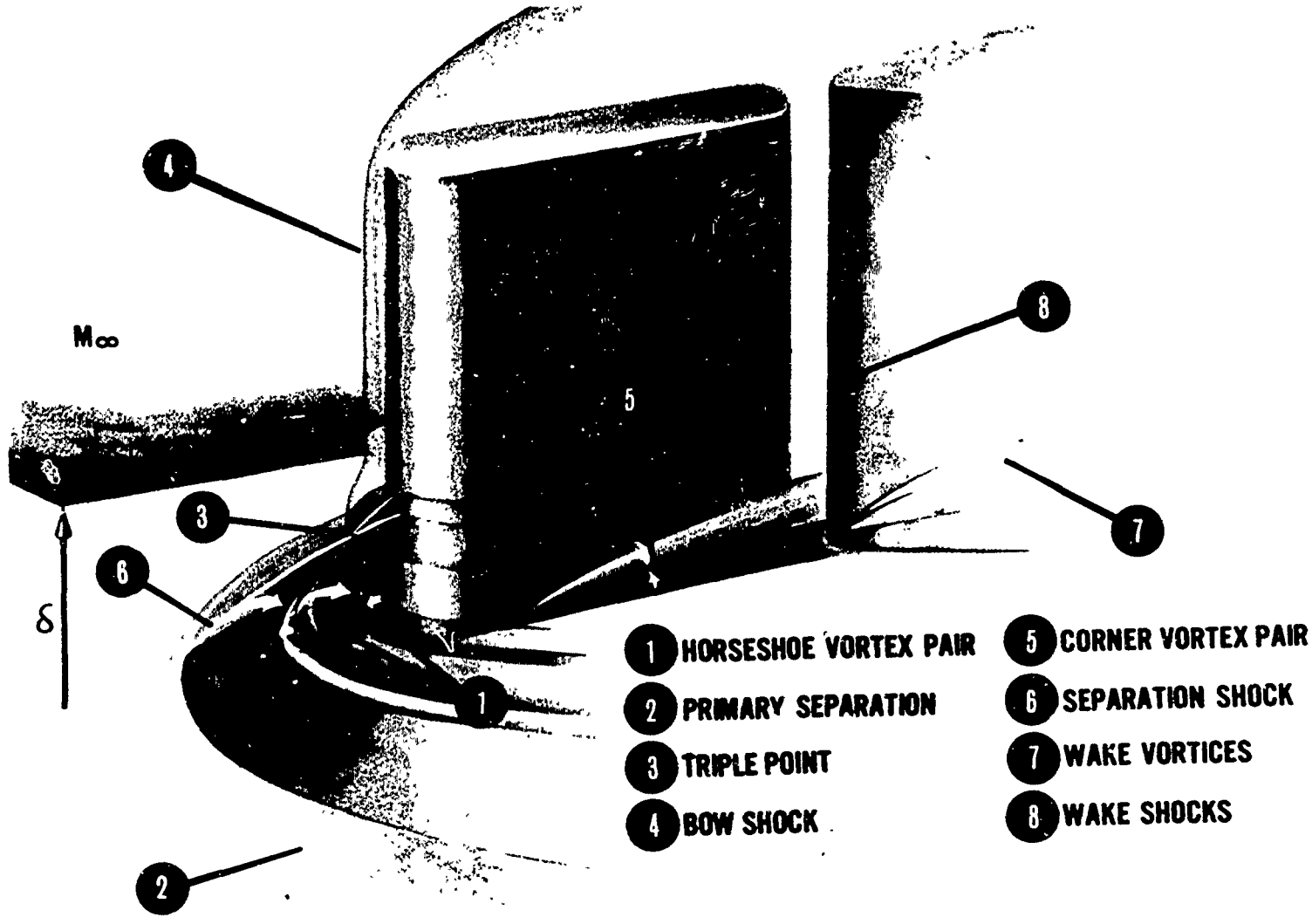

FIG. 2 POSSIBLE FLOW-FIELD MODEL OF THE INTERACTION PRODUCED BY A FIN PROTUBERANCE

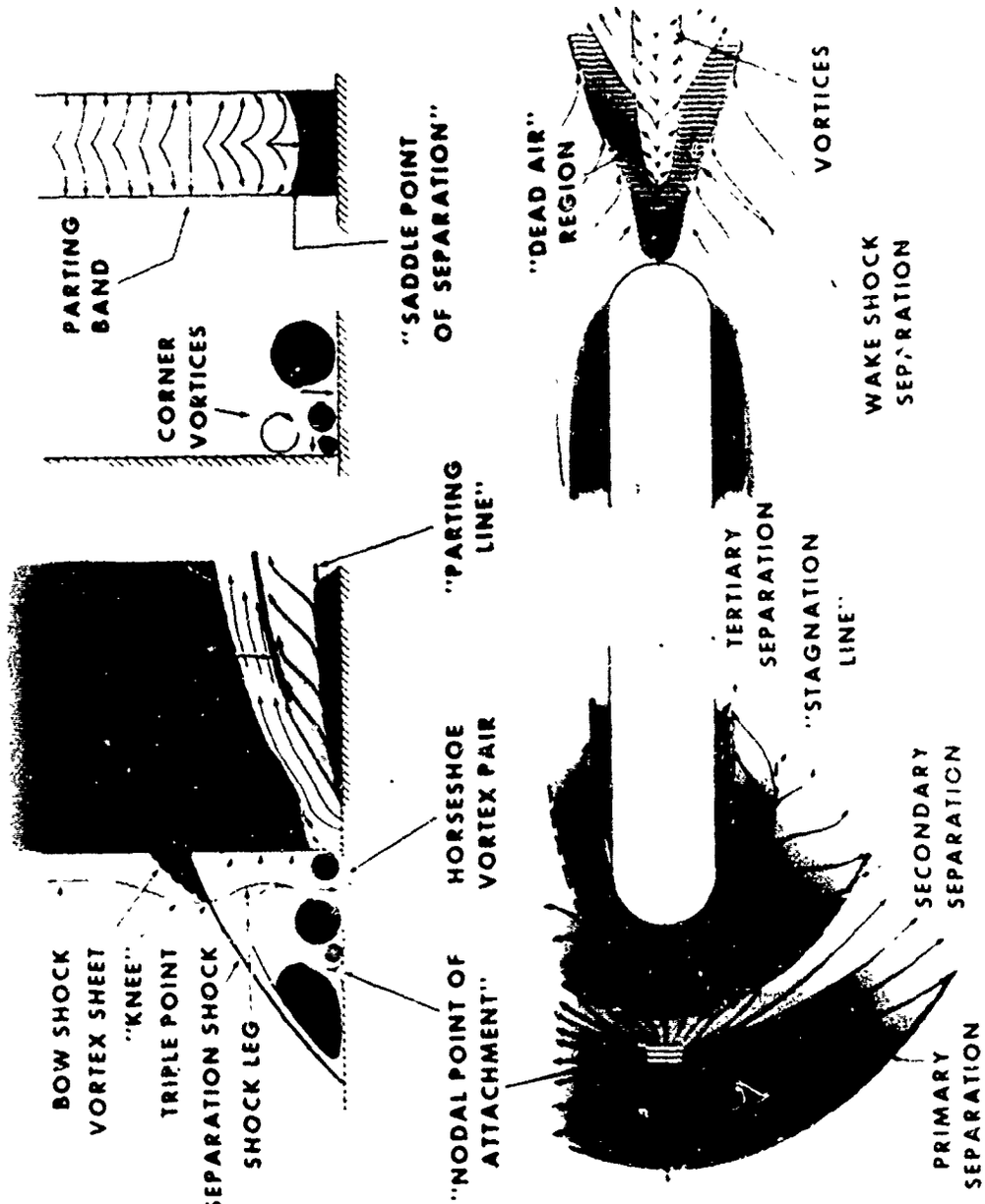

FIG. 2 (CONCLUDED)

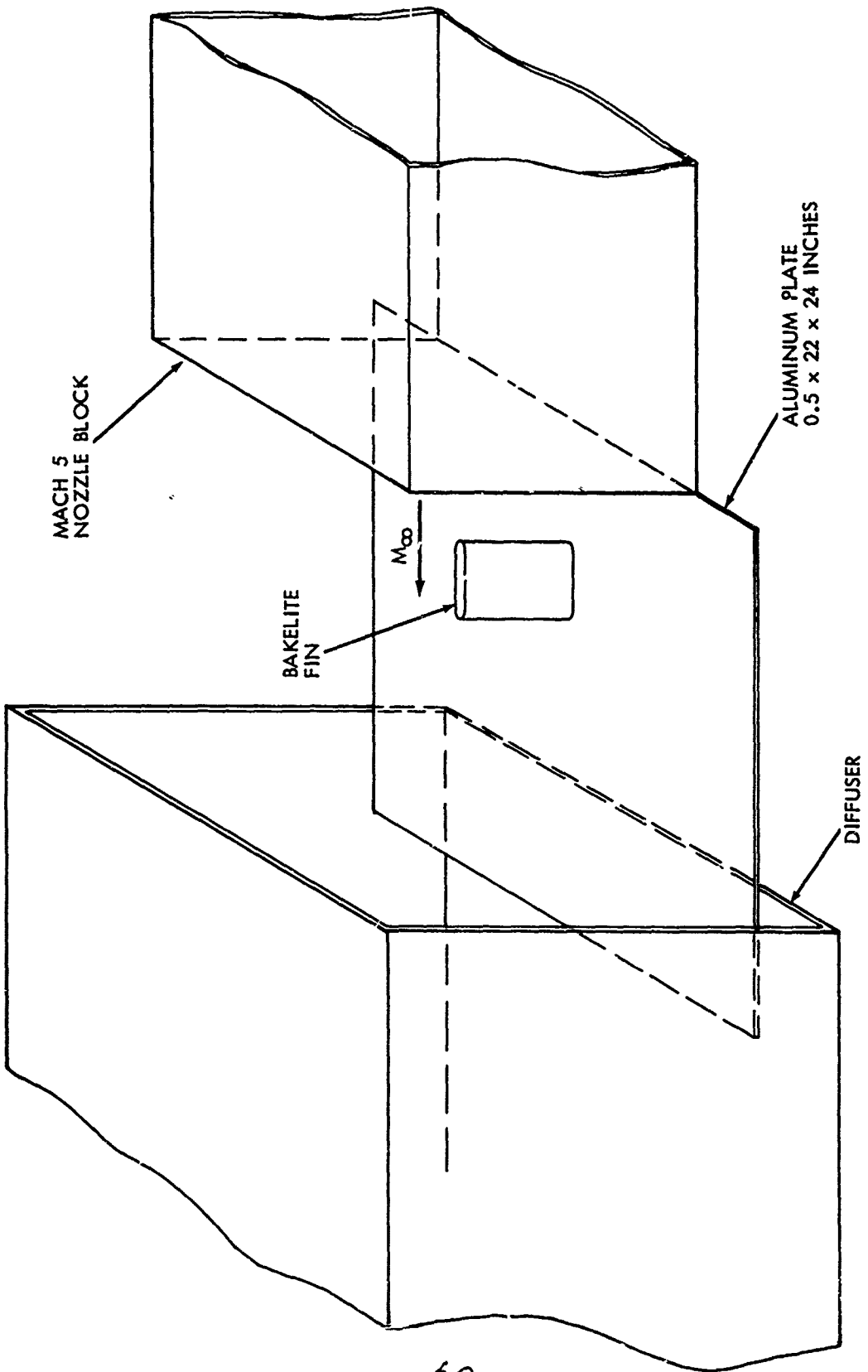

FIG. 3 NOL SUPERSONIC TUNNEL NO. 2 WITH FIN-FLAT PLATE MODEL

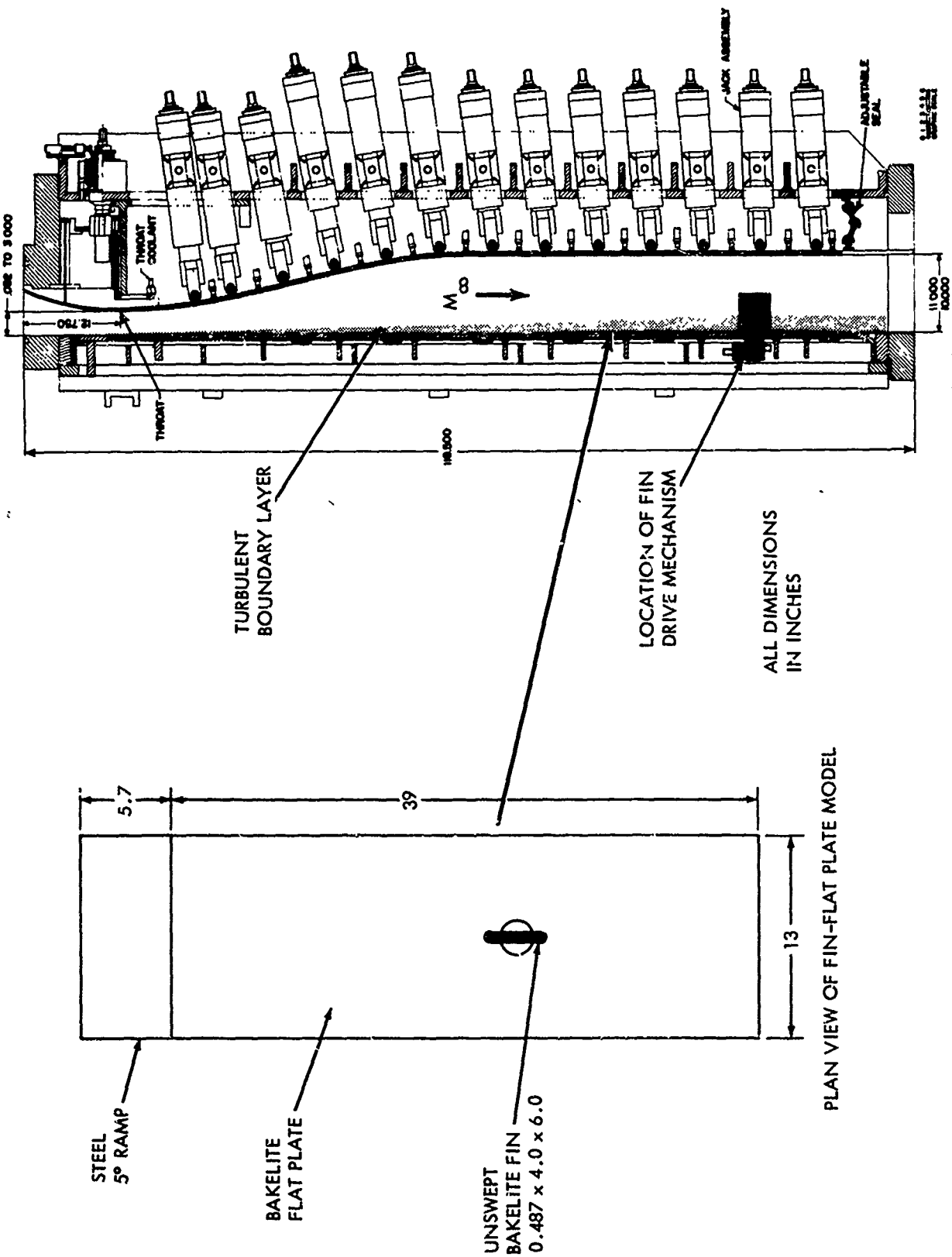

FIG. 4 NOL BOUNDARY LAYER CHANNEL WITH FIN-FLAT PLATE MODEL

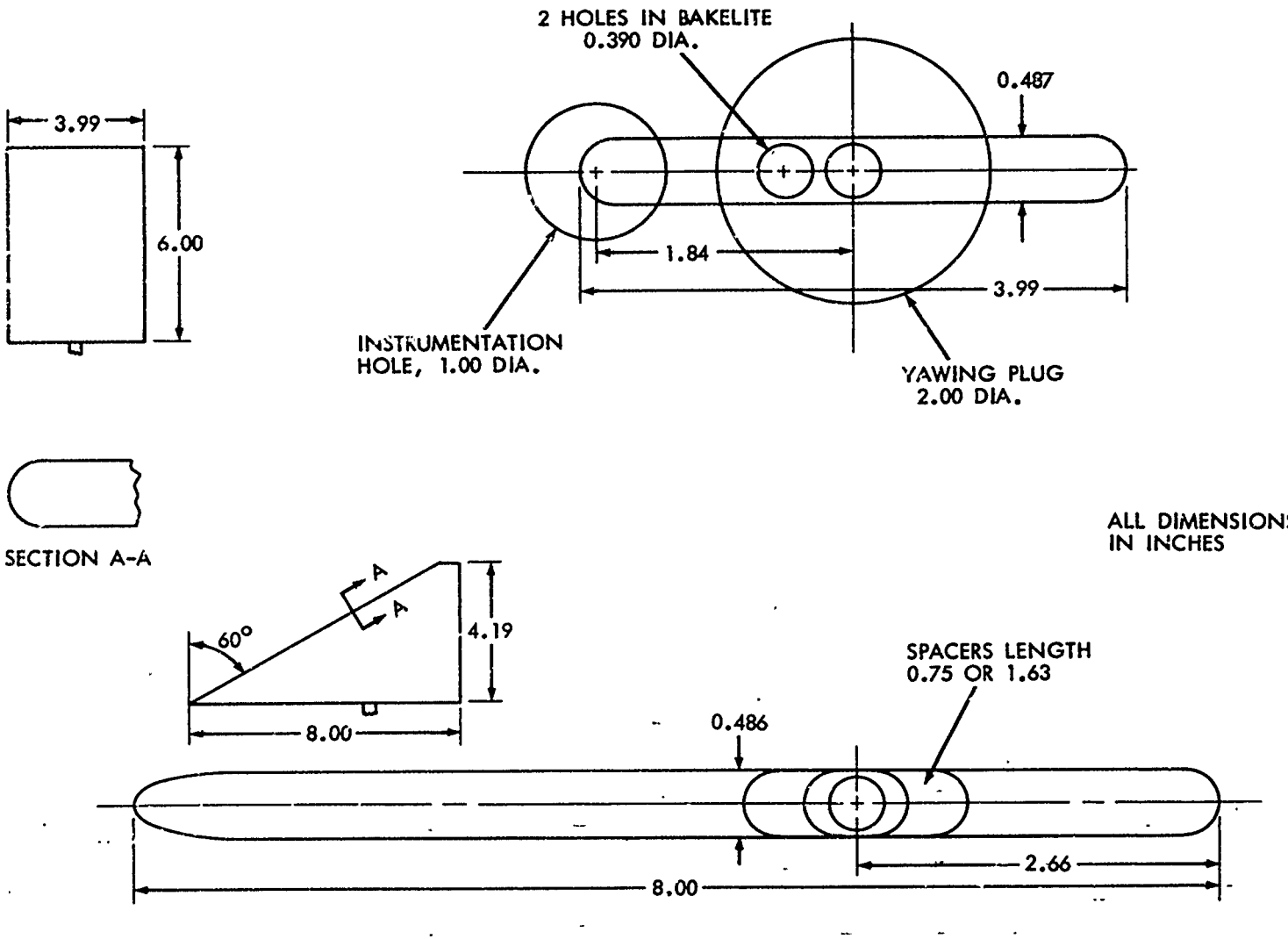

FIG. 5 PLAN VIEWS OF FIN MODELS ON BAKELITE FLAT PLATE

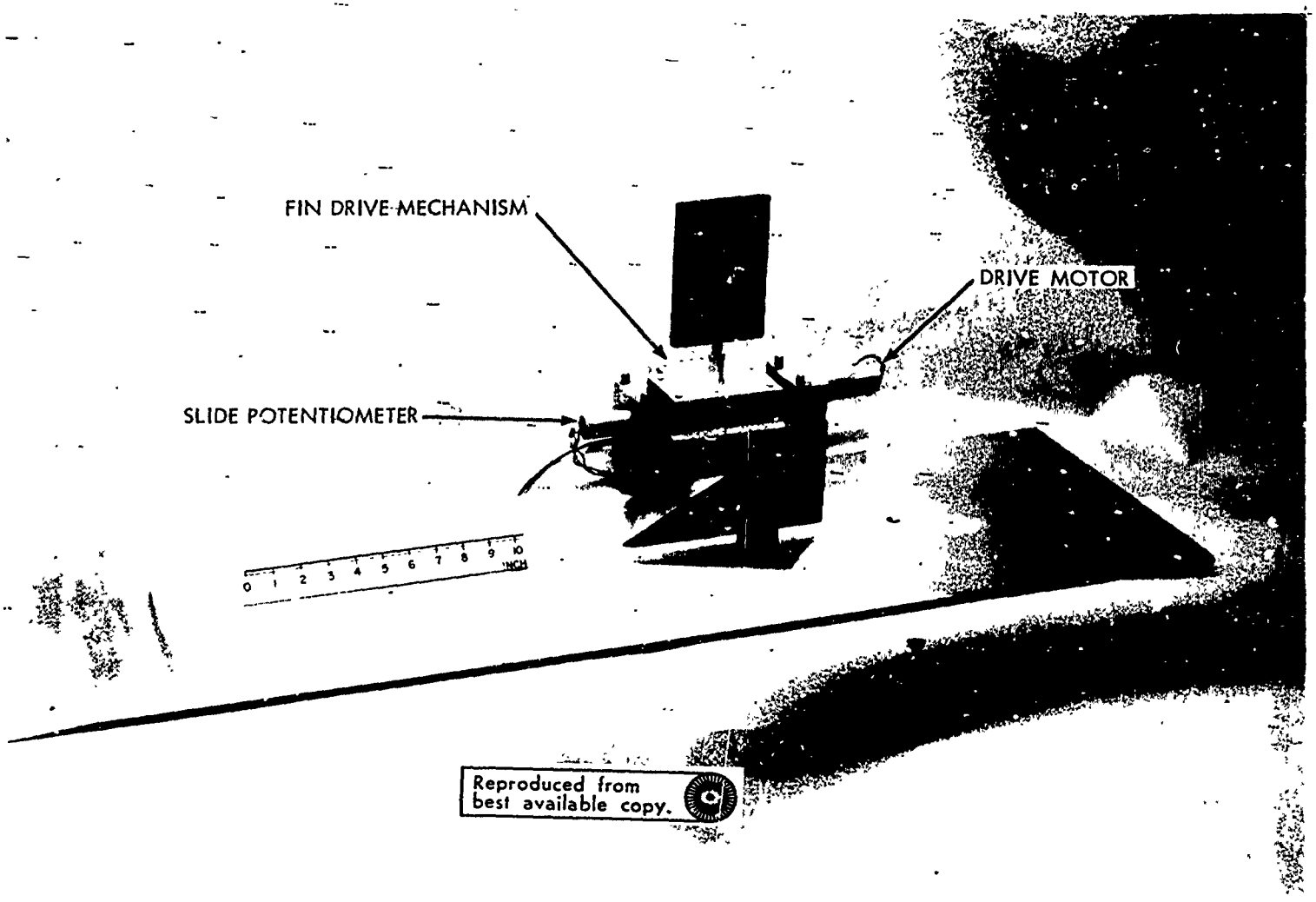

FIG. 6 FIN FLAT PLATE PRES L

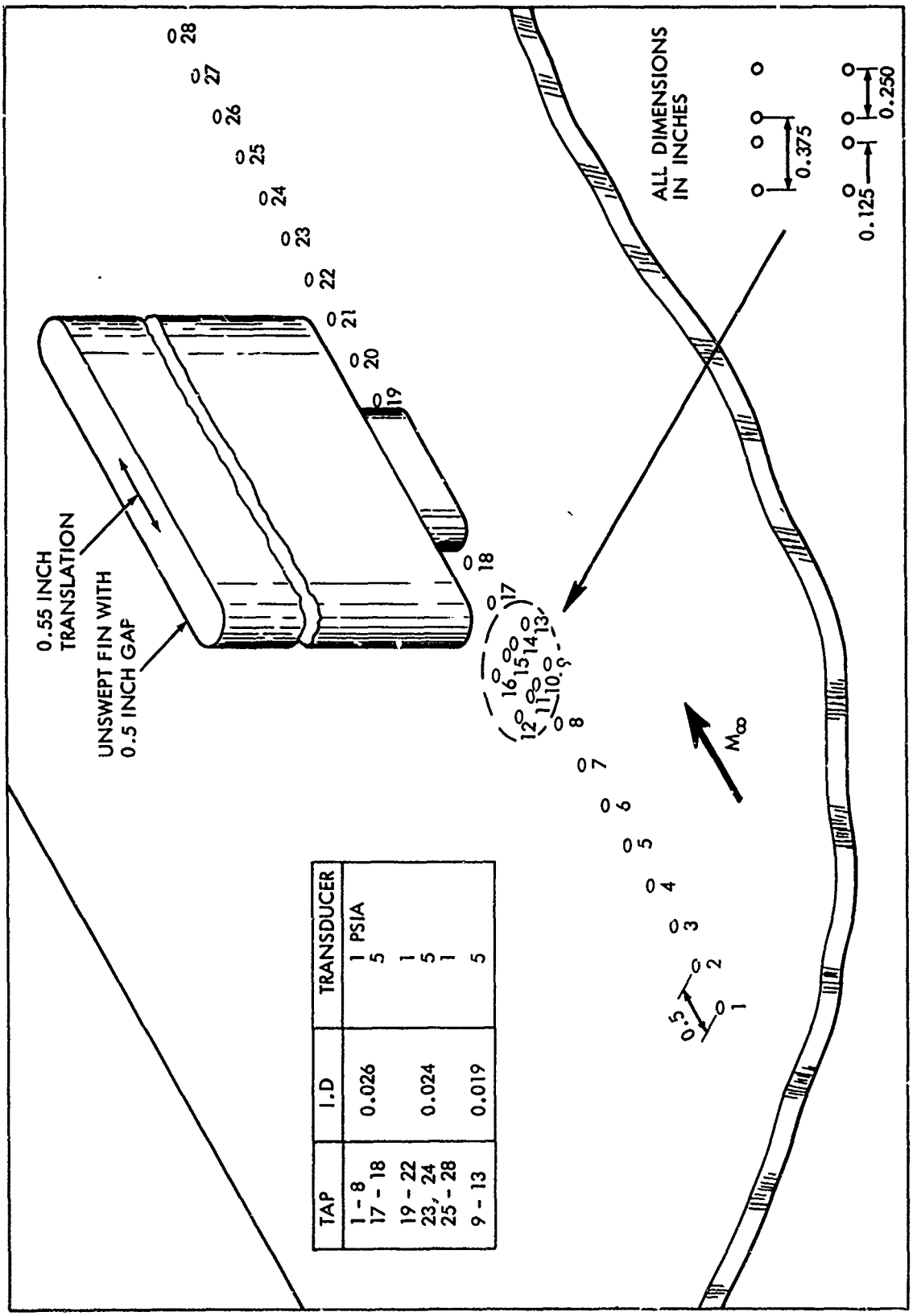

TAP	I.D	TRANSDUCER
1 - 8	0.026	1 PSIA
17 - 18		5
19 - 22	0.024	1
23, 24		5
25 - 28		1
9 - 13	0.019	5

FIG. 7 STATIC PRESSURE TAP LOCATIONS ON FLAT PLATE

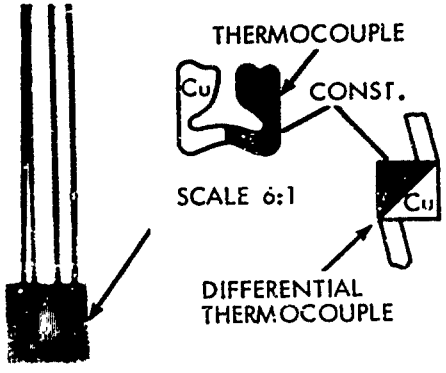

Rd F MICRO-FOIL
HEATED FLOW SENSOR

MINCO
BUTTON HEATER

PHENOLIC PLUG

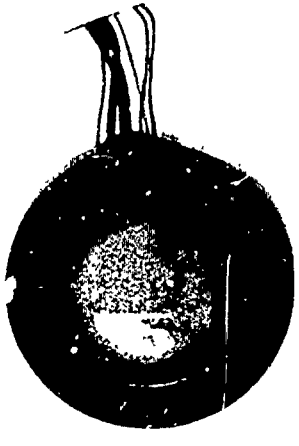

FIG. 8 HEATED DIFFERENTIAL HEAT TRANSFER GAGE

FIG. 9 OIL SMEAR TEST IN SUPERSONIC TUNNEL NO. 2

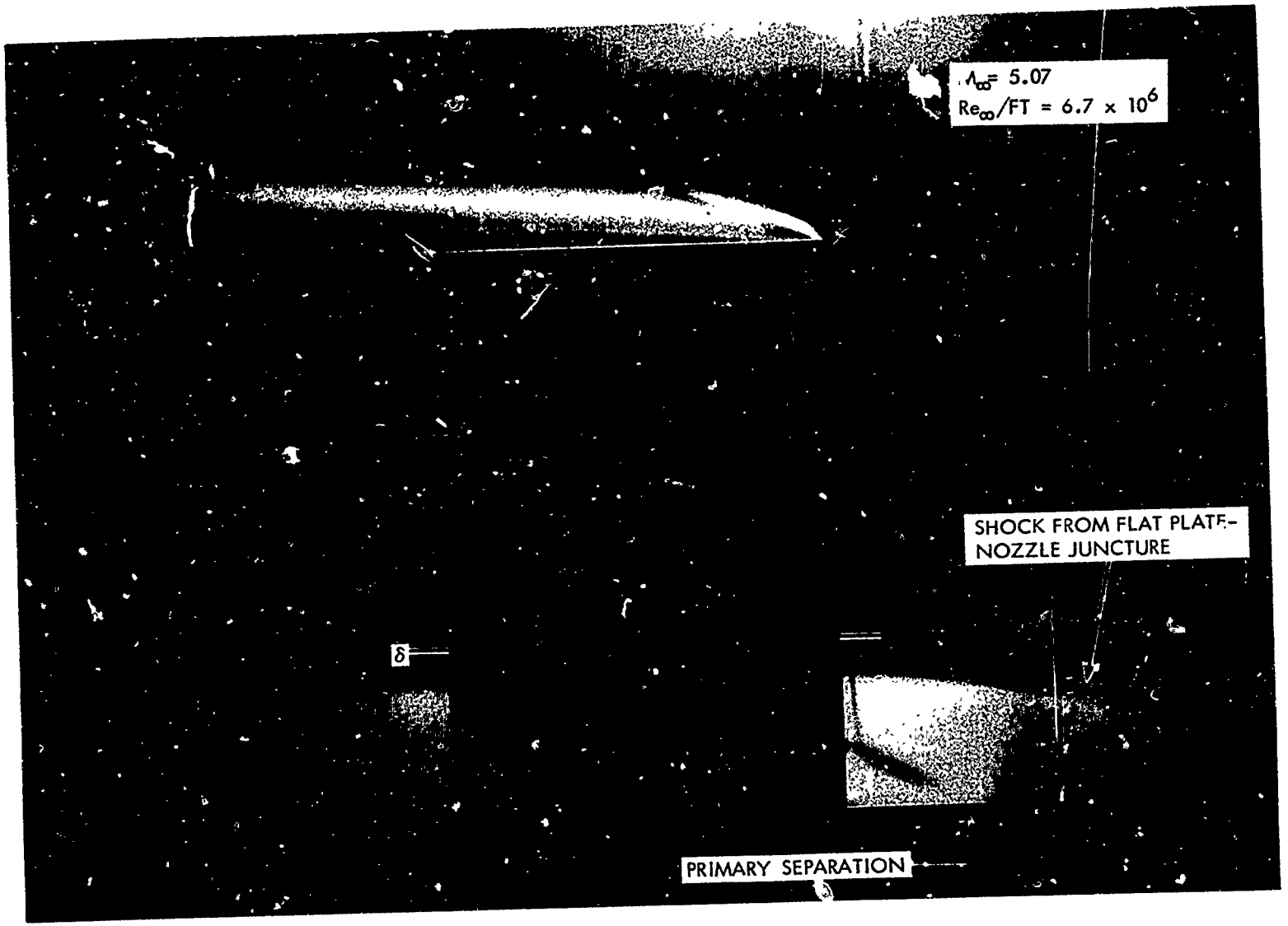

FIG. 10 SCHLIEREN PHOTOGRAPH OF UNSWEPT FIN IN SUPERSONIC TUNNEL NO. 2

FIG. 11 SCHLIEREN PHOTOGRAPH OF 60° SWEPT FIN IN SUPERSONIC TUNNEL NO. 2

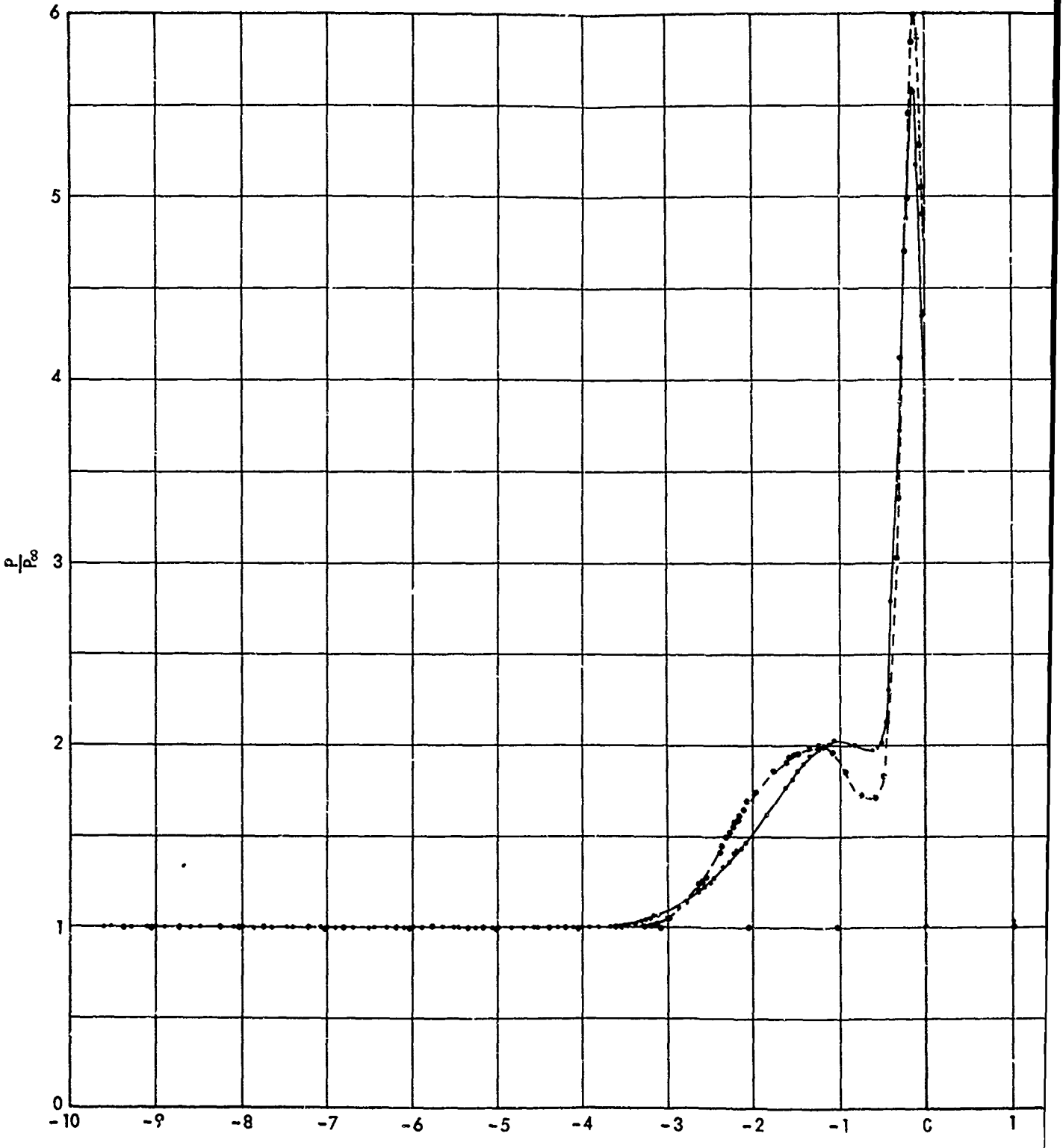
6
5
4
3
2
1
0
p/p∞
-10
-9
-8
-7
-6
-5
-4
-3
-2
-1
0
1

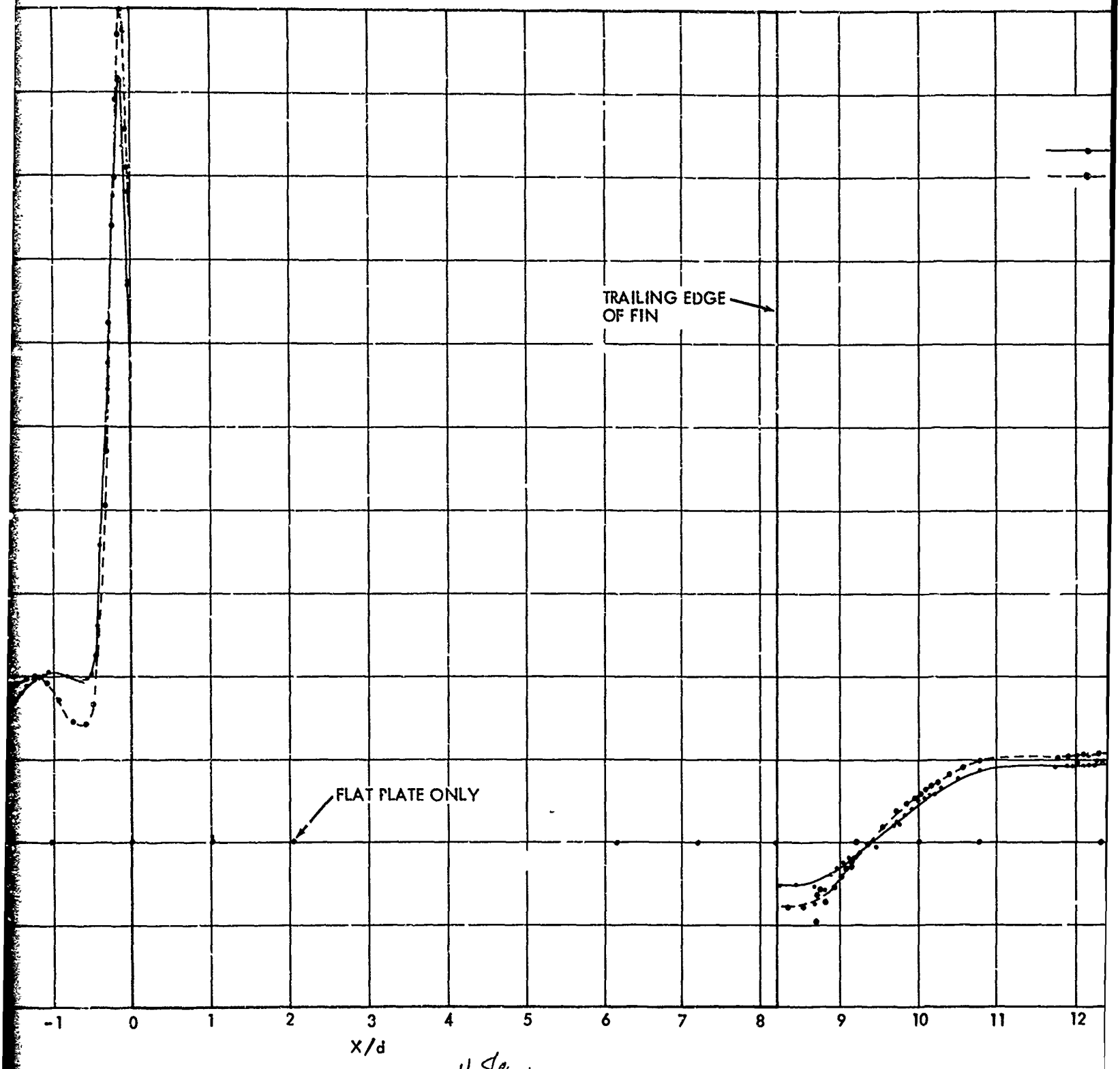

FIG. 12A FLAT PLATE PRESSURE DISTRIBUTION

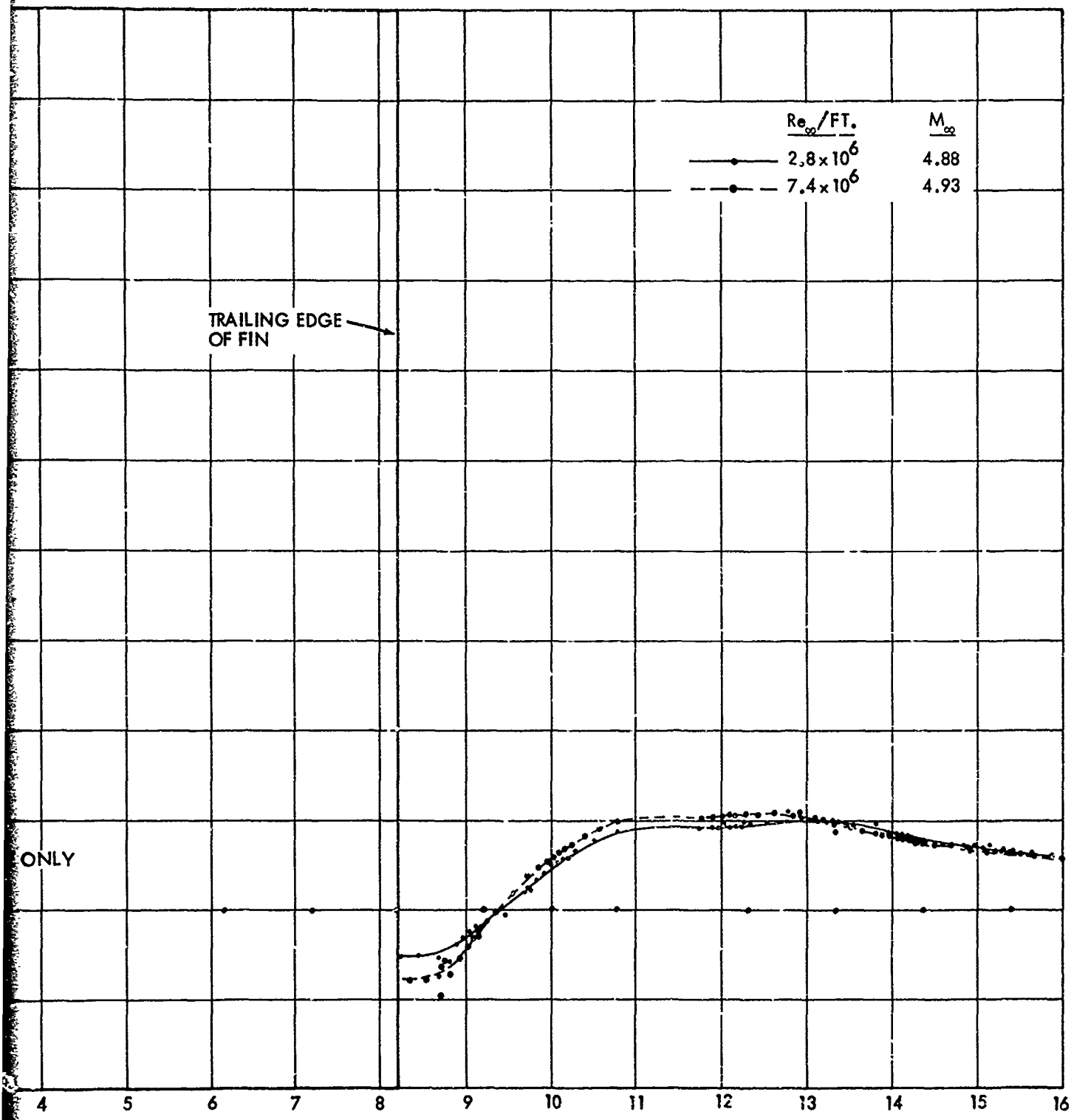

48a

FIG. 12A FLAT PLATE PRESSURE DISTRIBUTION PRODUCED BY AN UNSWEPT FIN

48a

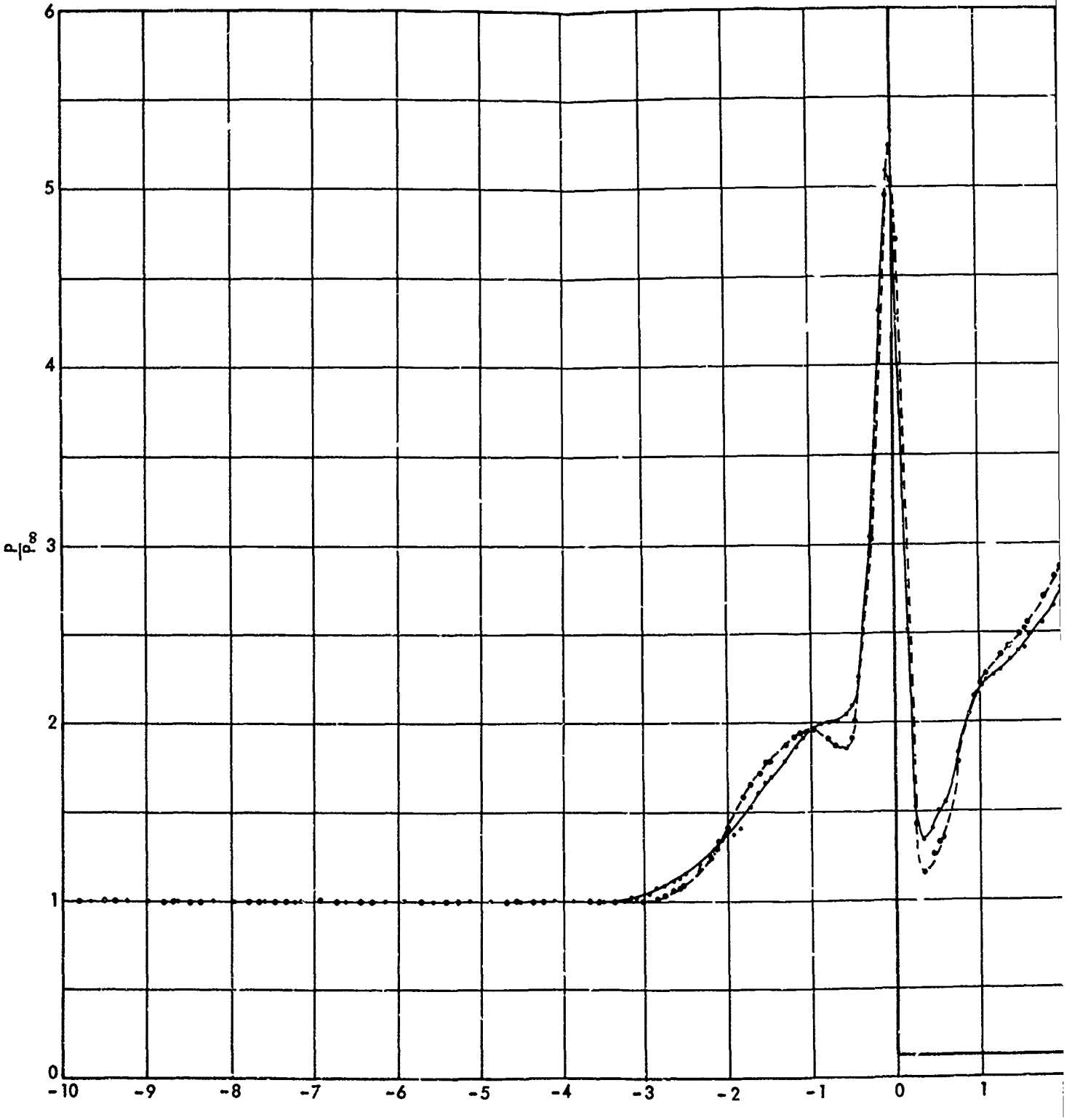
6
5
4
3
2
1
0
$\frac{P}{P_\infty}$
-10
-9
-8
-7
-6
-5
-4
-3
-2
-1
0
1

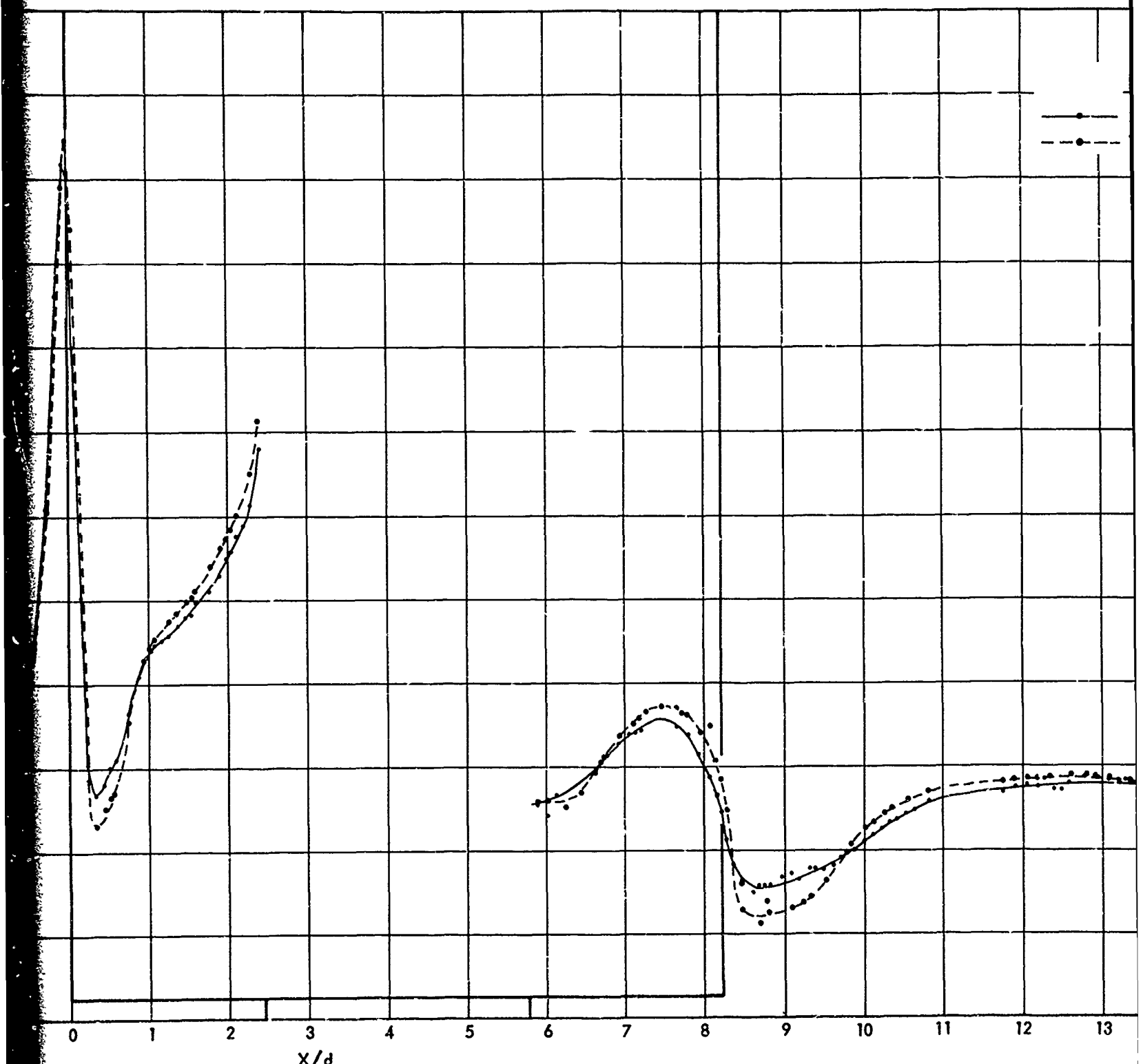

FIG. 12B UNSWEPT FIN WITH 0.125 INCH CLEAR

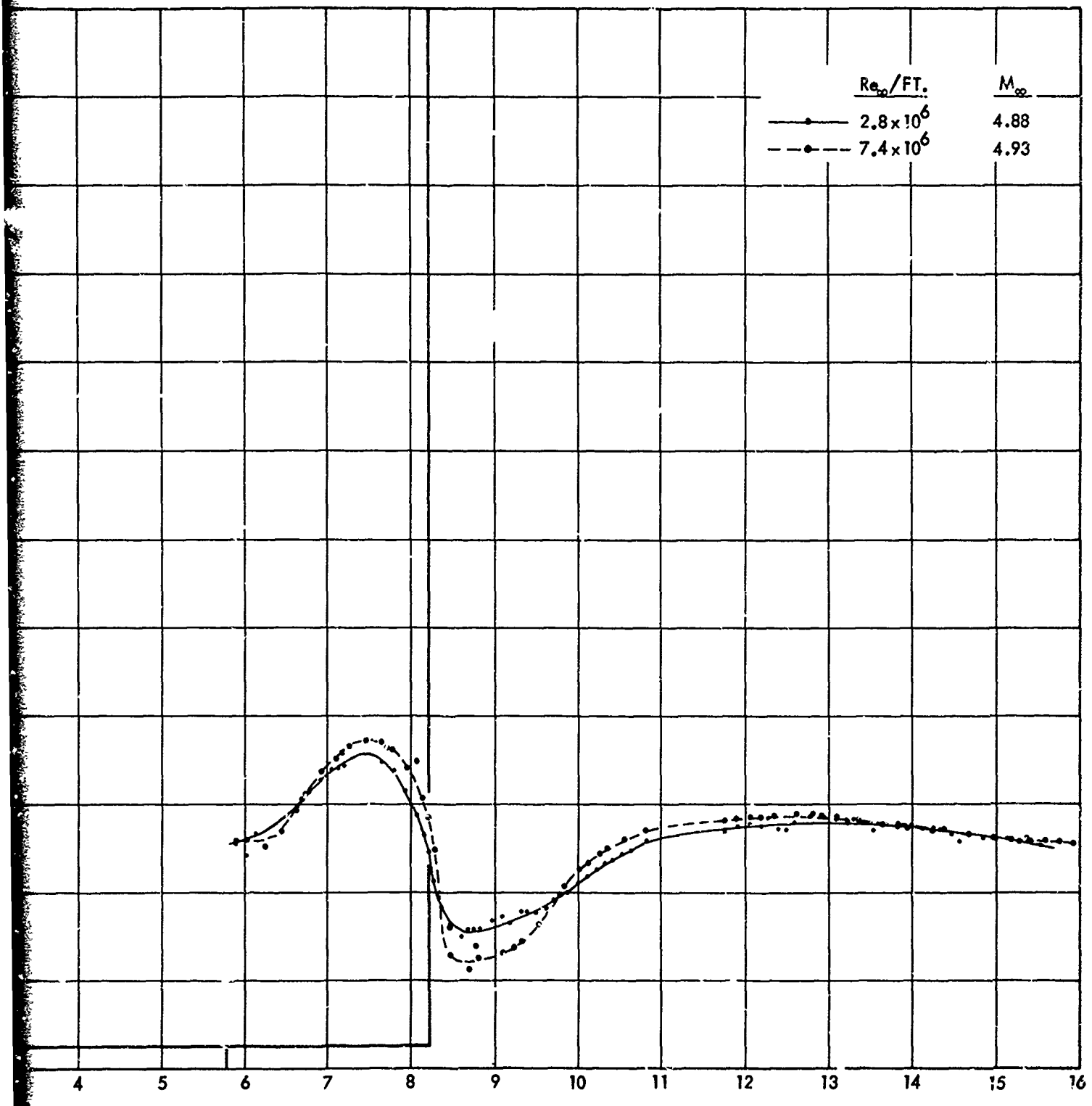

49R

FIG. 12B UNSWEPT FIN WITH 0.125 INCH CLEARANCE GAP

49C

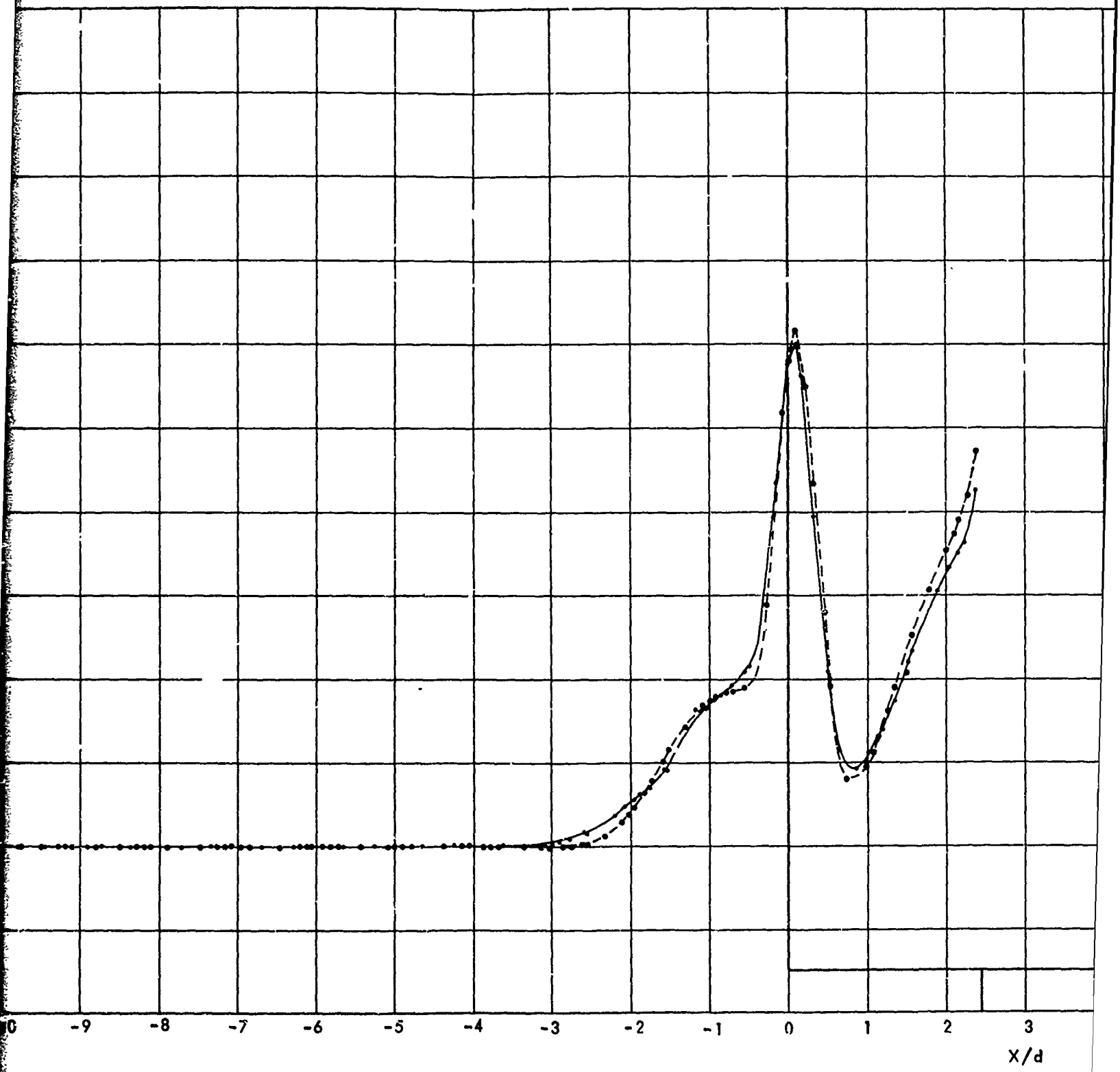

50

50a

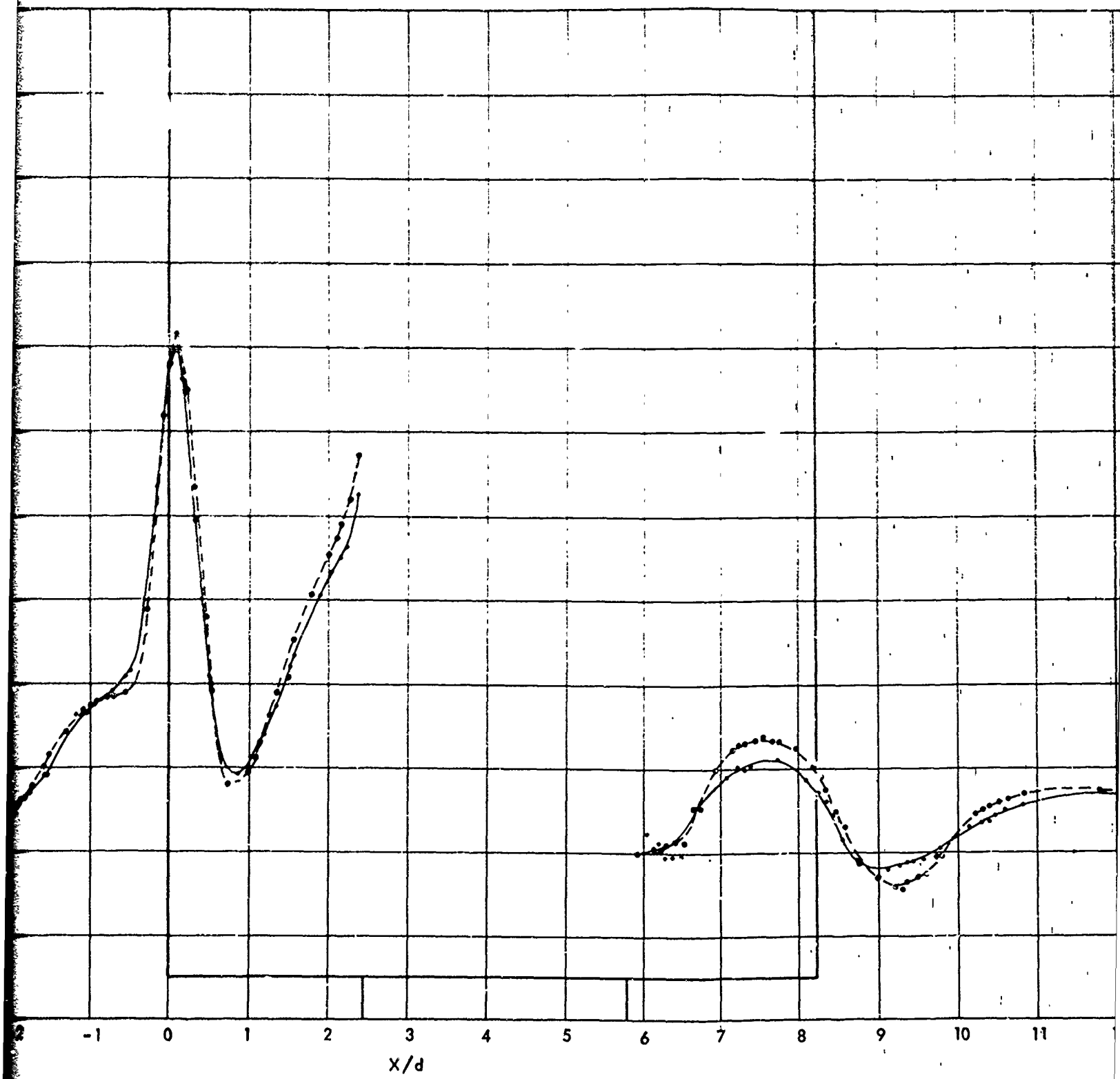

FIG. 12C UNSWEPT FIN WITH 0.25

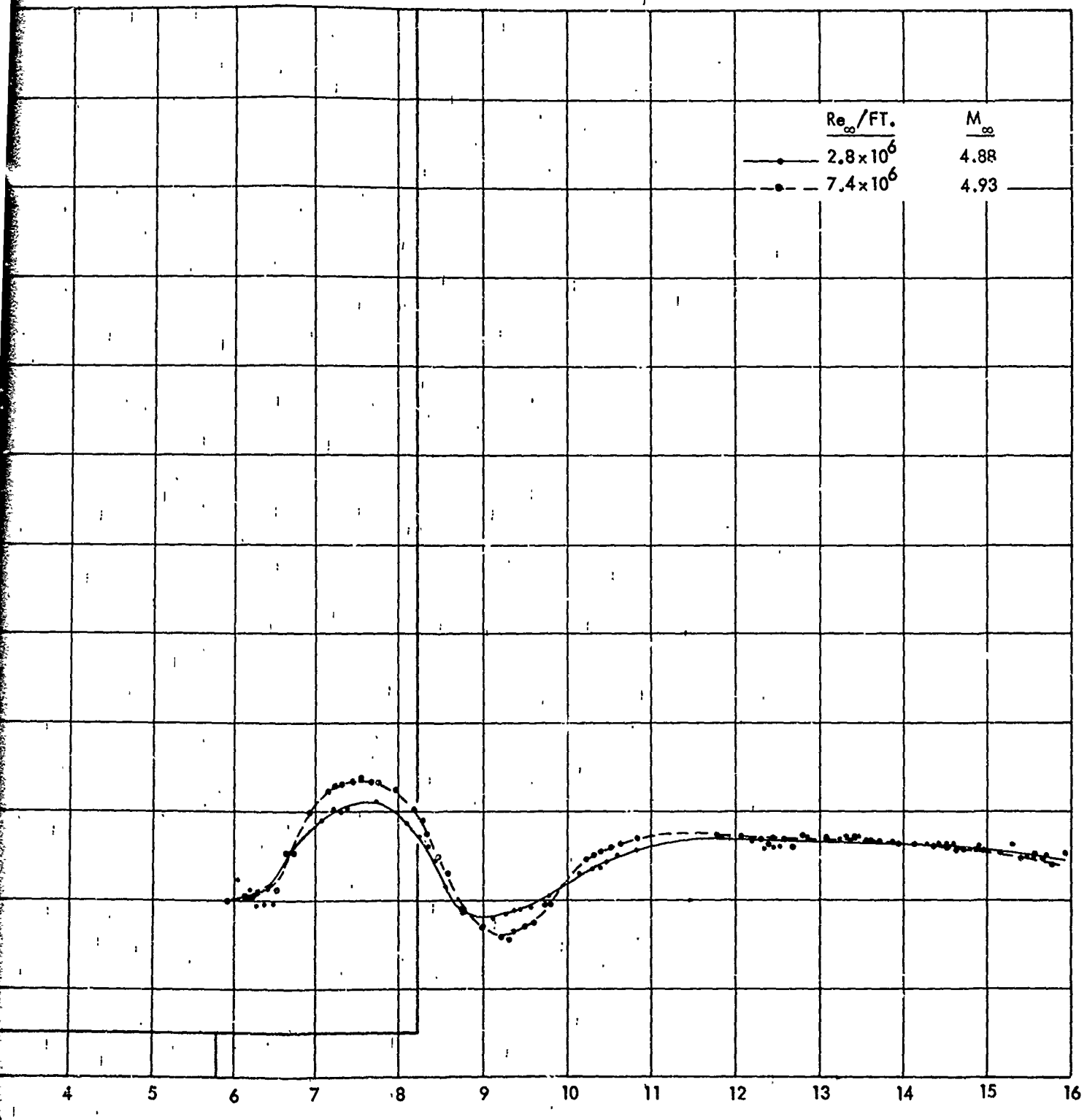

FIG. 12C UNSWEPT FIN WITH 0.25 INCH CLEARANCE GAP

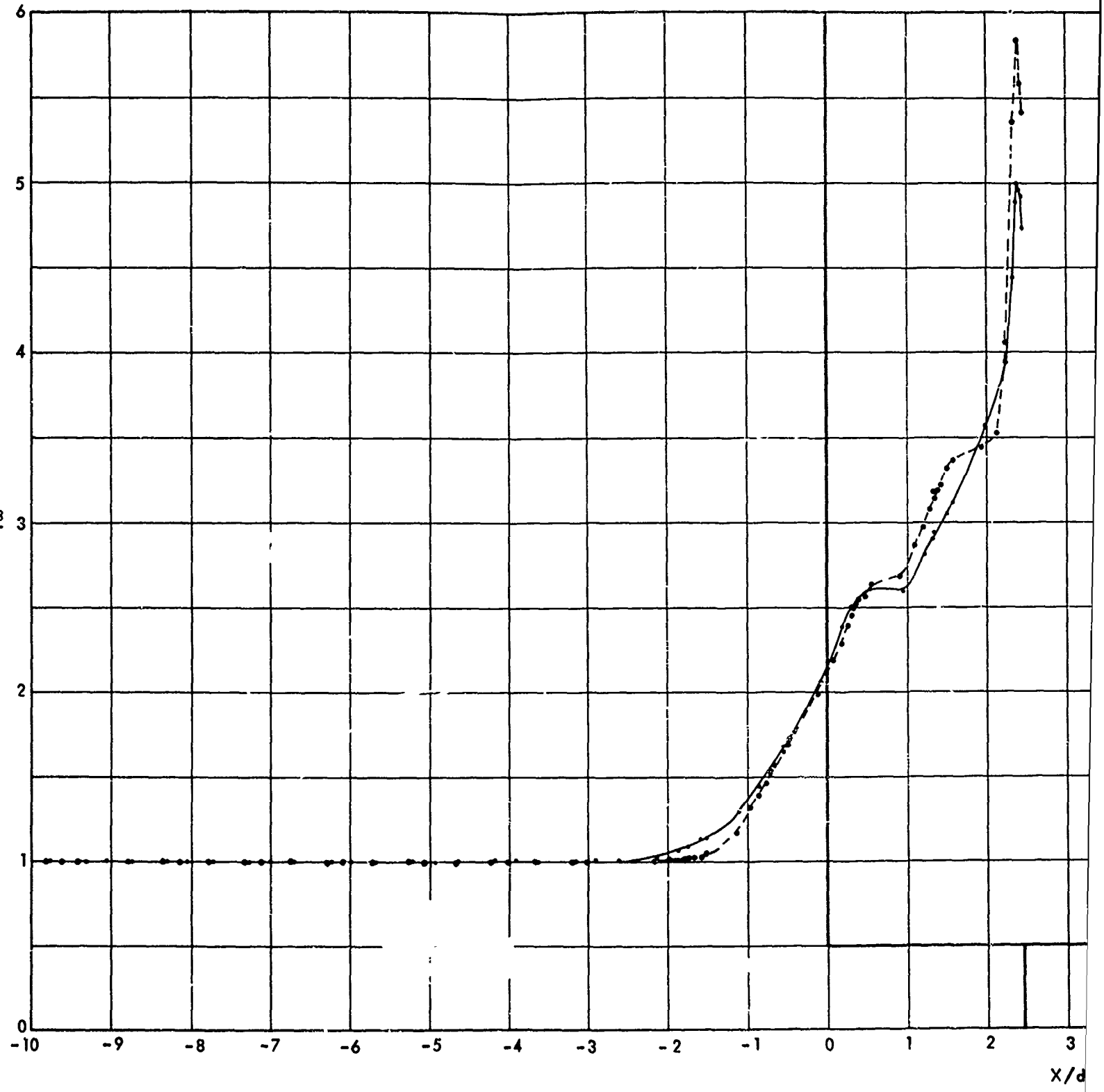

F.C

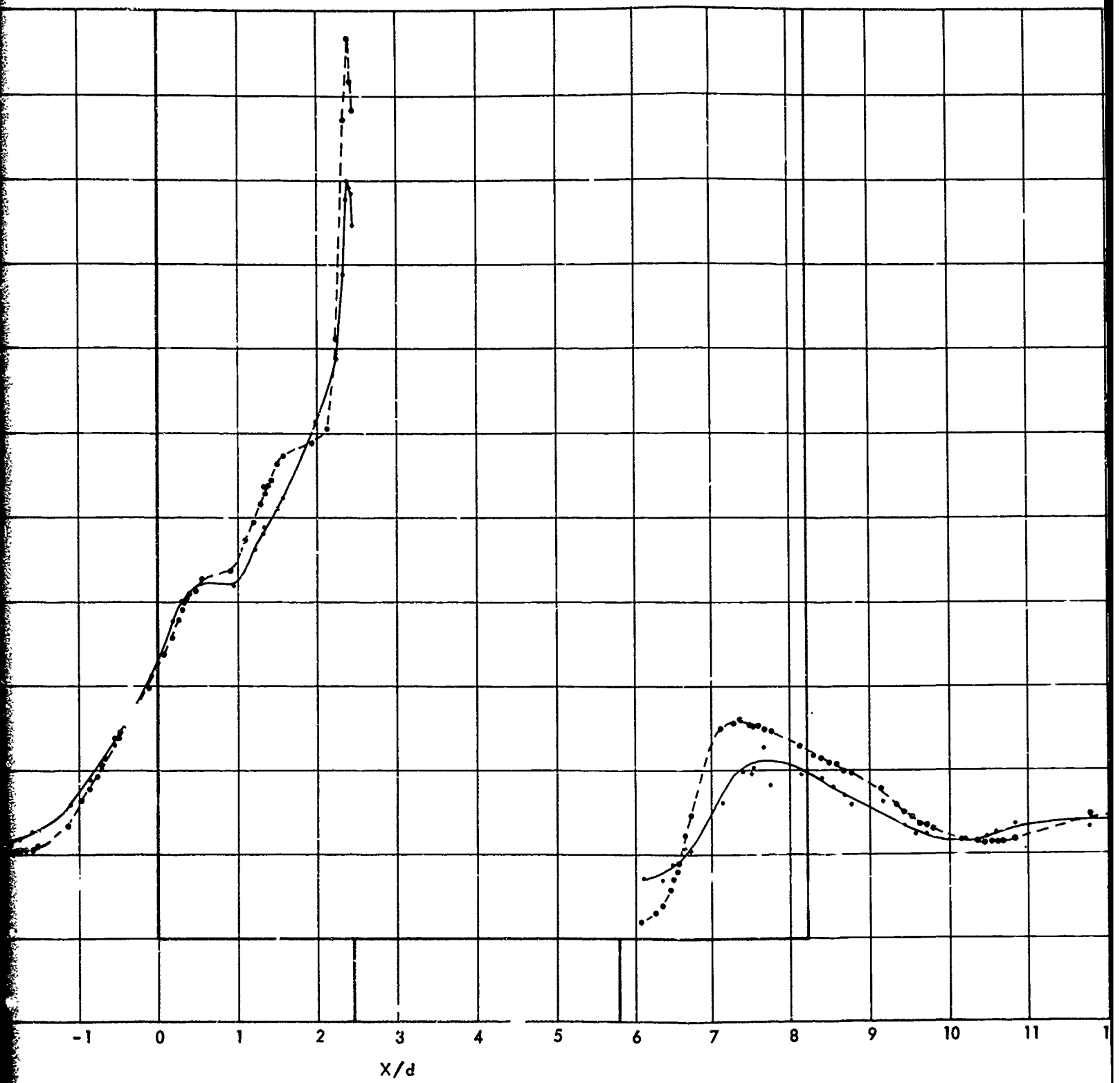

FIG. 12D UNSWEPT FIN WITH

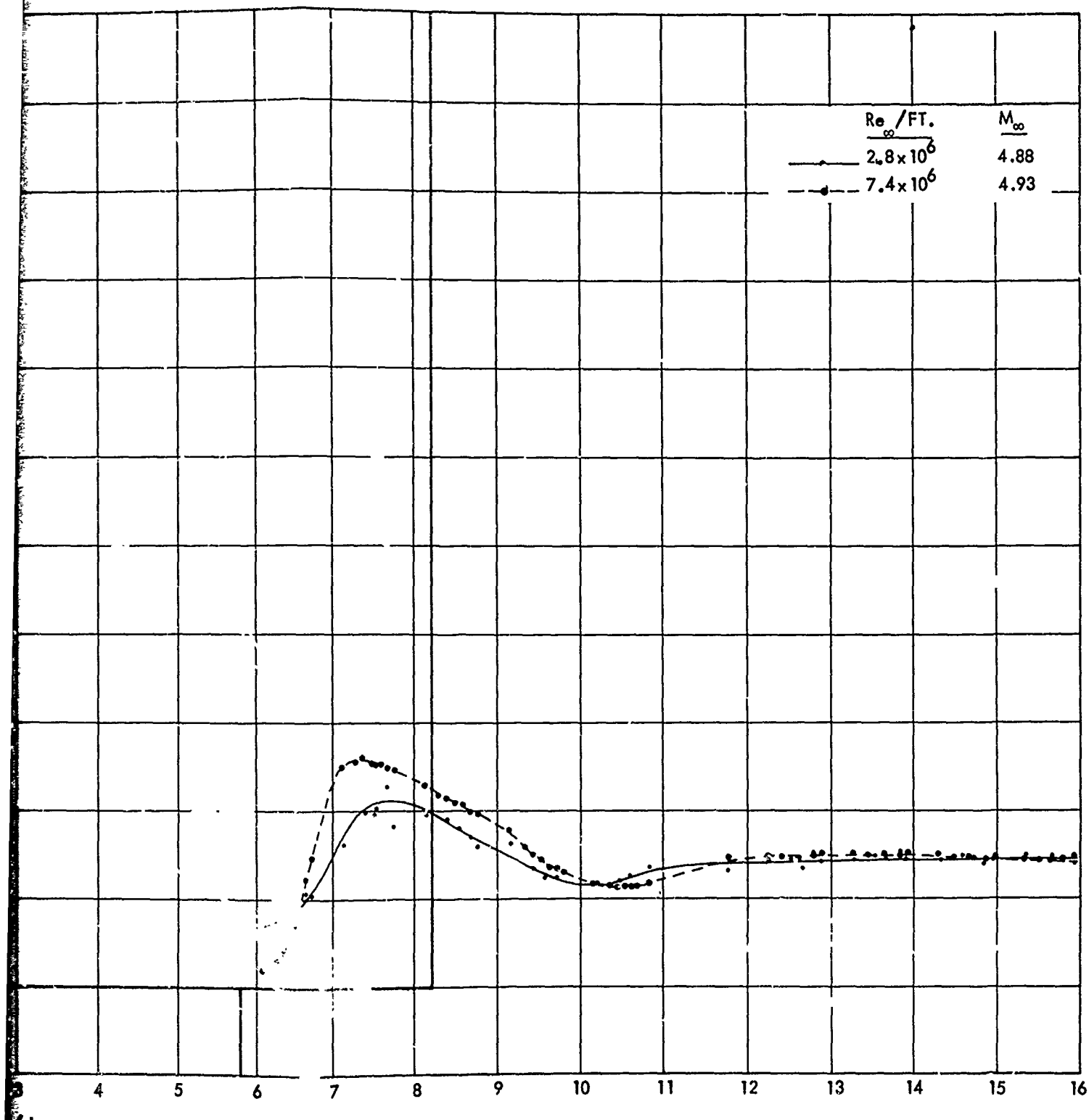

FIG. 12D UNSWEPT FIN WITH 0.50 INCH CLEARANCE GAP

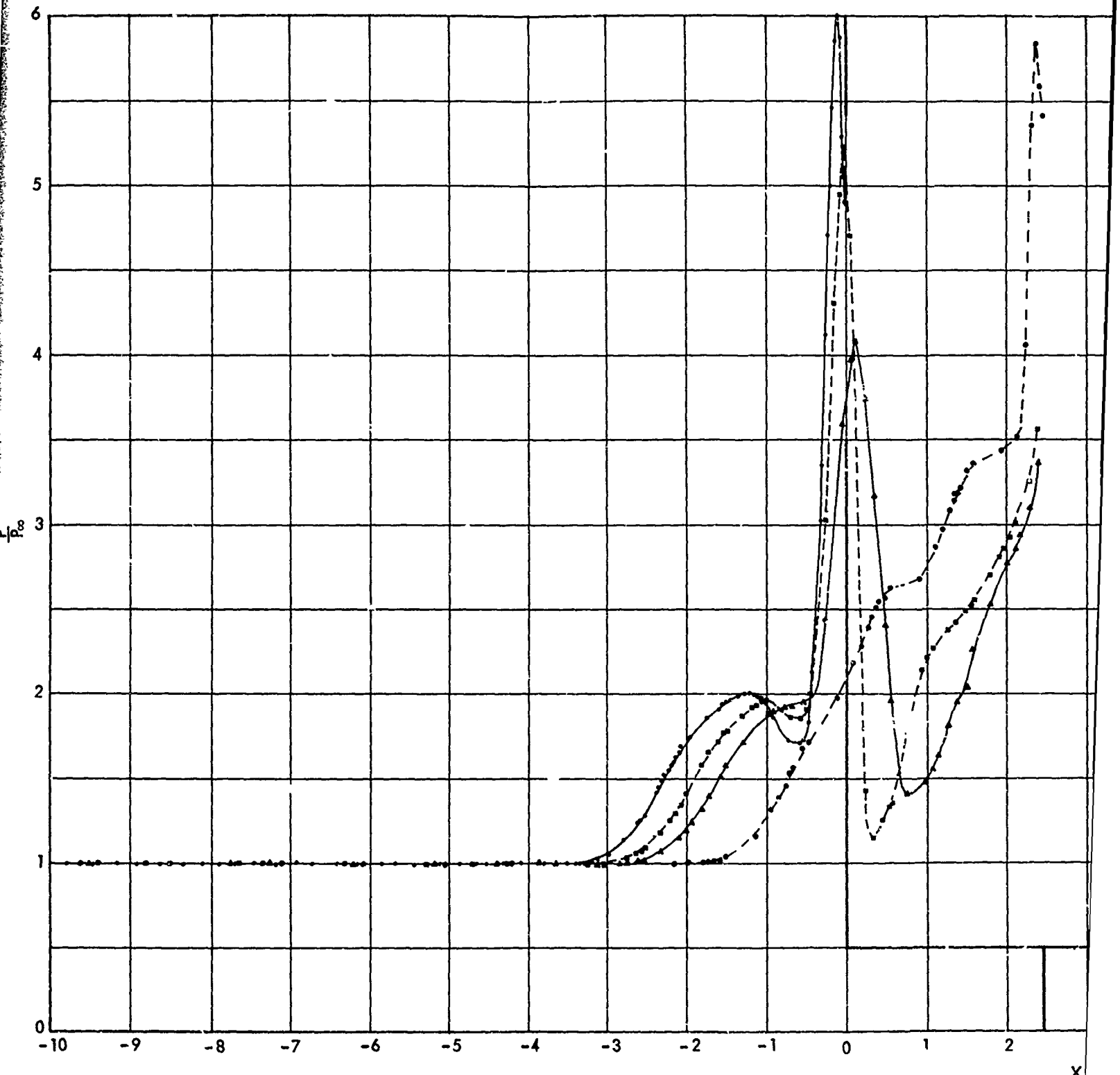
6
5
4
3
2
1
0
ρ/ρ∞
-10
-9
-8
-7
-6
-5
-4
-3
-2
-1
0
1
2
X
P

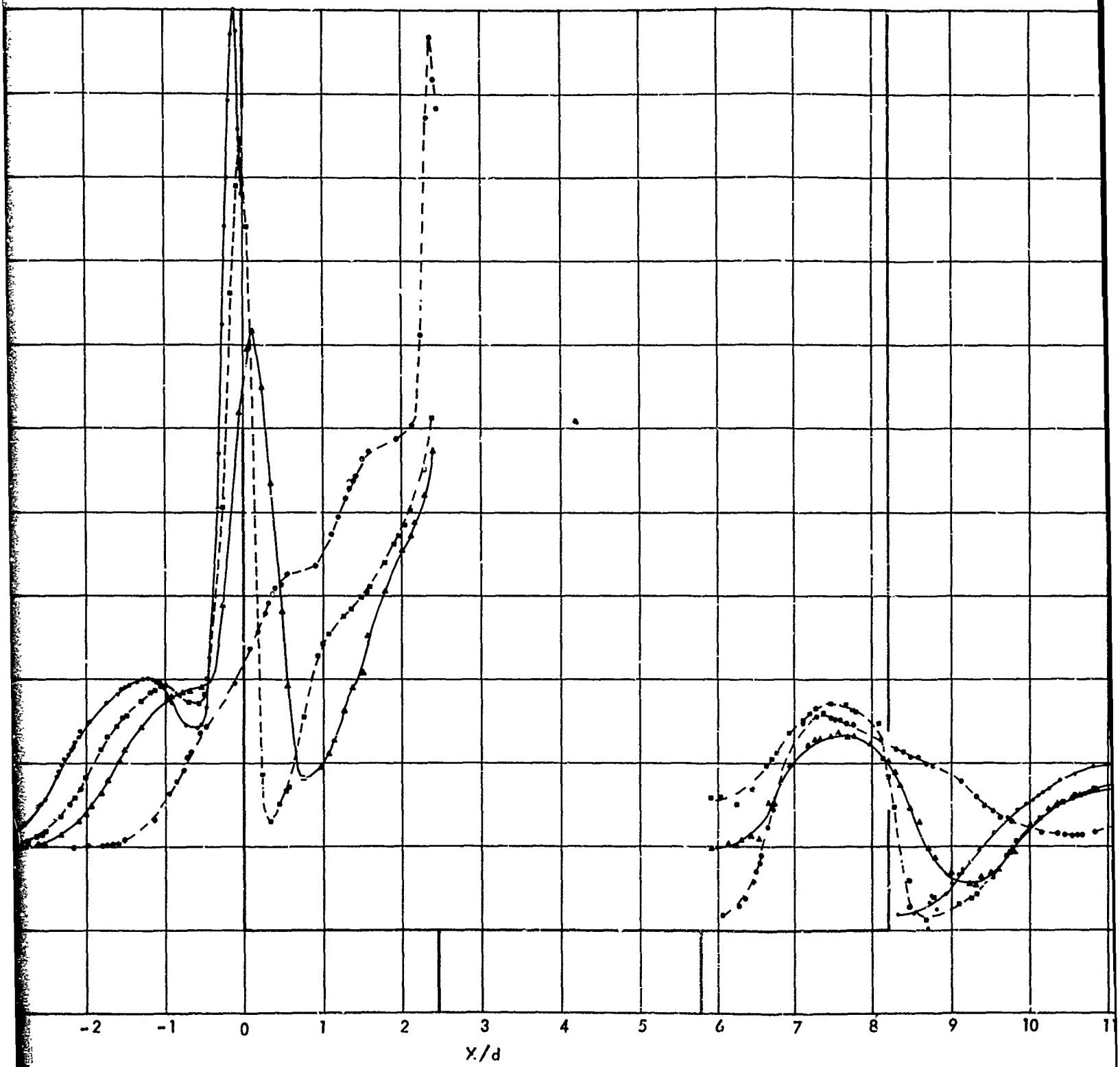

FIG. 13 FLAT PLATE PRESSURE DISTRIBUTIO I FOR VARY

52a

52a

5

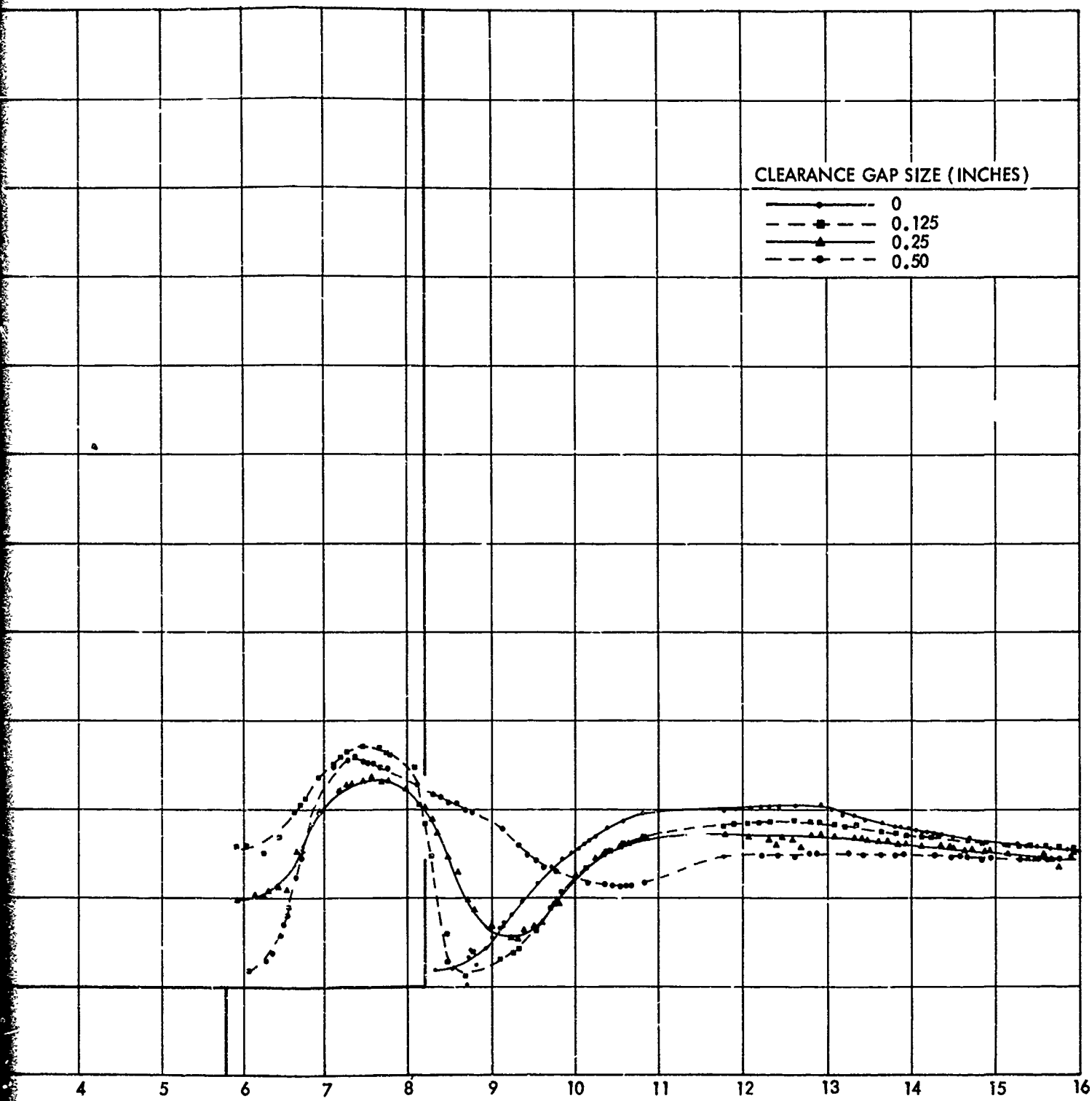

FIG. 13 FLAT PLATE PRESSURE DISTRIBUTION FOR VARYING CLEARANCE GAPS OF AN UNSWEPT FIN

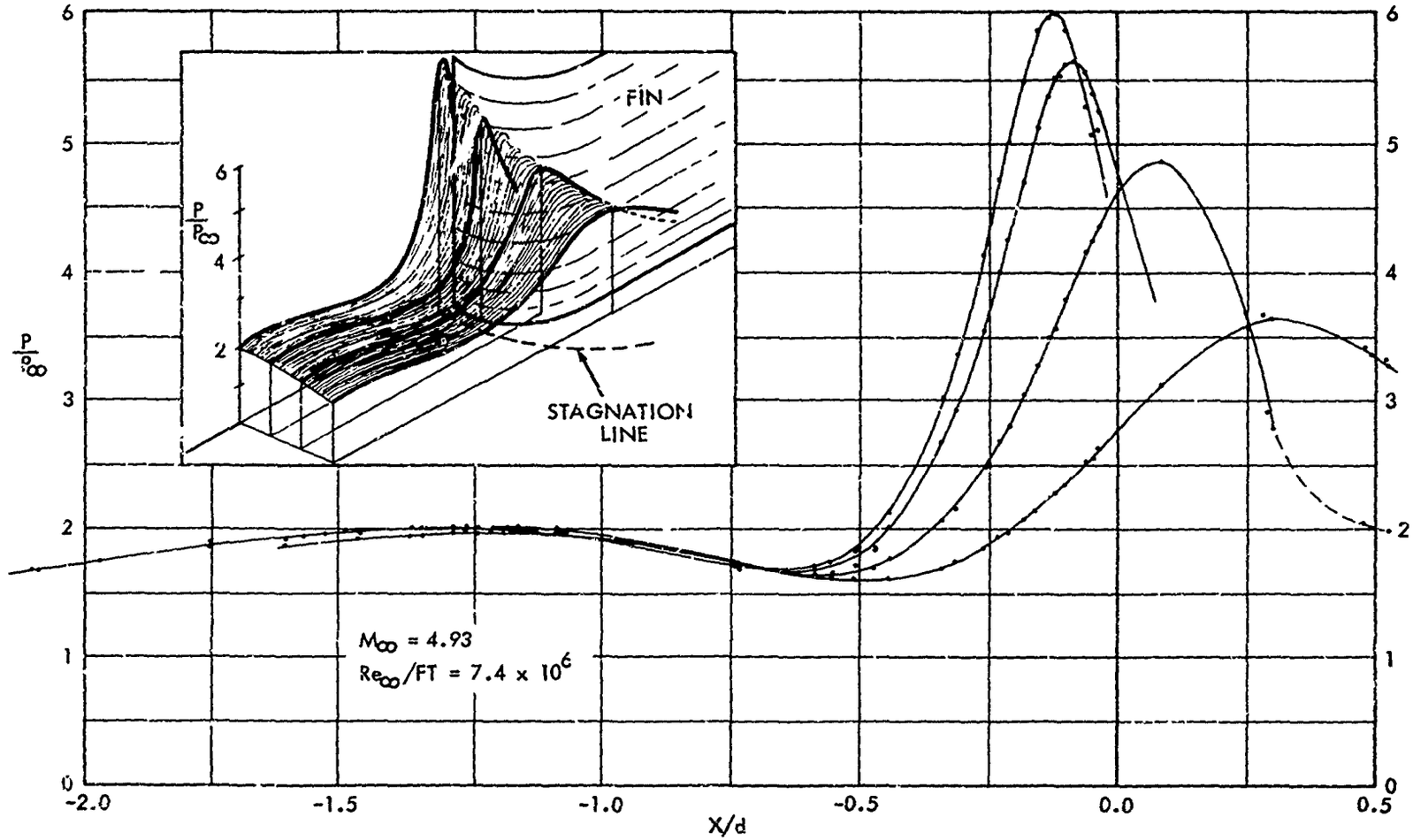

FIG. 14 PR. RE DISTRIBUTION ON FLAT PLATE AROUND LEADING EDGE OF FIN

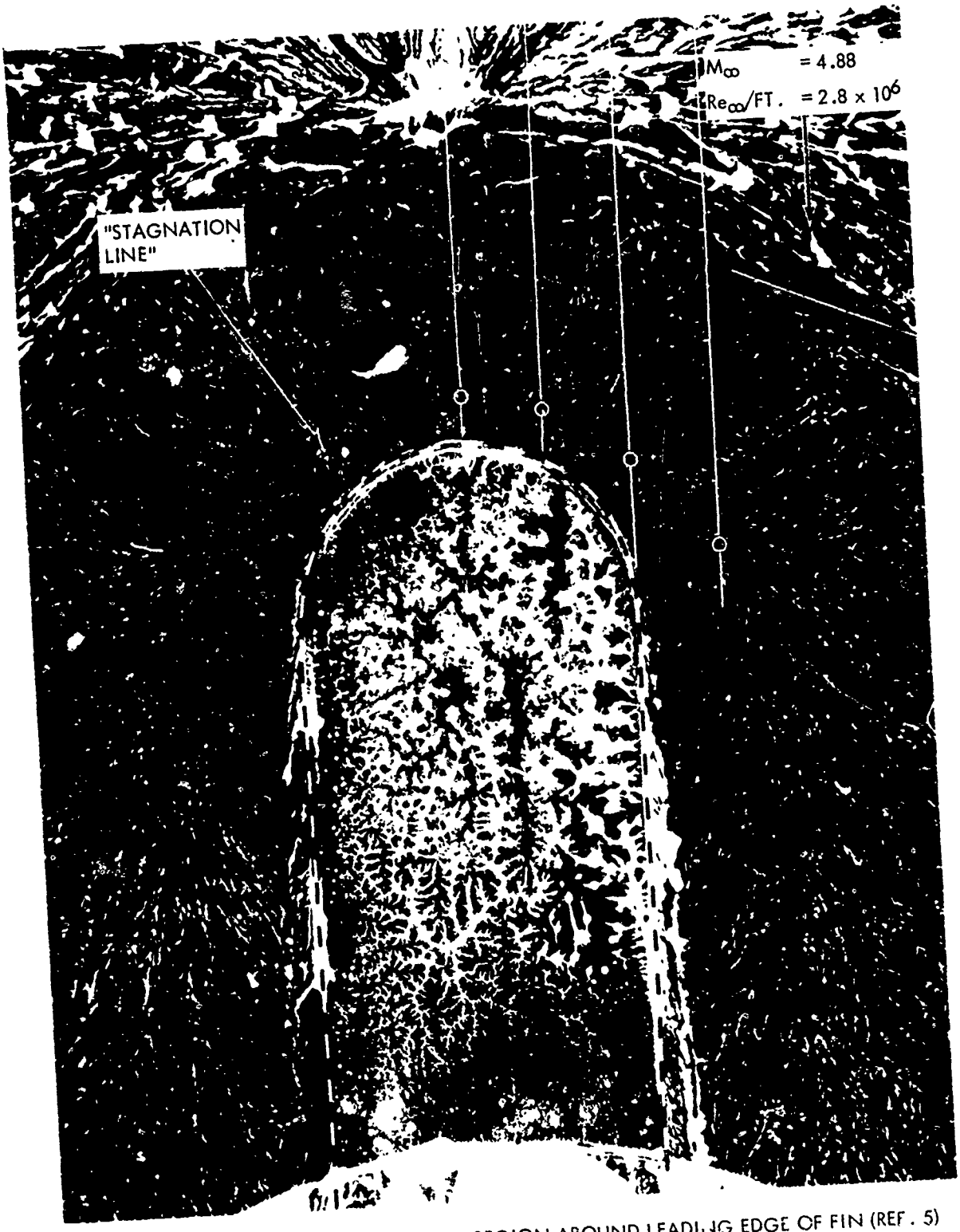

FIG. 15 OIL SMEAR PHOTOGRAPH OF REGION AROUND LEADING EDGE OF FIN (REF. 5)

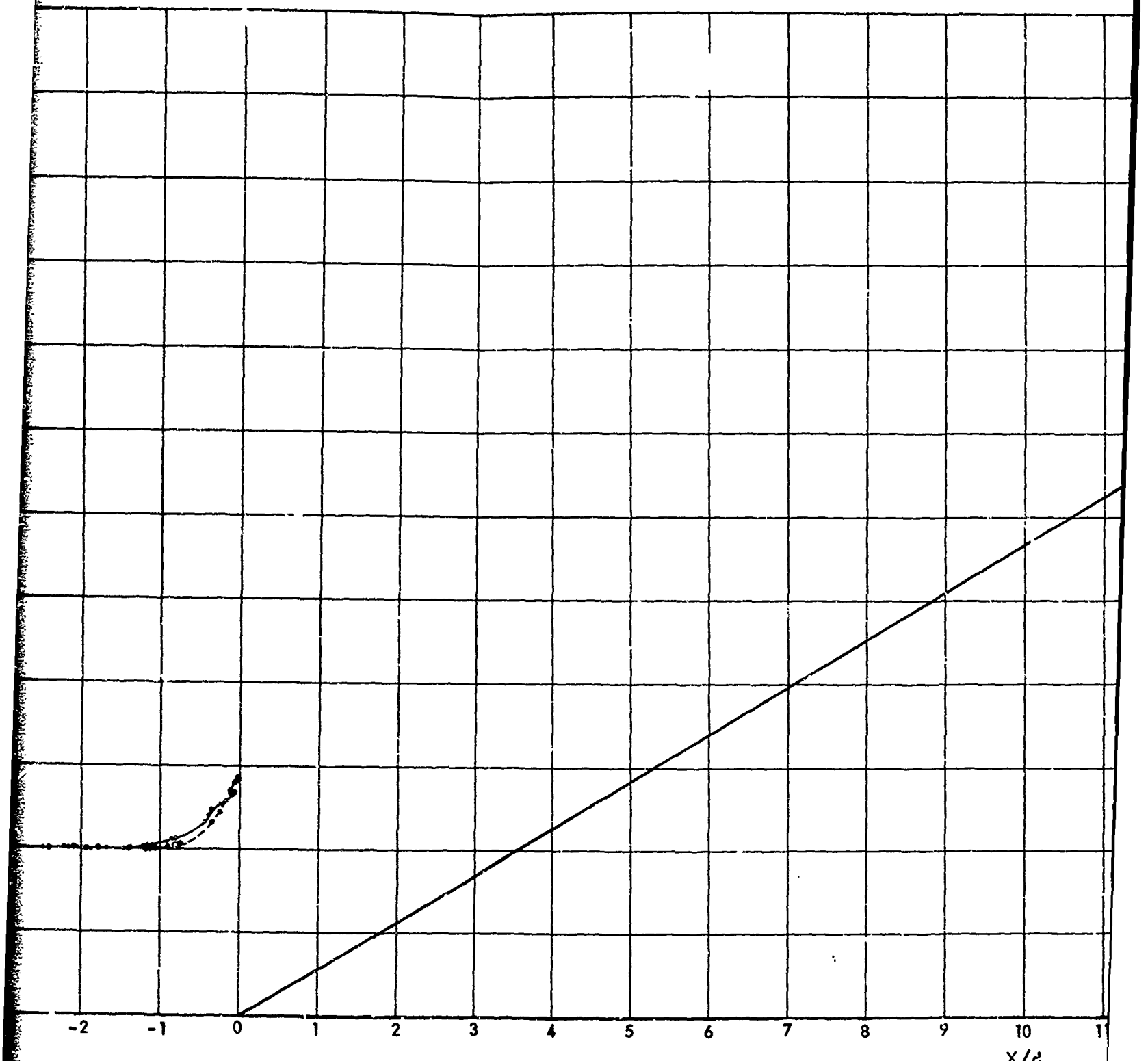

55 54

55a

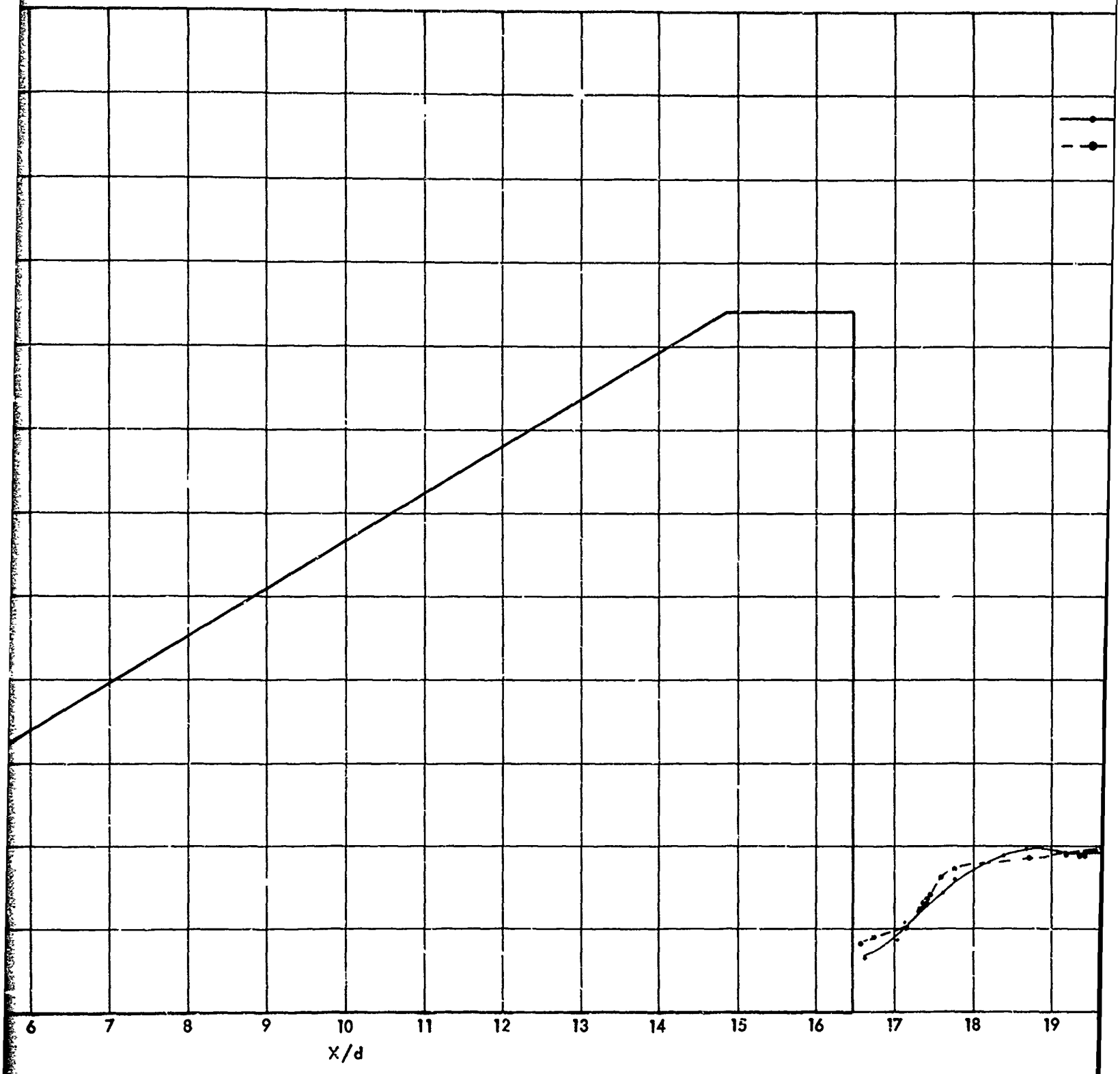

FIG. 16A FLAT PLATE PRESSURE DISTRIBUTION PRO

55a

55b

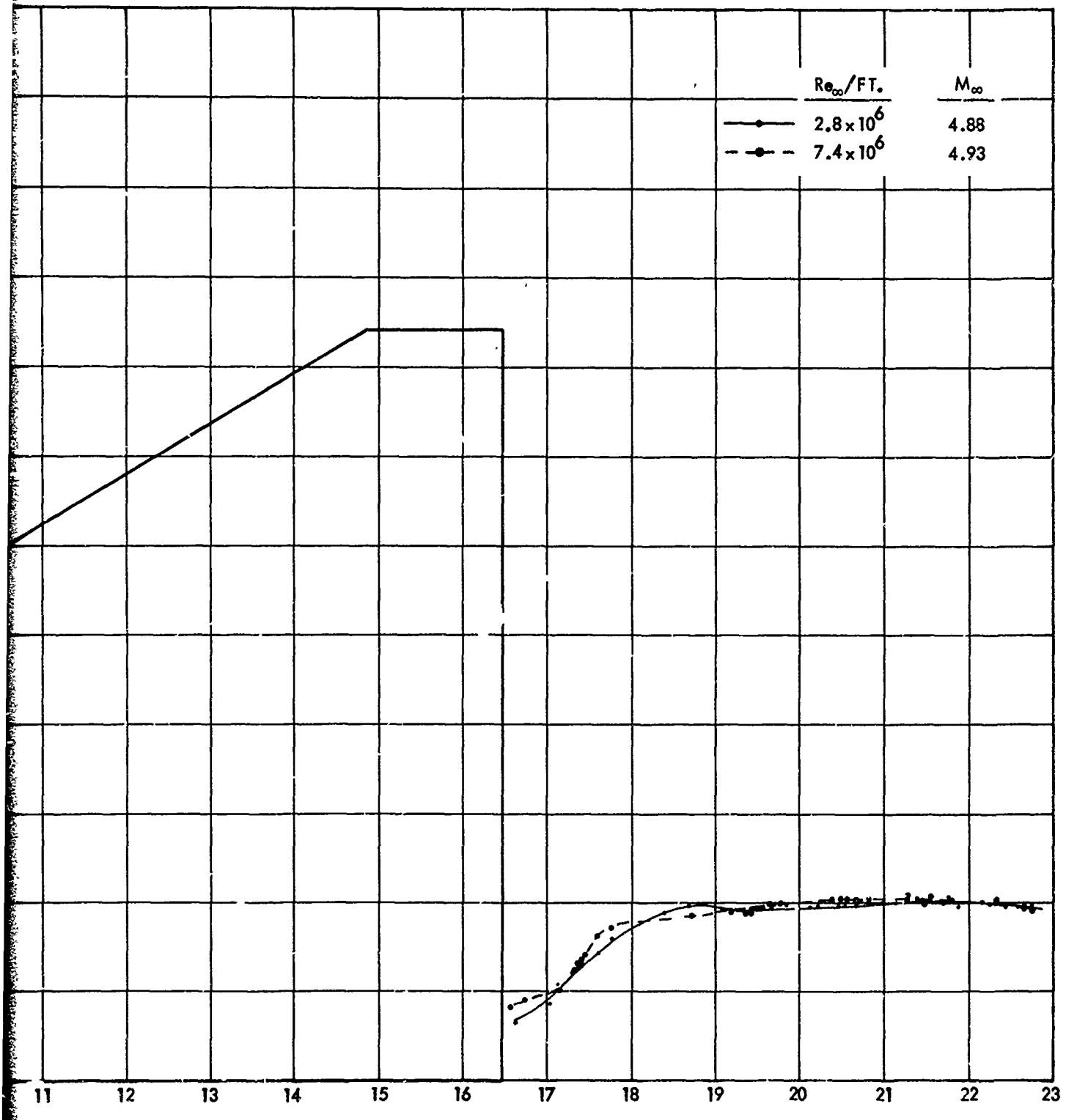

FIG. 16A FLAT PLATE PRESSURE DISTRIBUTION PRODUCED BY A 60° SWEPT FIN

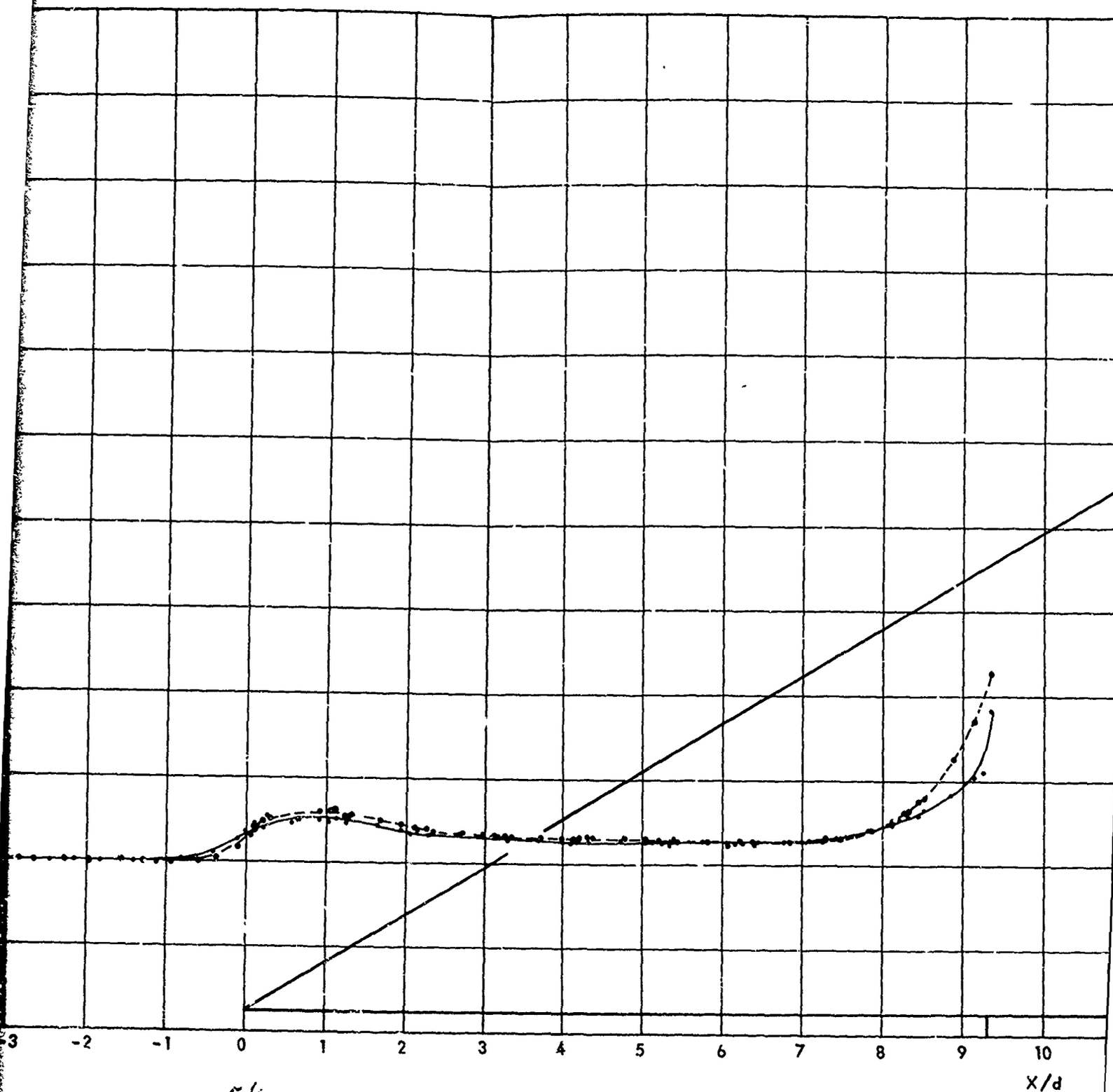

54

56a

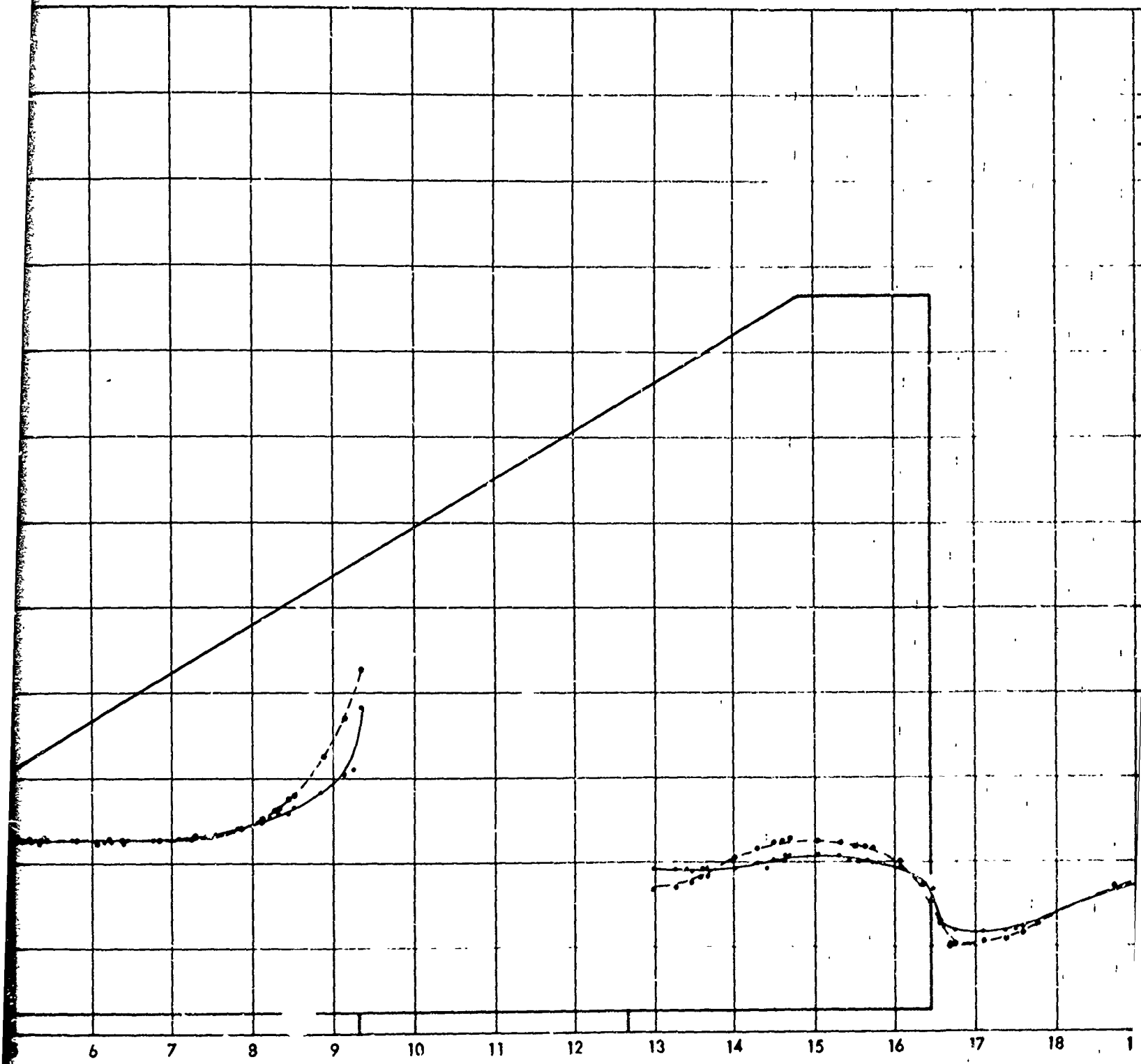

5ka

FIG. 16 B 60° SWEPT FIN WIT

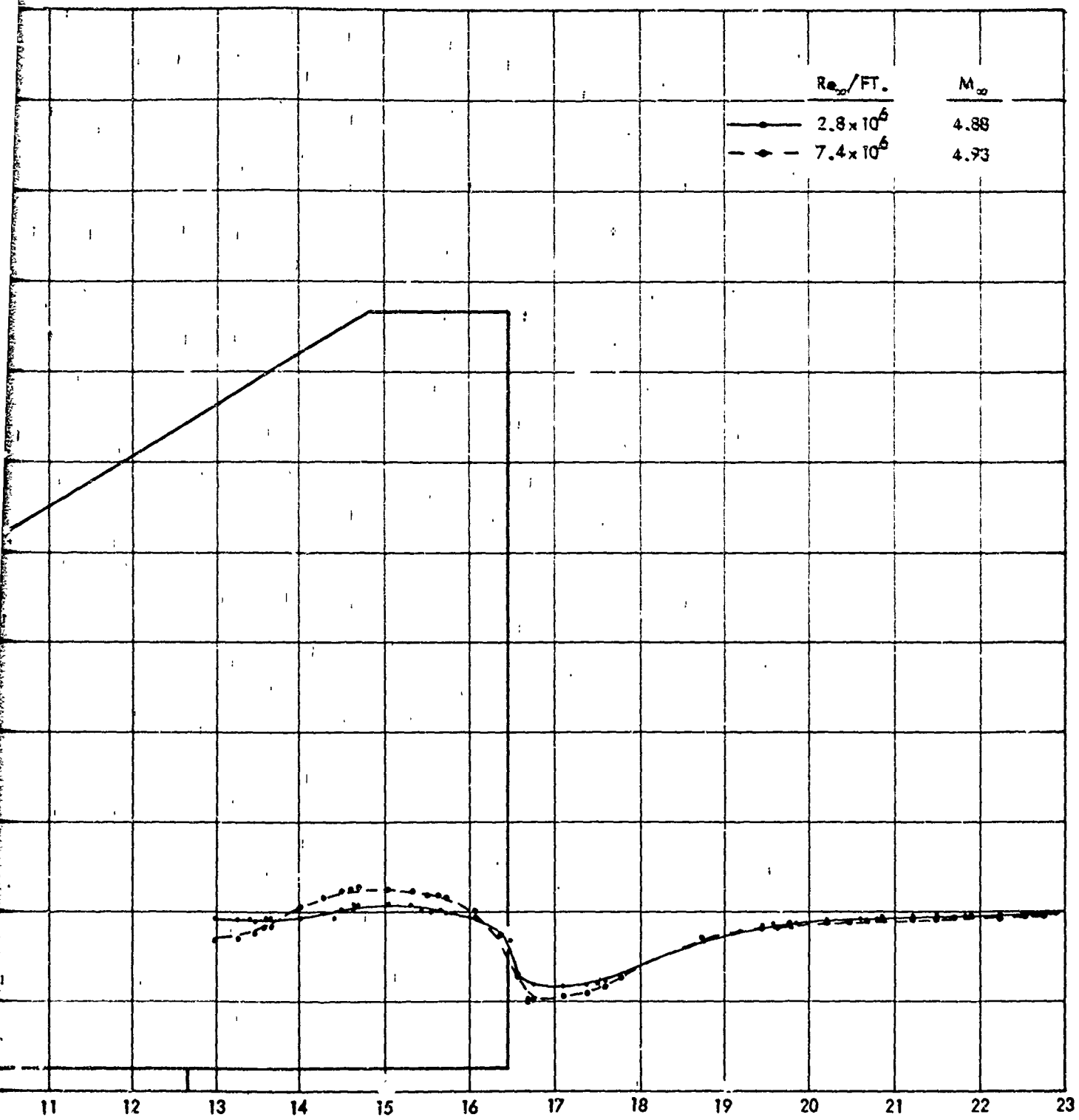

FIG. 16 B 60° SWEPT FIN WITH 0.125 INCH CLEARANCE GAP

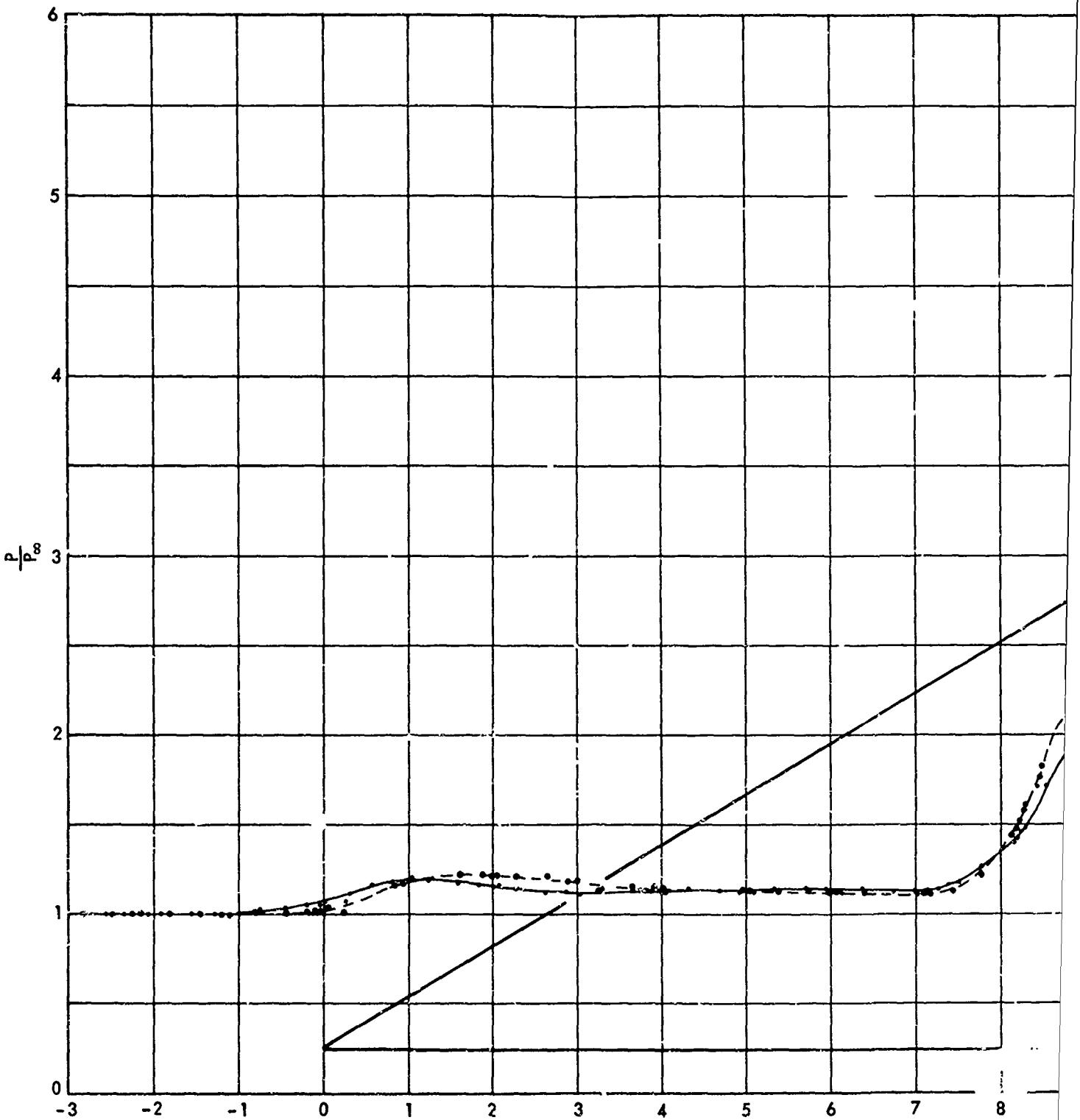
6
5
4
3
2
1
0
$\frac{p}{p^8}$
-3
-2
-1
0
1
2
3
4
5
6
7
8

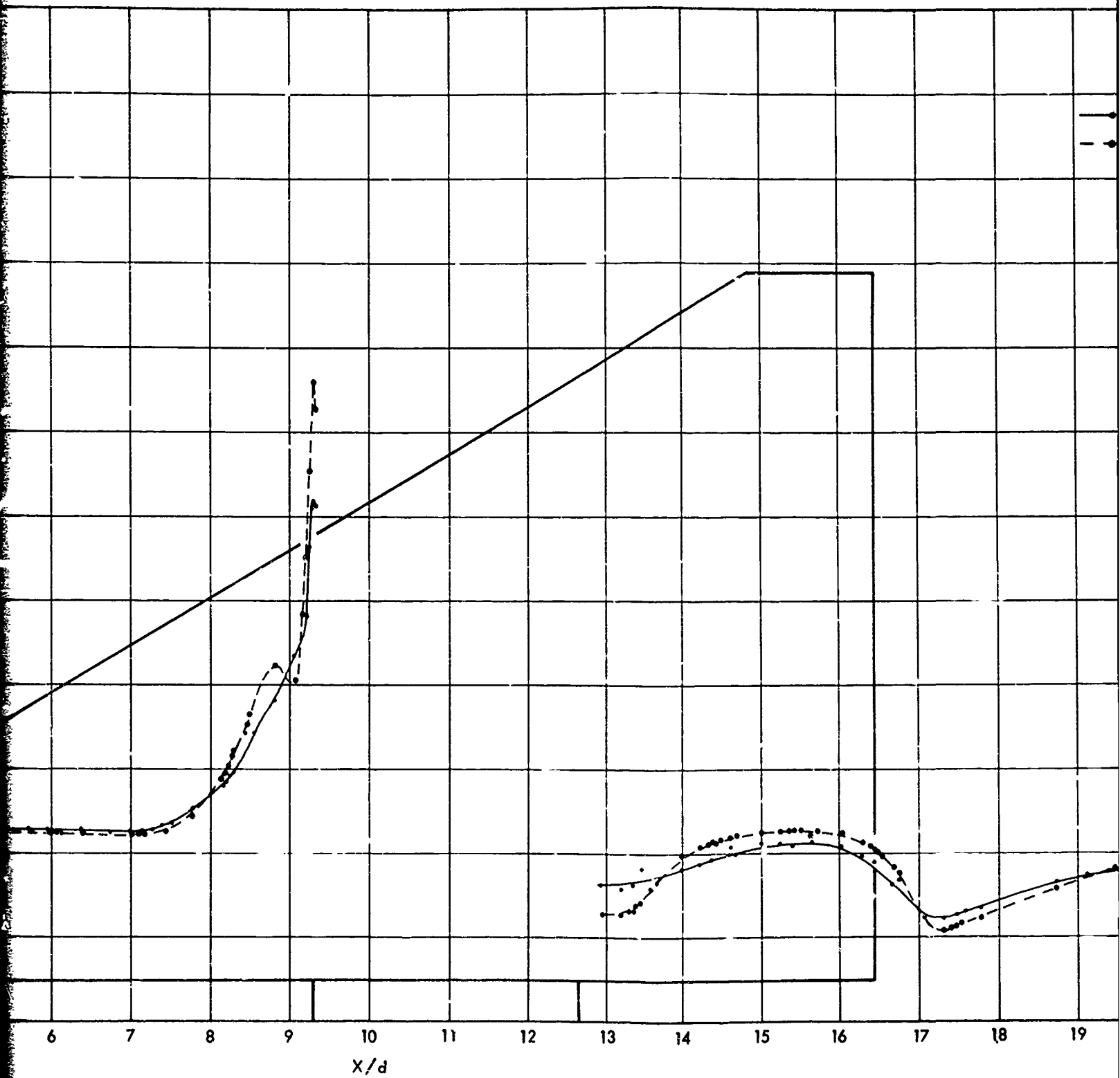

FIG. 16C 60° SWEPT FIN WITH 0.25

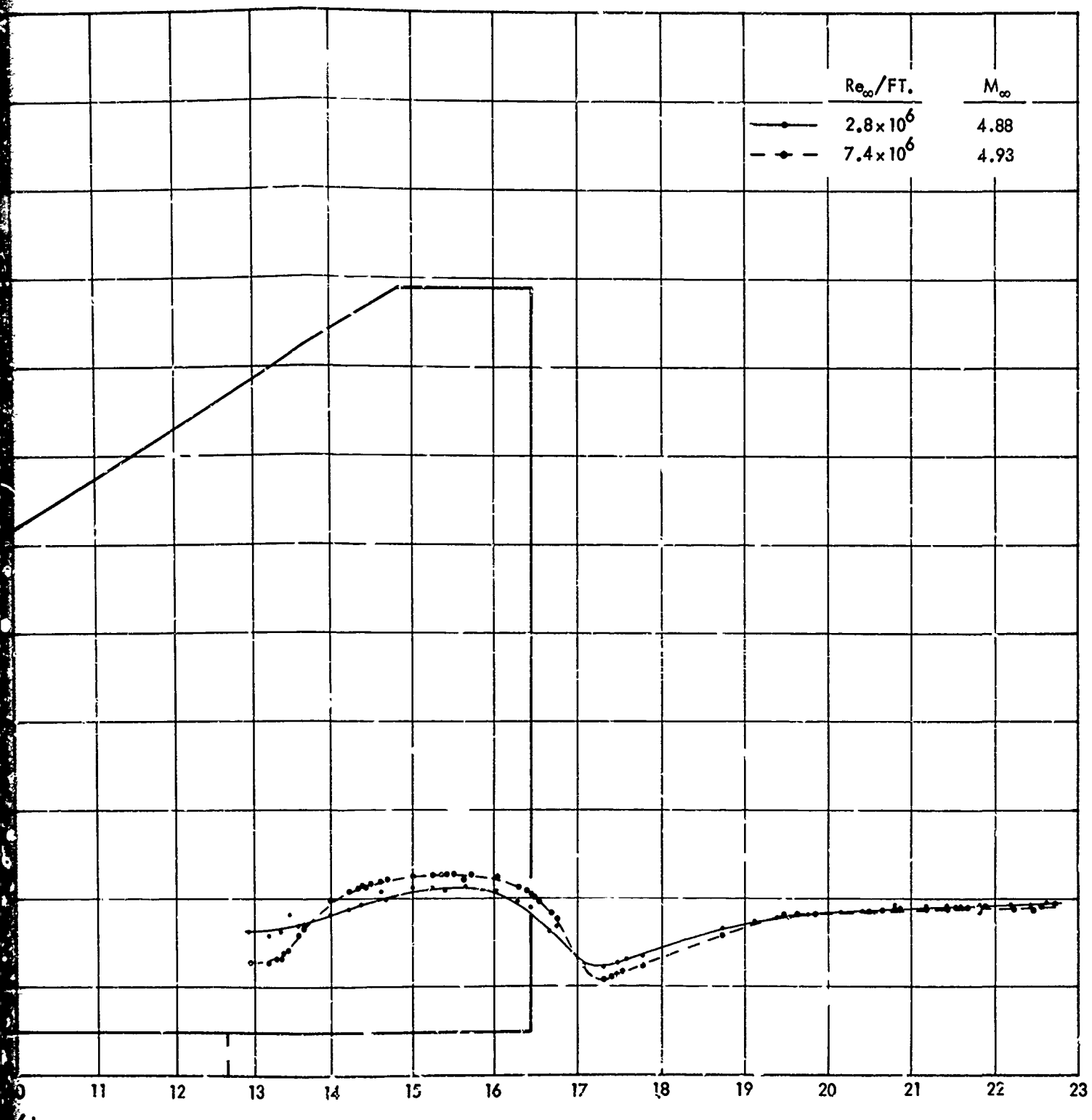

FIG. 16C 60° SWEPT FIN WITH 0.25 INCH CLEARANCE GAP

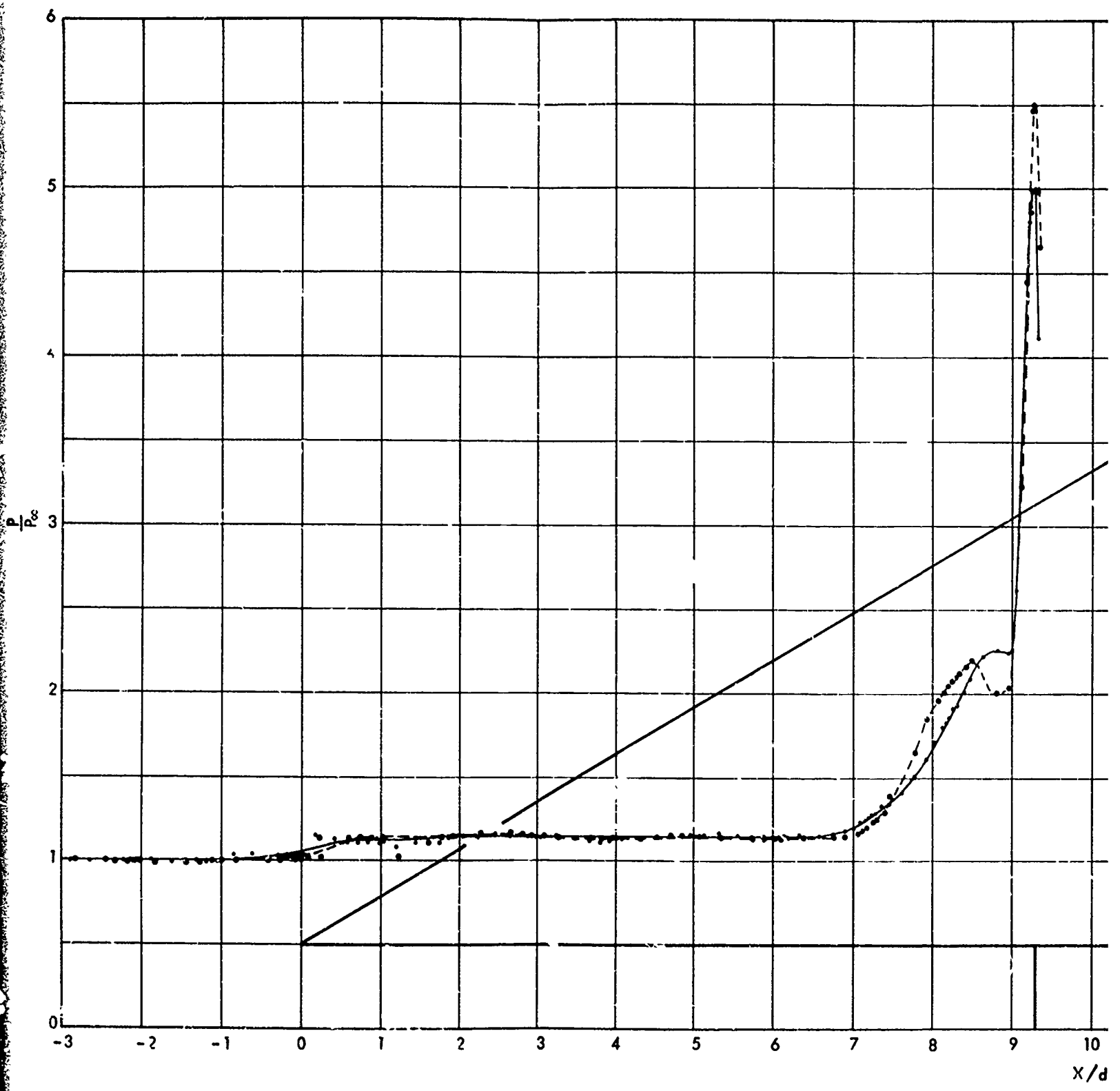

58

58a

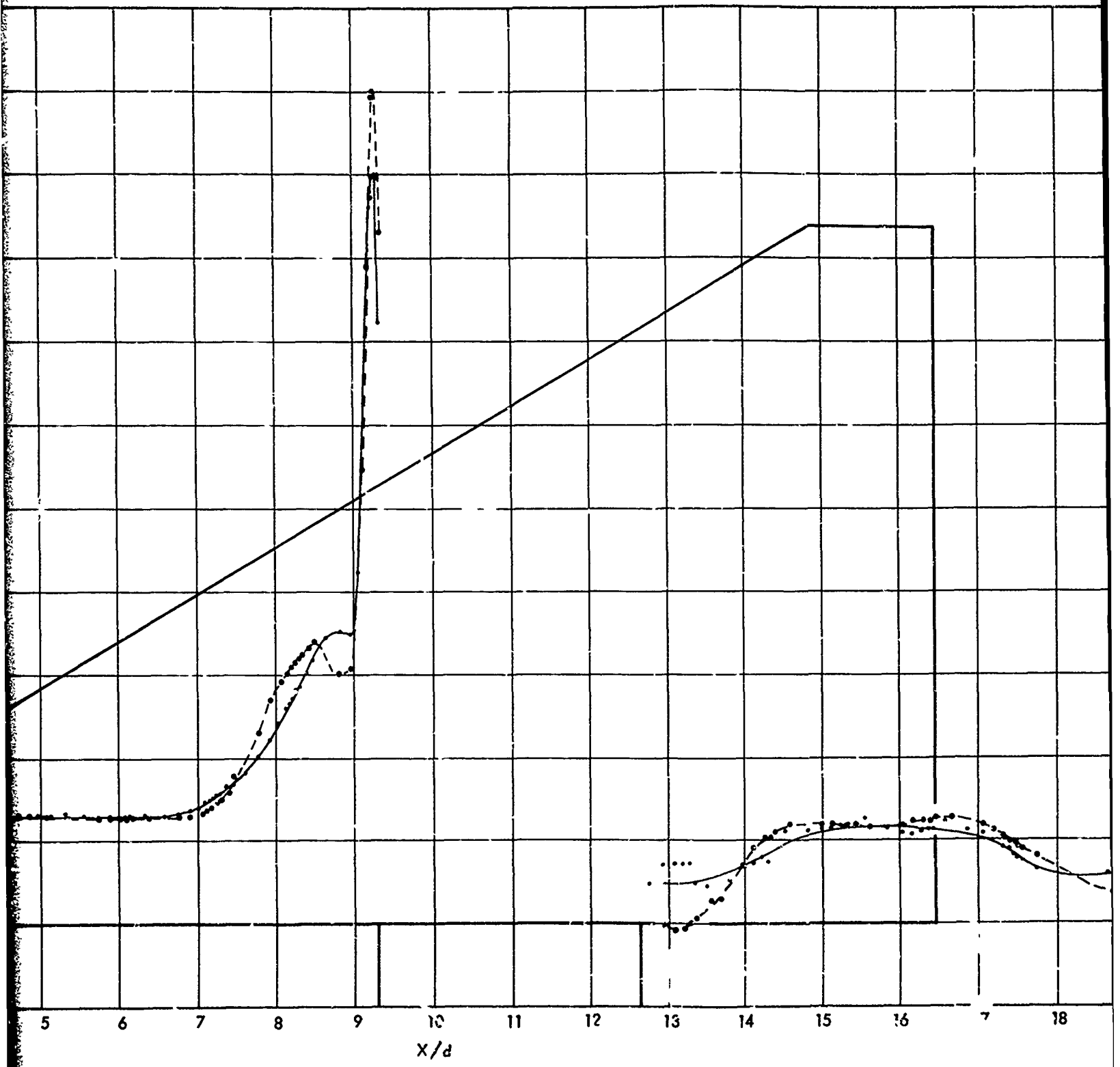

FIG. 16 D 60° SWEPT FIN W

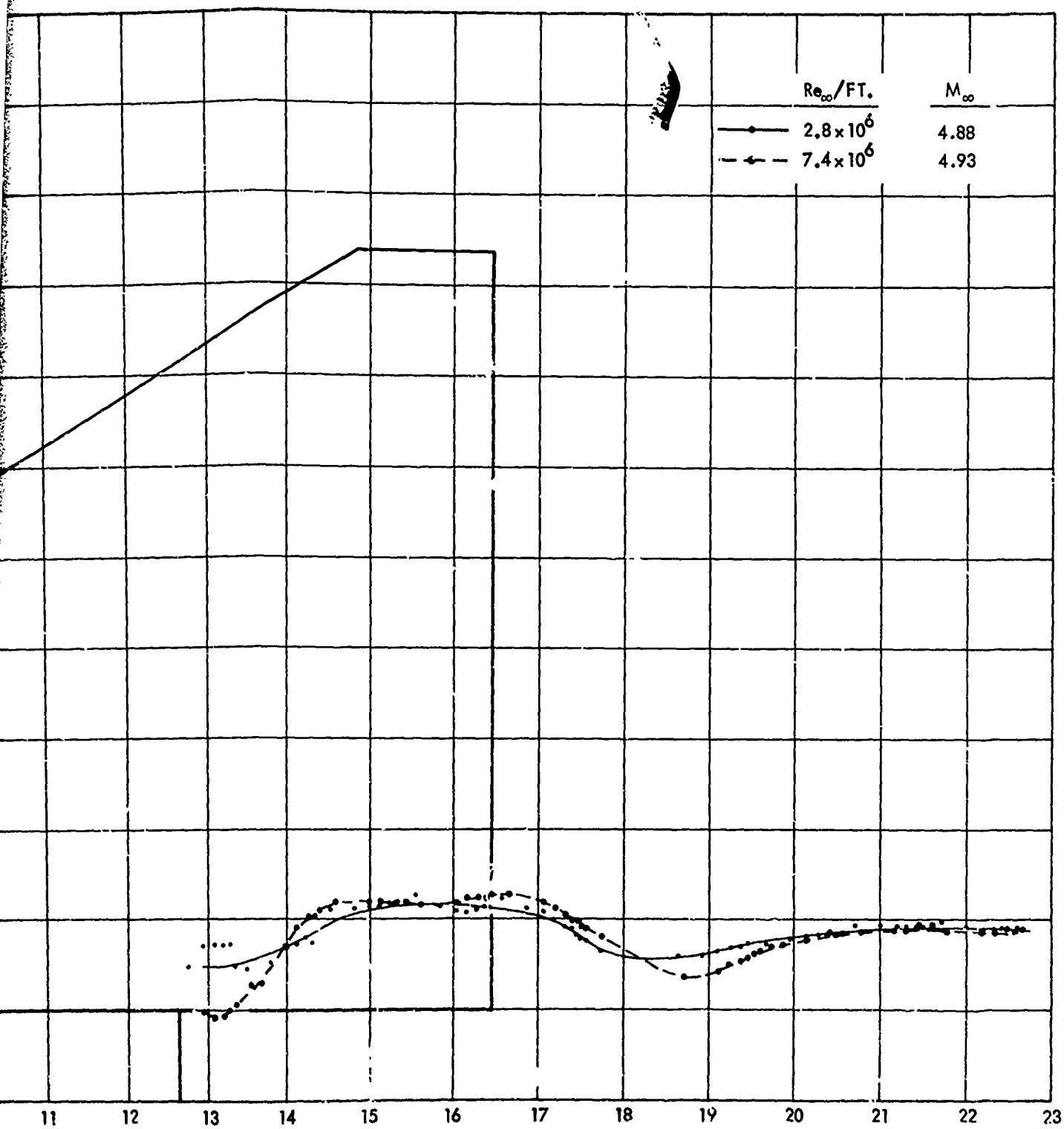

FIG. 16 D 60° SWEPT FIN WITH 0.50 INCH CLEARANCE GAP

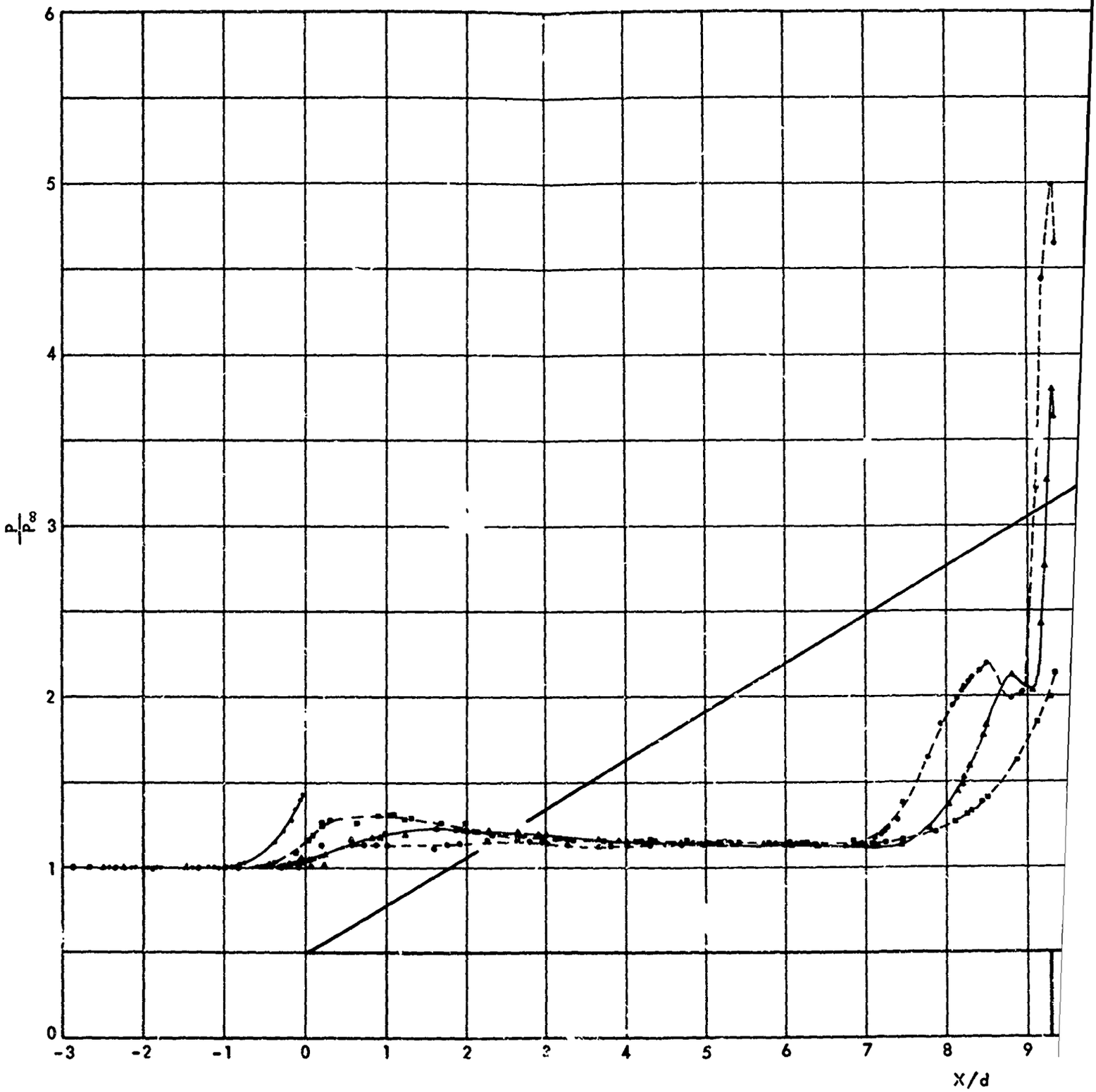

59

59a

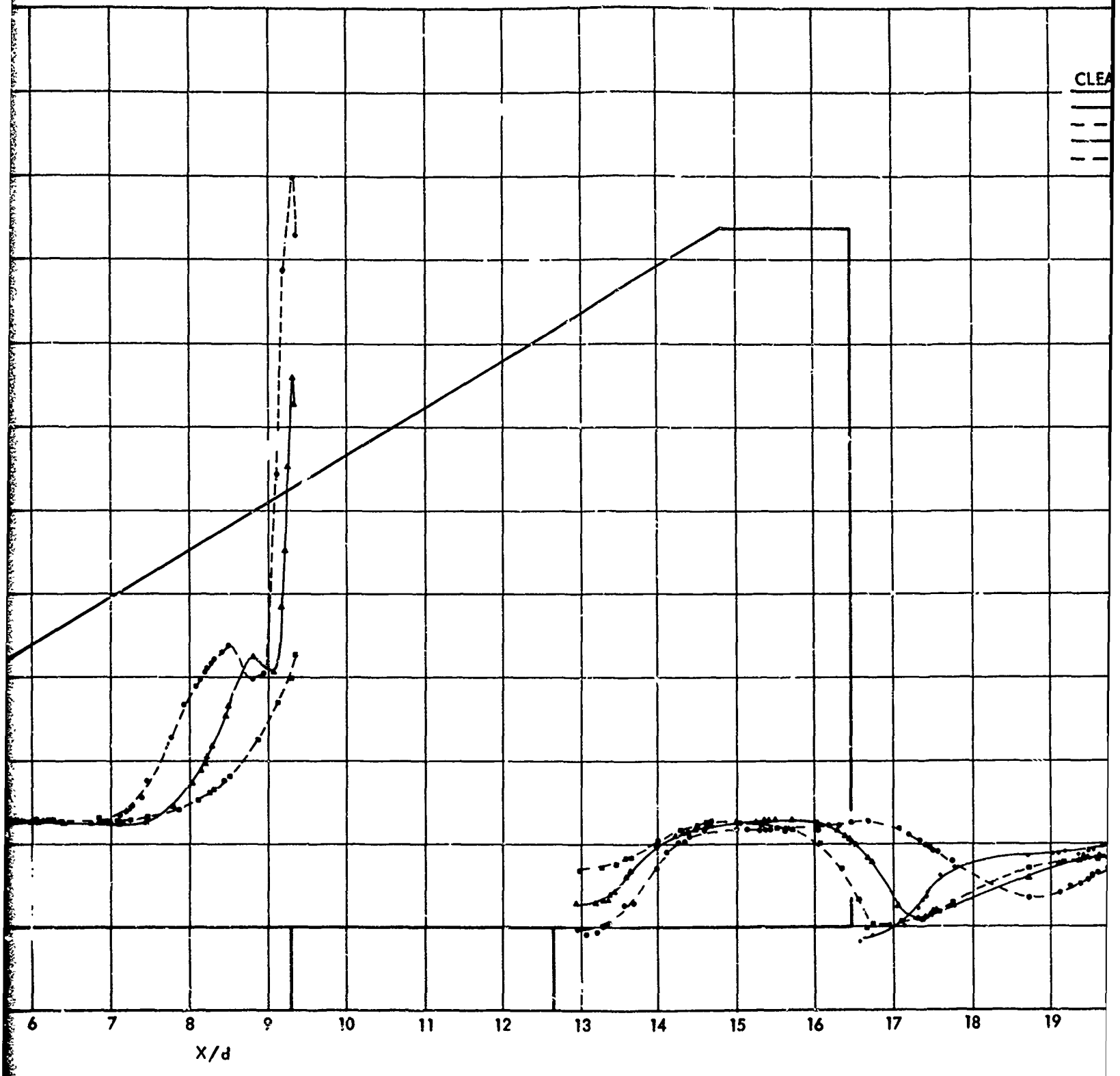

FIG. 17 FLAT PLAT PRESSURE DISTRIBUTION FOR VARYING CLEARANCE

59a

59b

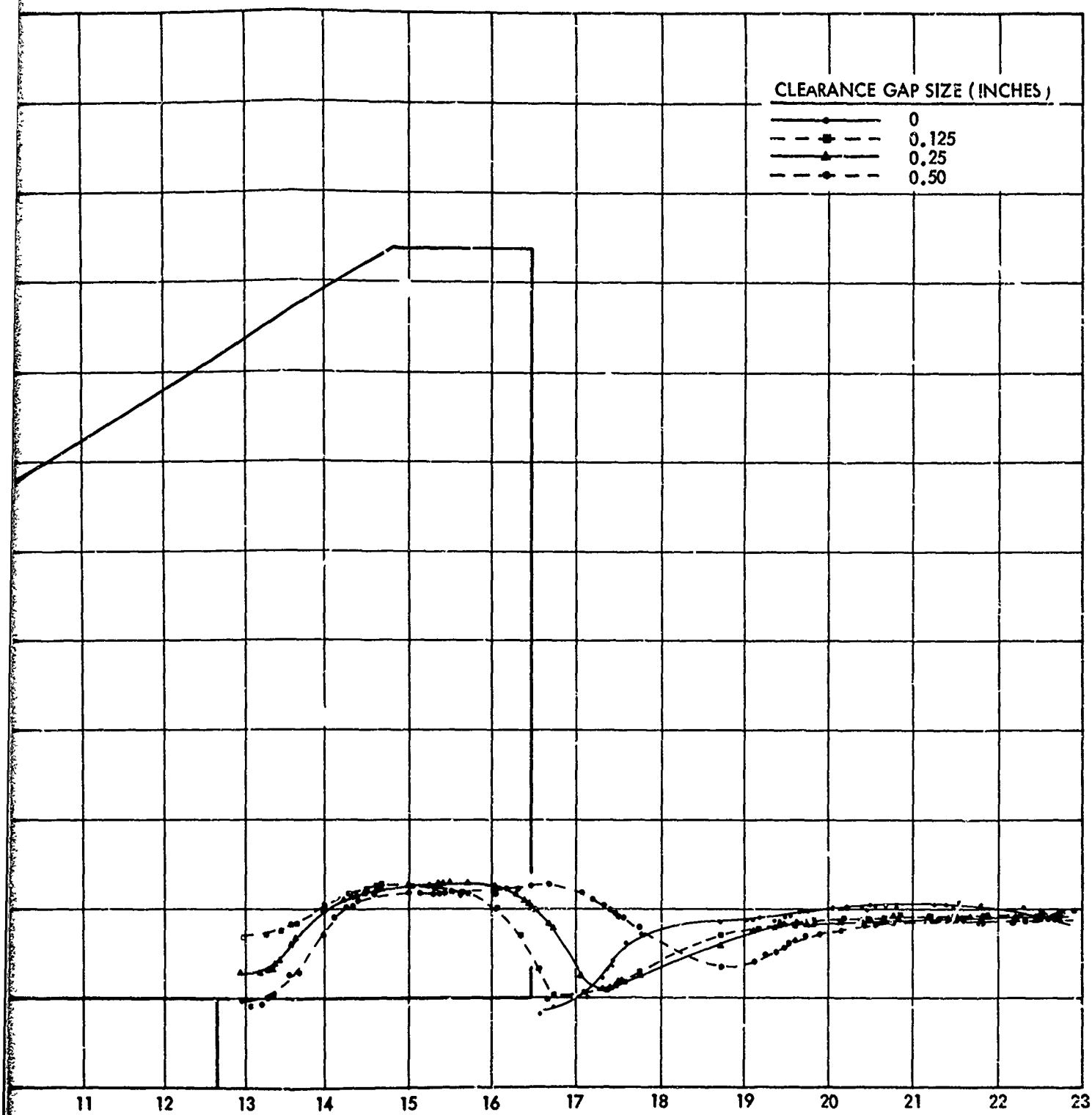

FIG. 17 FLAT PLAT PRESSURE DISTRIBUTION FOR VARYING CLEARANCE GAPS ON A 60° SWEPT FIN

FIG. 18 AZOBENZENE PATTERN SHOWING REGION OF HIGH HEAT TRANSFER PRODUCED BY A BLUNT UNSWEPT FIN (REF. 5)

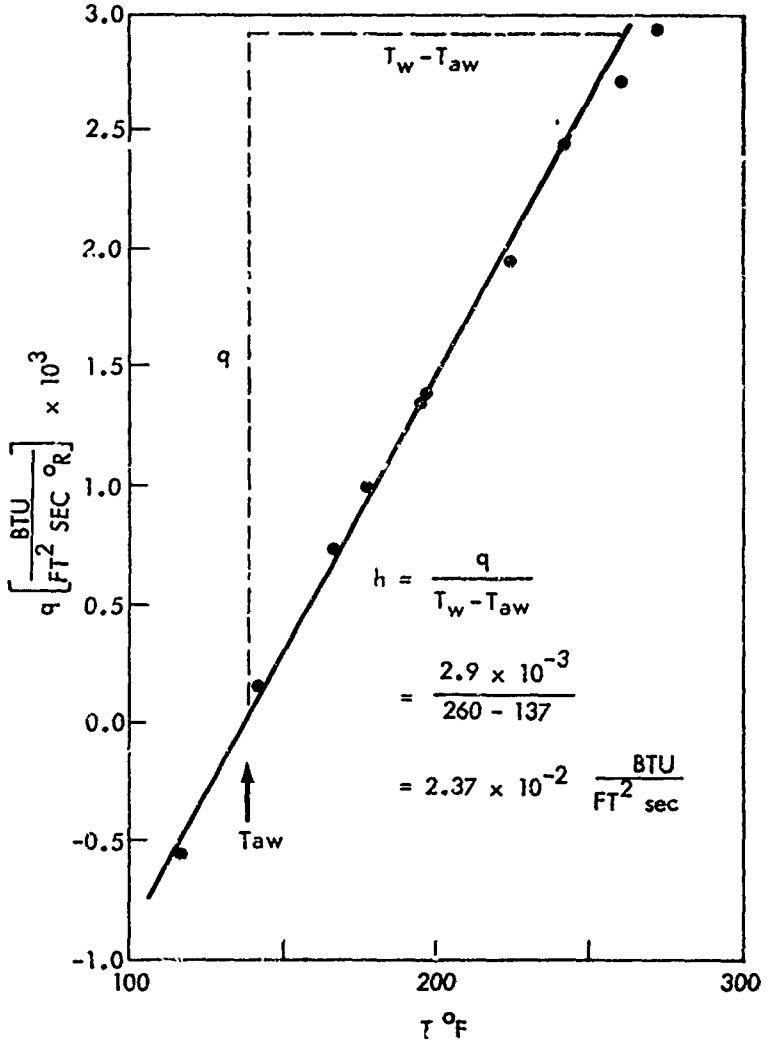

FIG. 19 TYPICAL DATA OBTAINED FROM HEATED DIFFERENTIAL HEAT TRANSFER GAGE

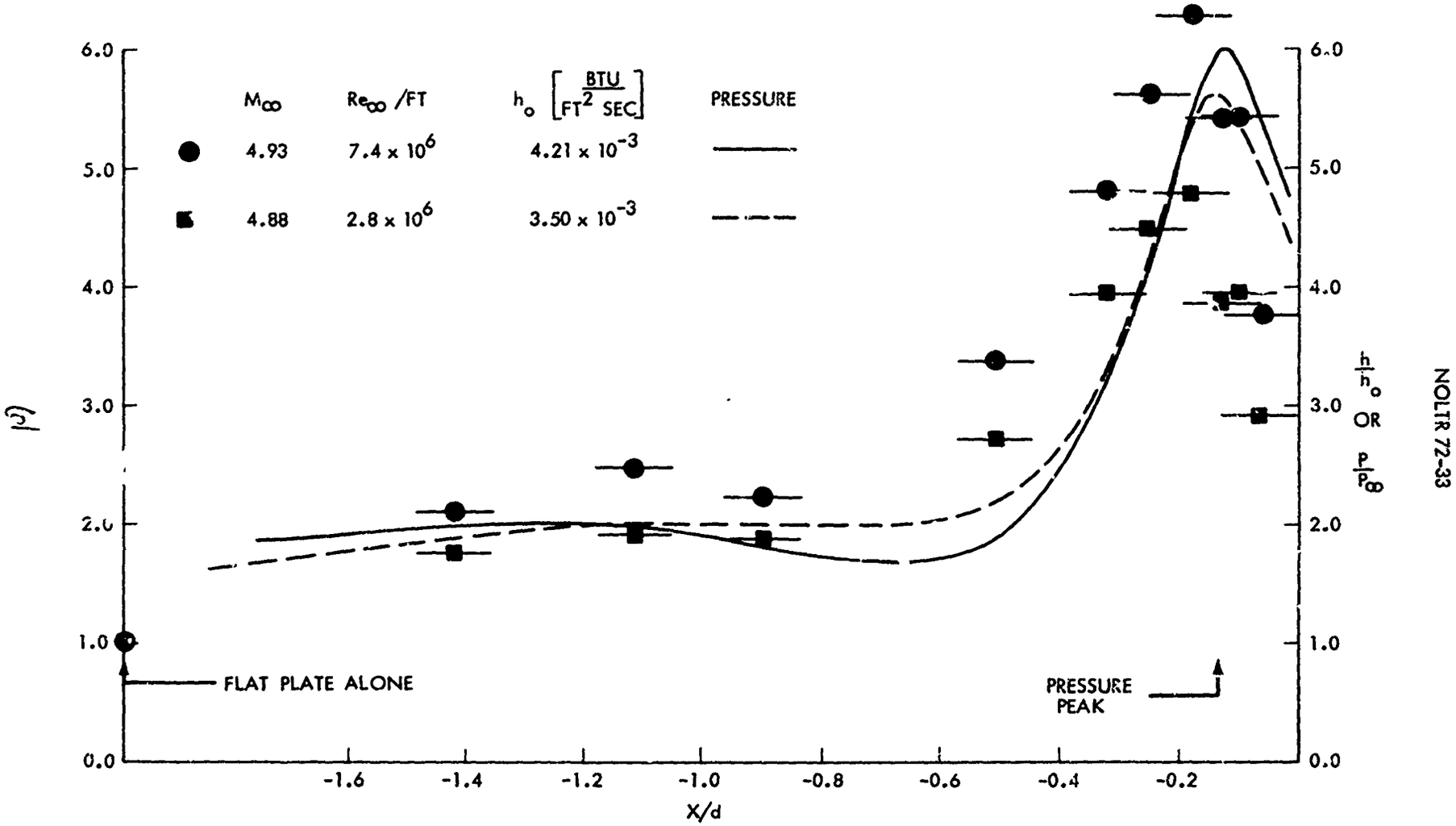

FIG. 20 HEAT TRANSFER DATA IN REGION AHEAD OF AN UNSWEPT FIN

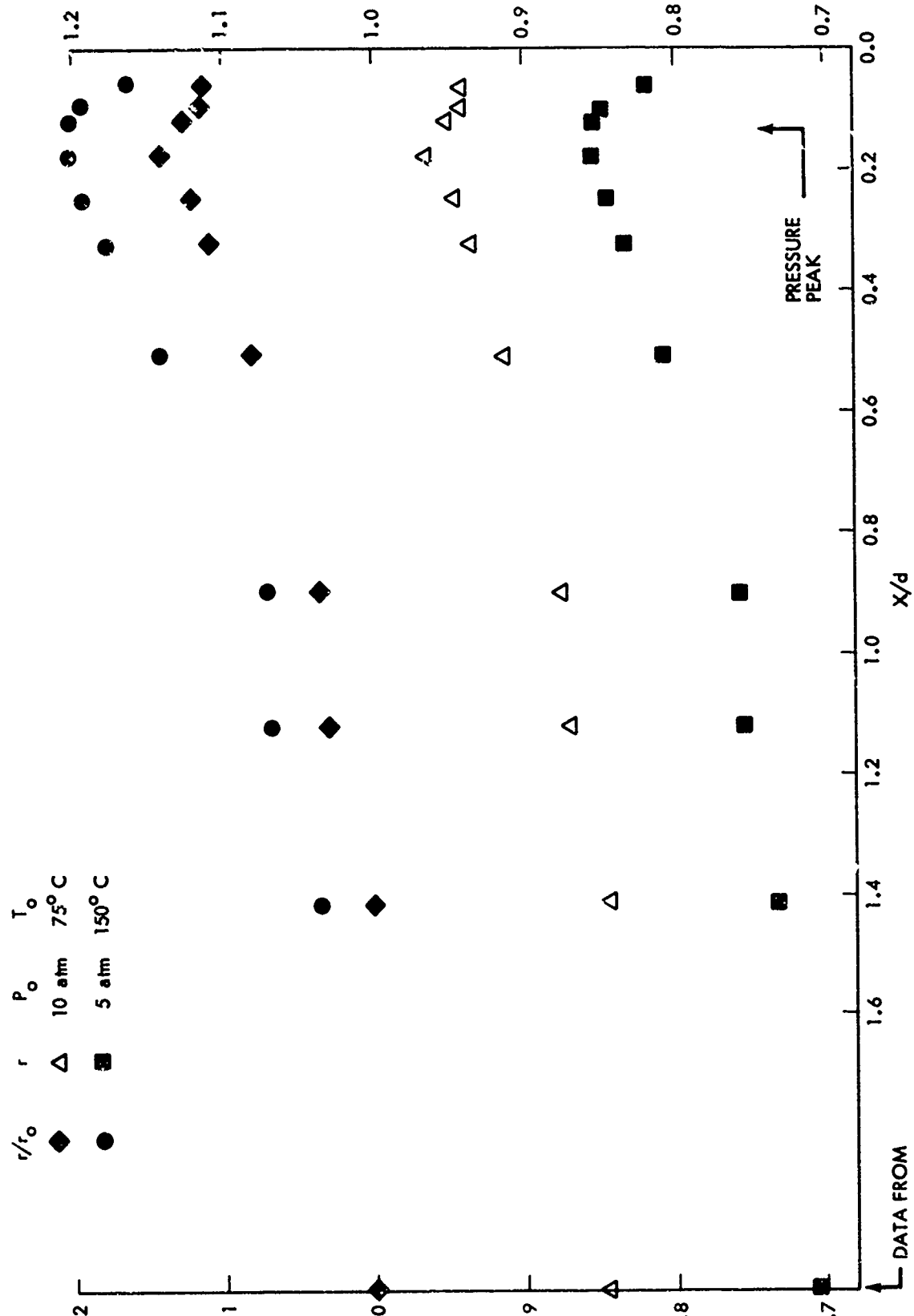

FIG. 21 RECOVERY FACTORS IN REGION AHEAD OF AN UNSWEPT FIN

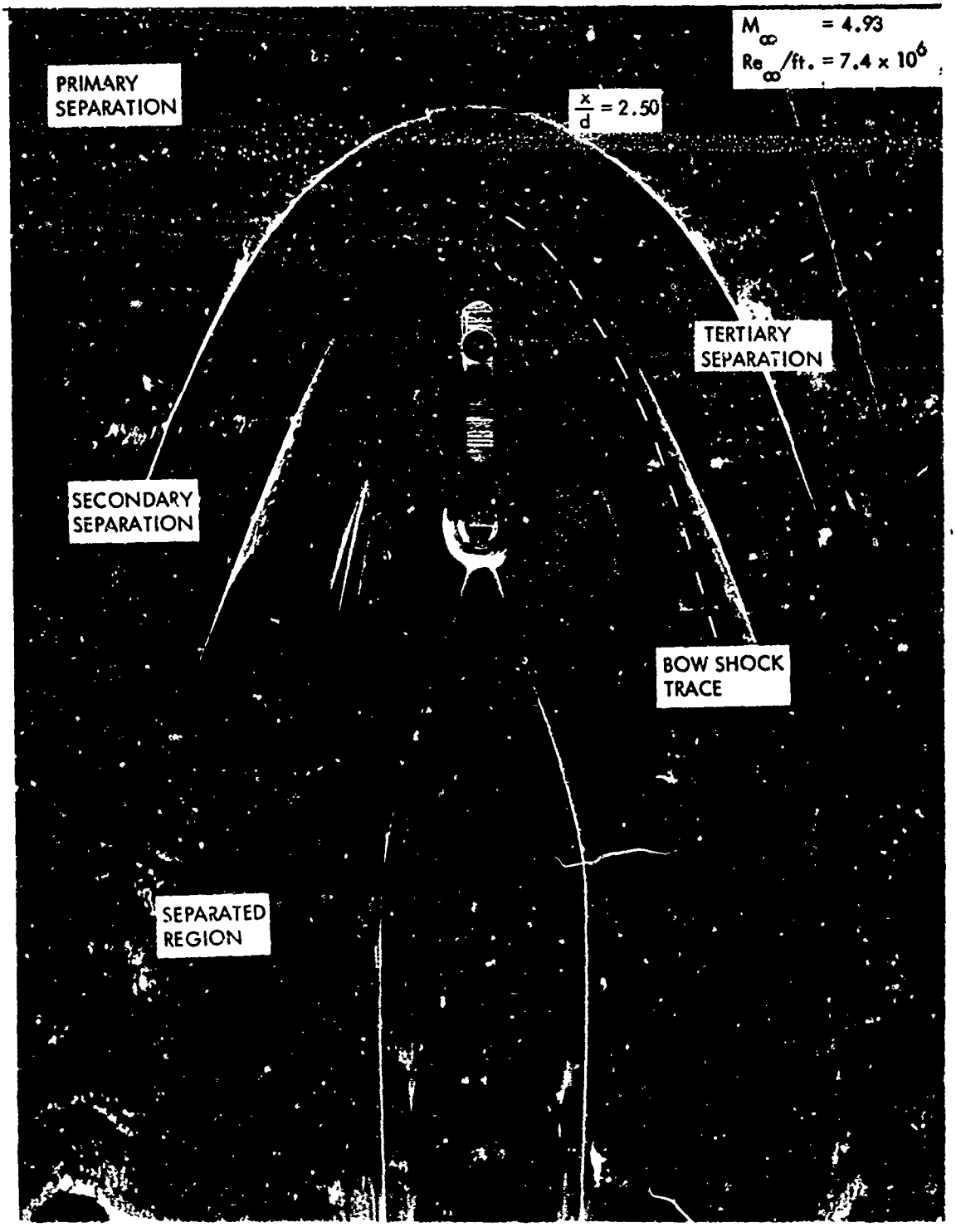

FIG. 22a OIL PATTERN ON THE FLAT PLATE FOR AN UNSWEPT FIN

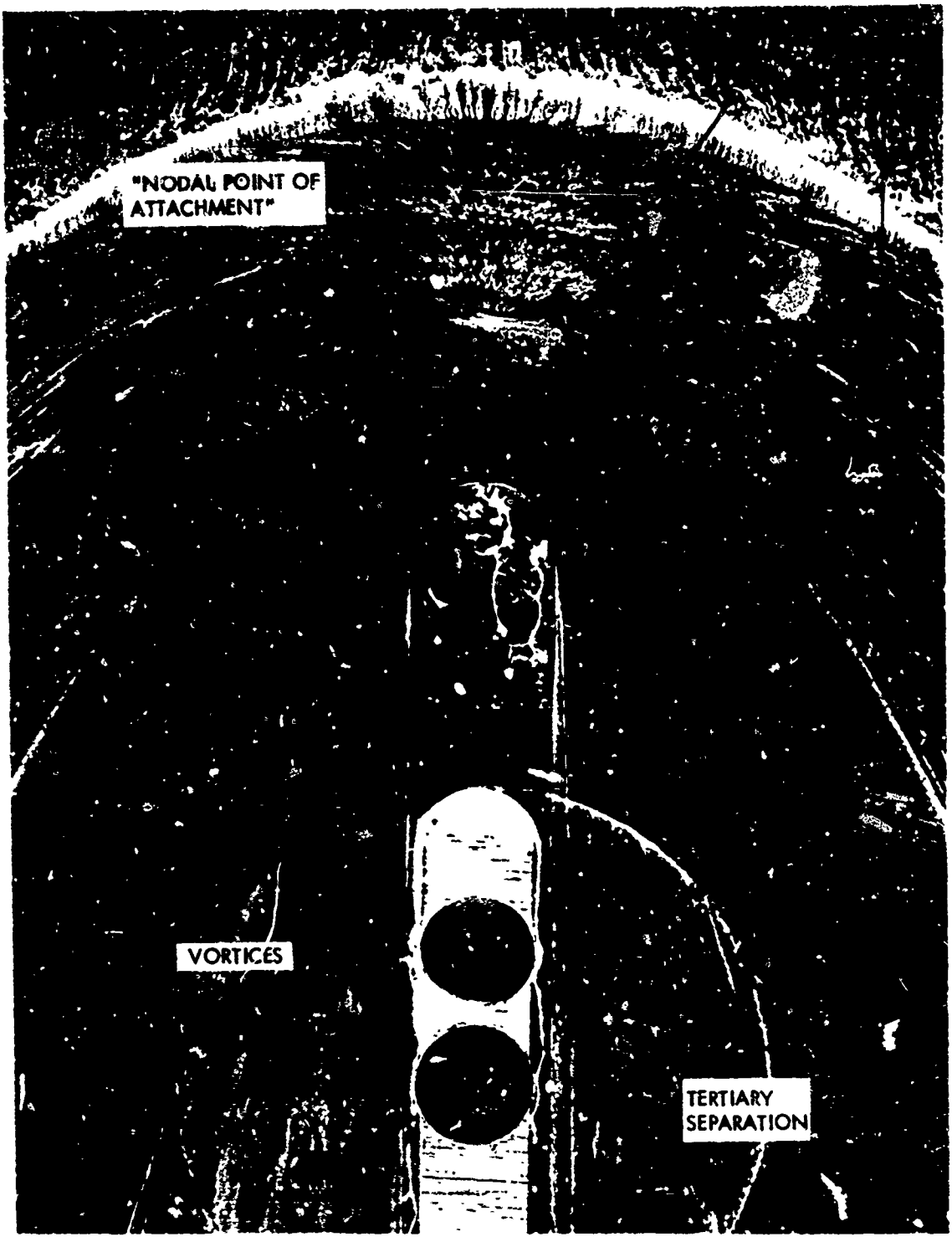

FIG. 22b ENLARGED VIEW-UPSTREAM OF UNSWEPT FIN

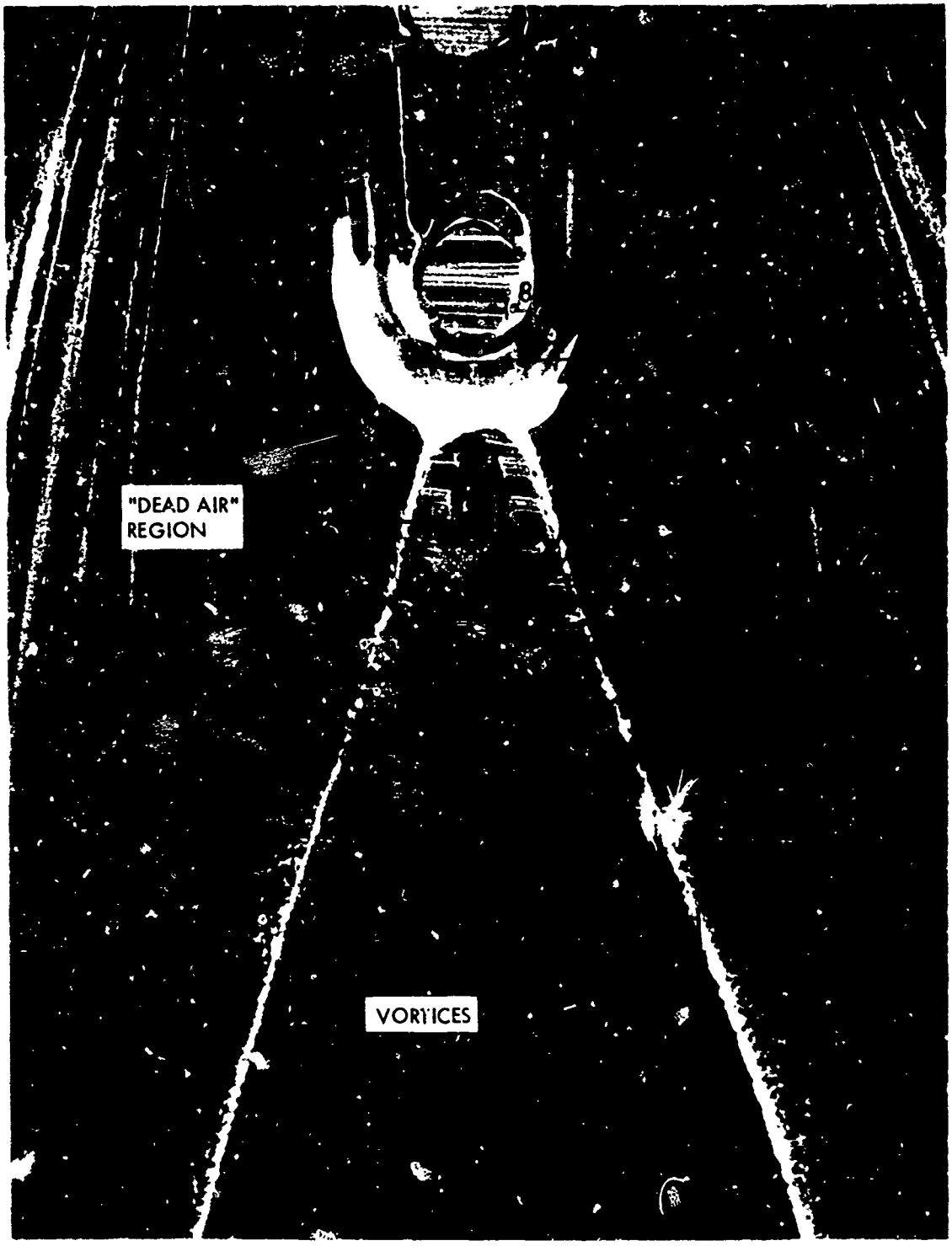

FIG. 22c ENLARGED VIEW-DOWNSTREAM OF UNSWEPT FIN

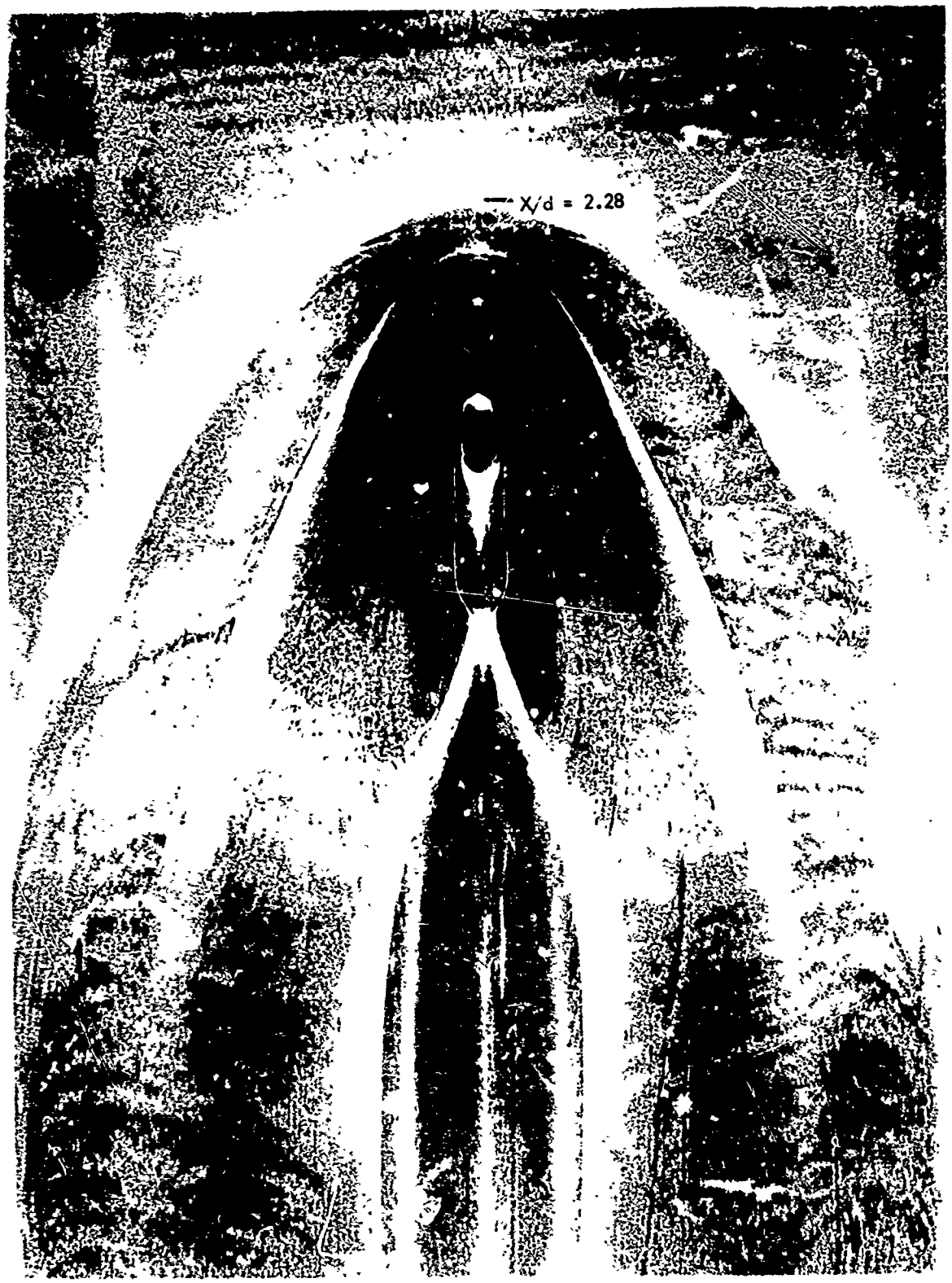

FIG. 23a UNSWEPT FIN WITH 0.075" CLEARANCE GAP

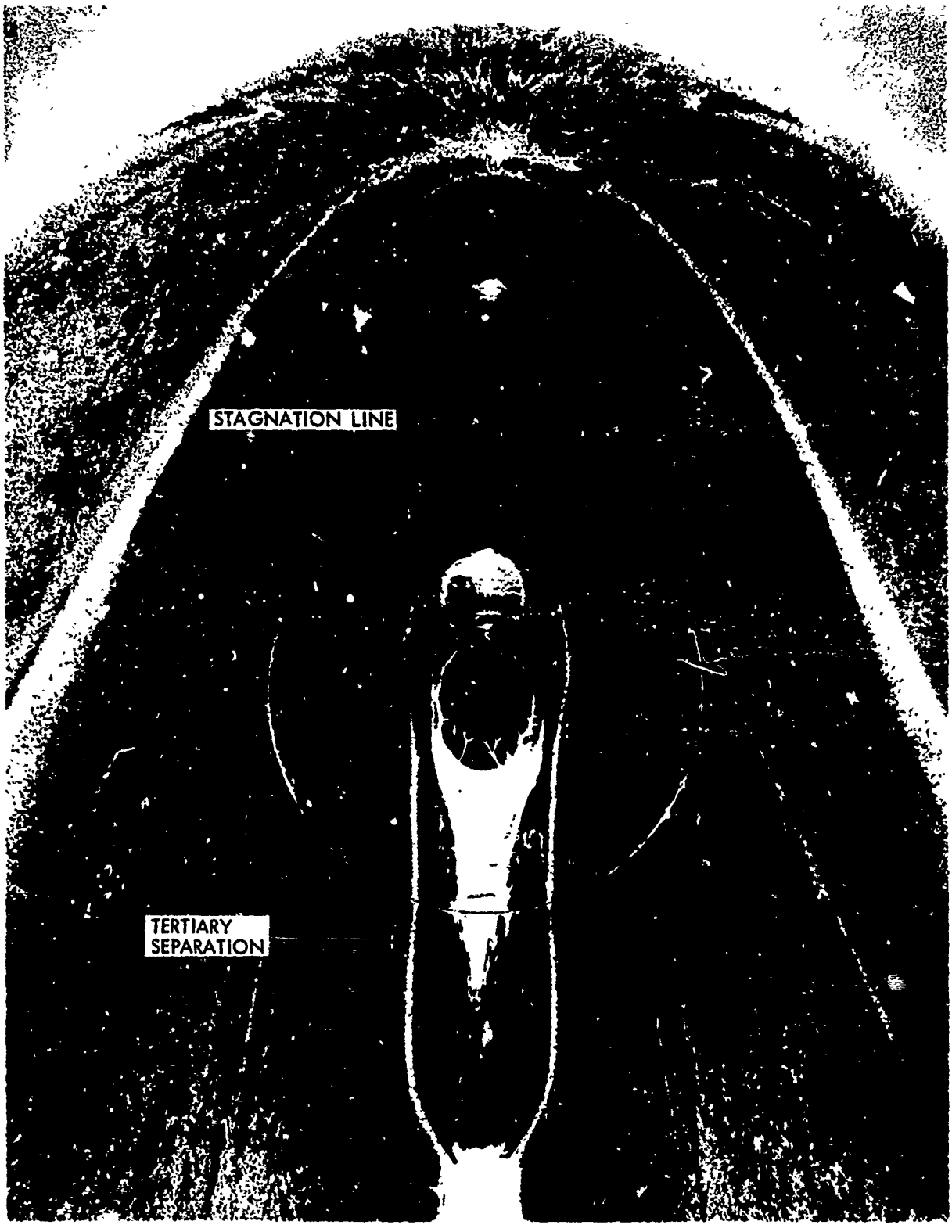

FIG. 23b ENLARGED VIEW-UNSWEPT FIN WITH 0.075" CLEARANCE GAP

FIG. 24 UNSWEPT FIN WITH 0.125" CLEARANCE GAP

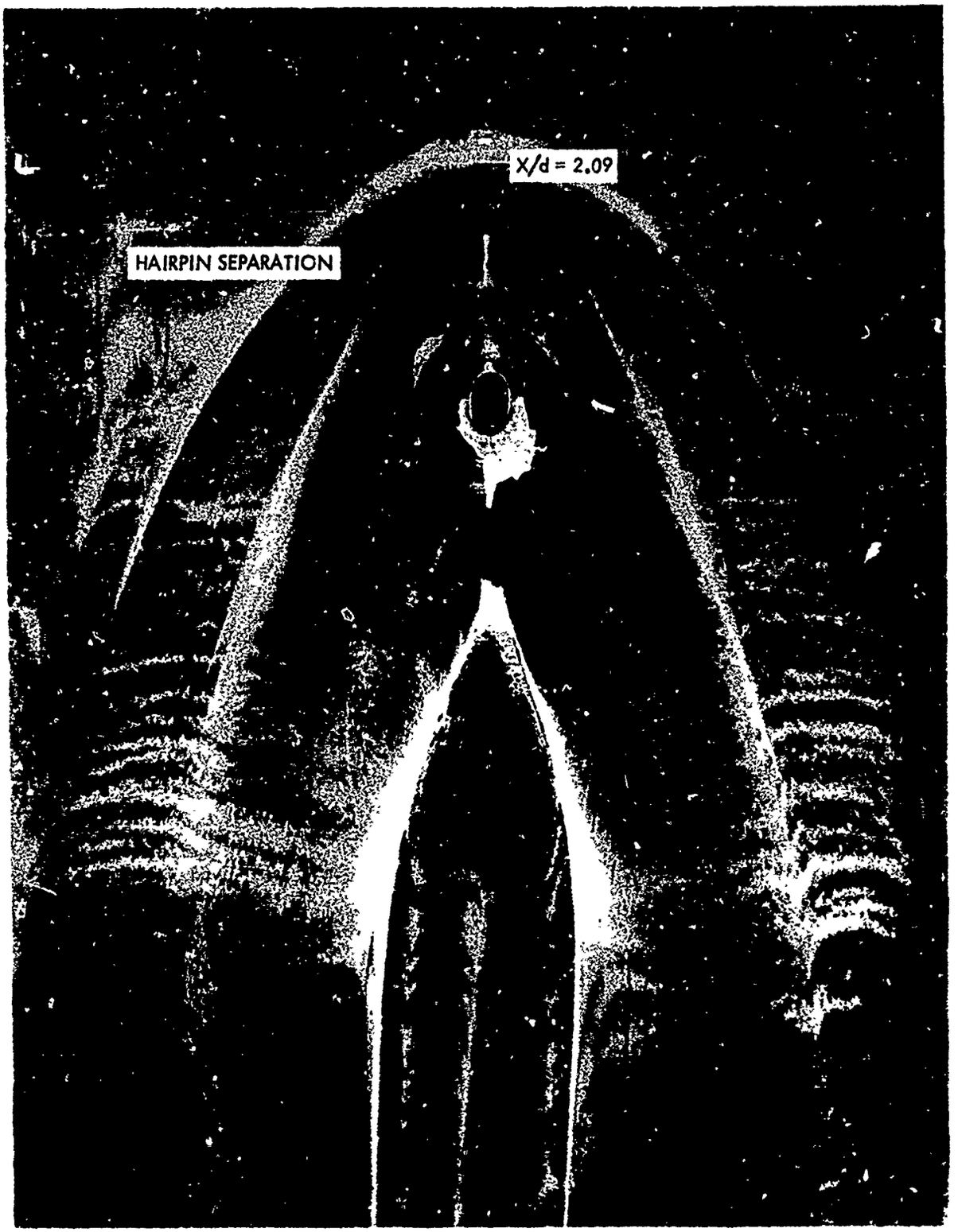

FIG. 25 UNSWEPT FIN WITH 0.25" CLEARANCE GAP

FIG. 26a UNSWEPT FIN WITH 0.5" CLEARANCE GAP

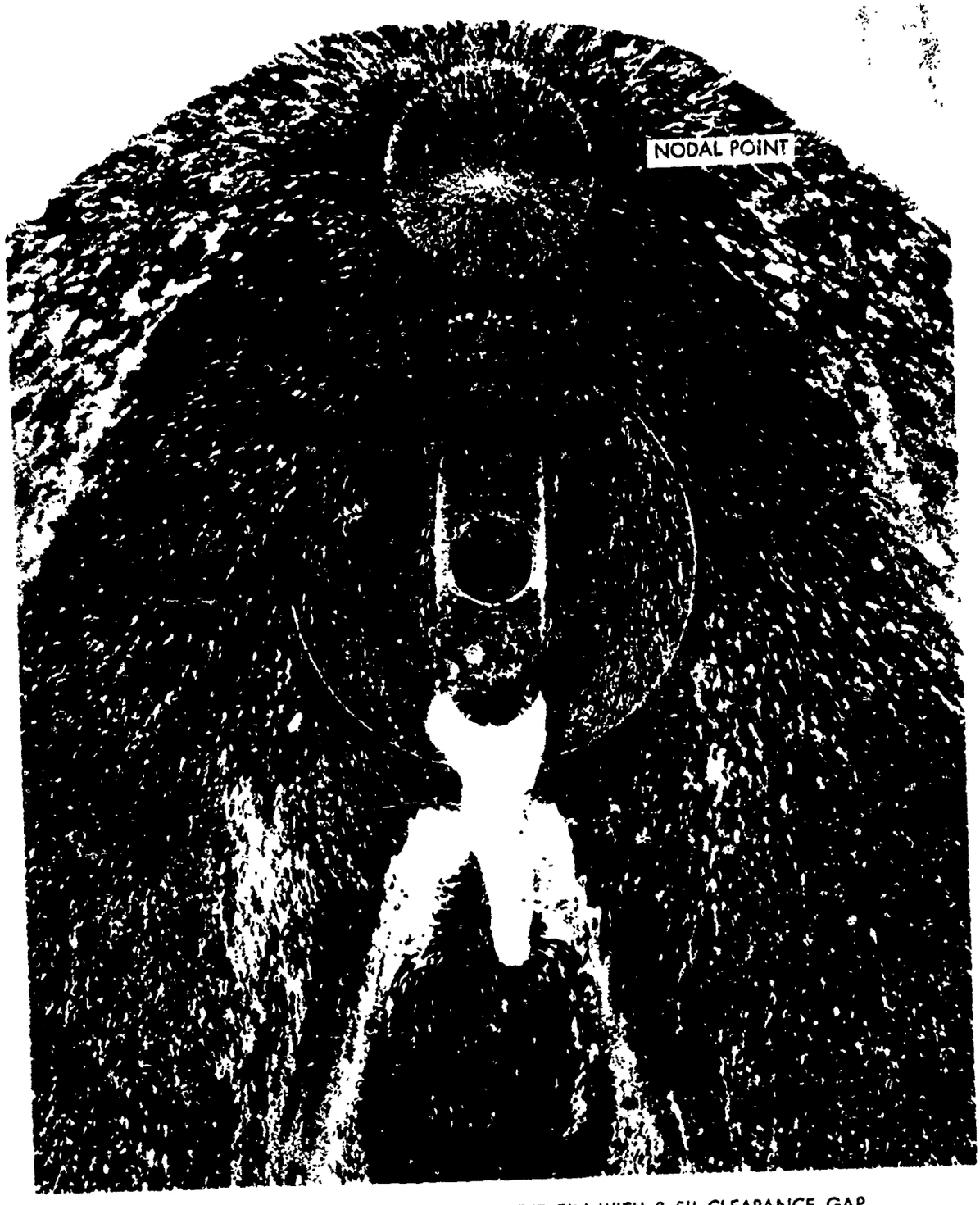

FIG. 26b ENLARGED VIEW-UNSWEPT FIN WITH 0.5" CLEARANCE GAP

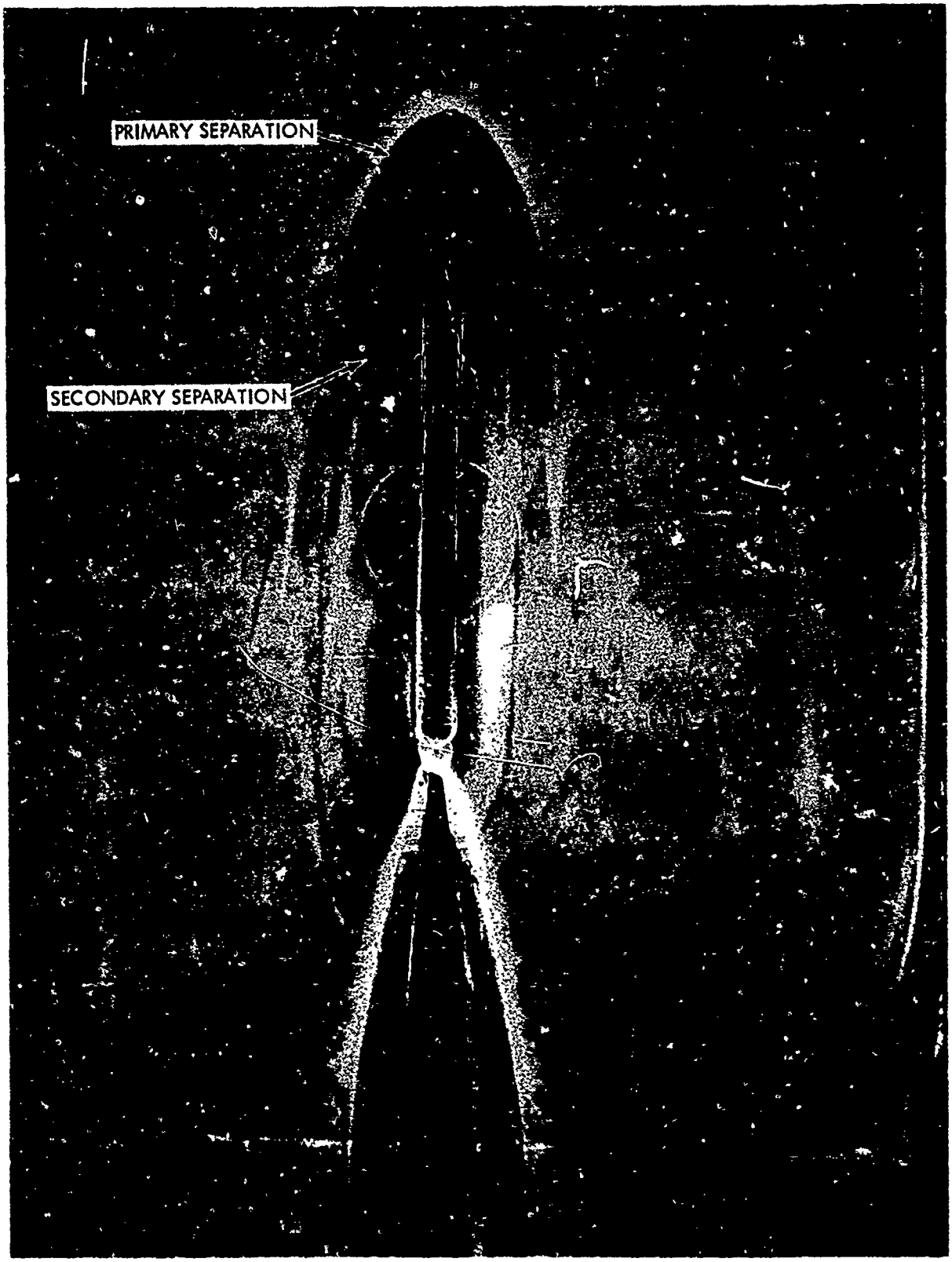

FIG. 27a OIL PATTERN ON THE FLAT PLATE FOR A 60° SWEPT FIN

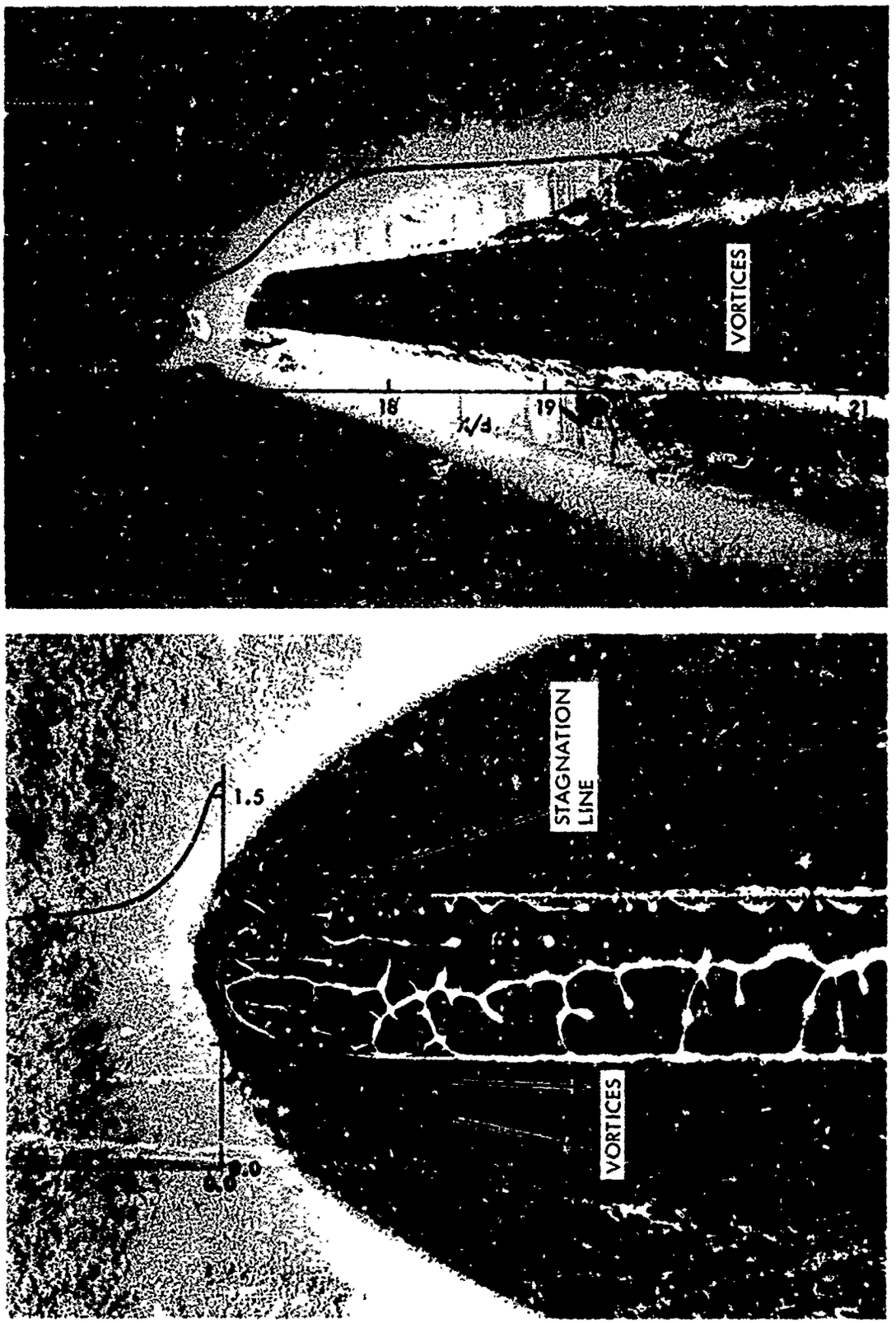

FIG. 27b ENLARGED VIEW - 60° SWEPT FIN

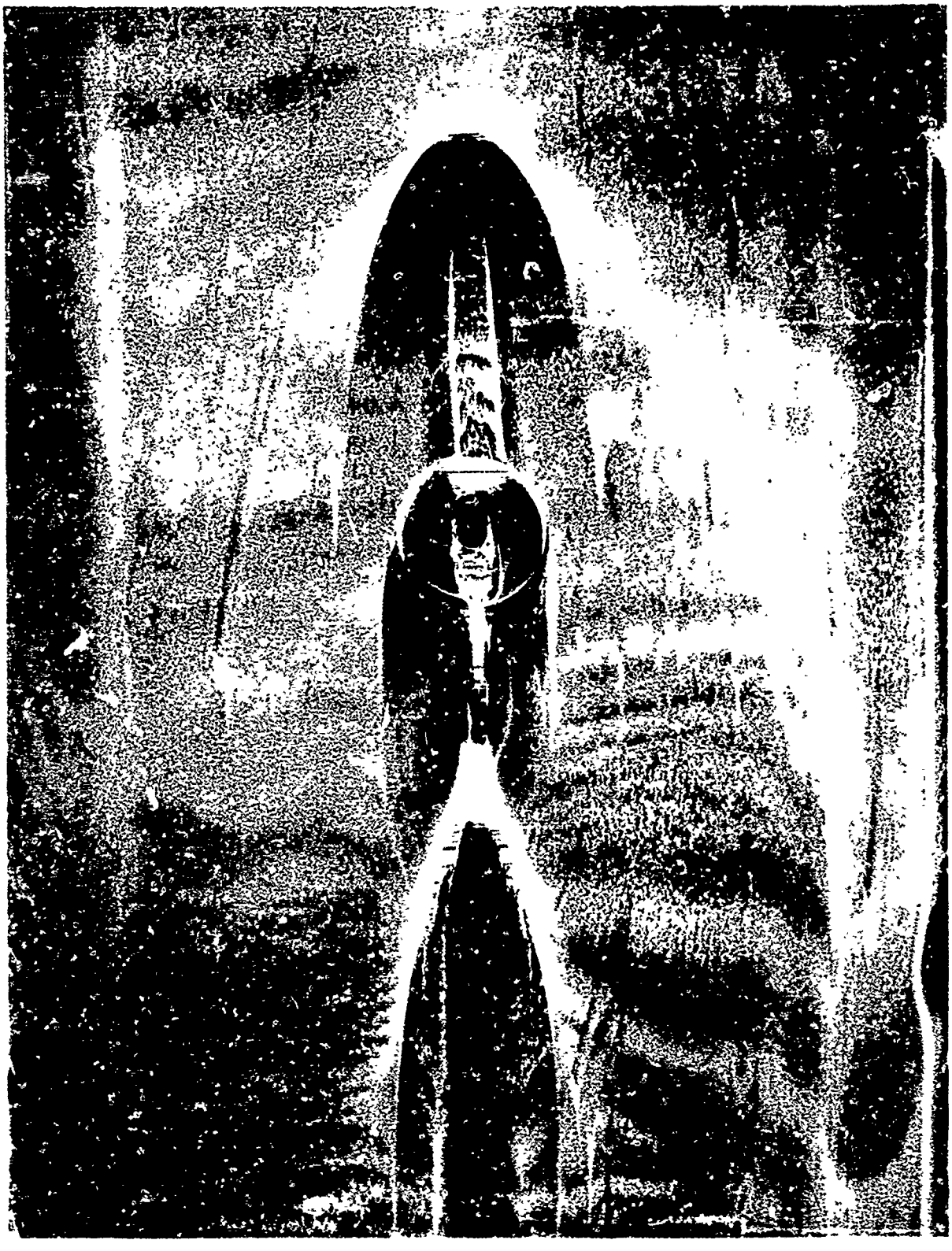

FIG. 8 60° SWEPT FIN WITH 0.125" CLEARANCE GAP

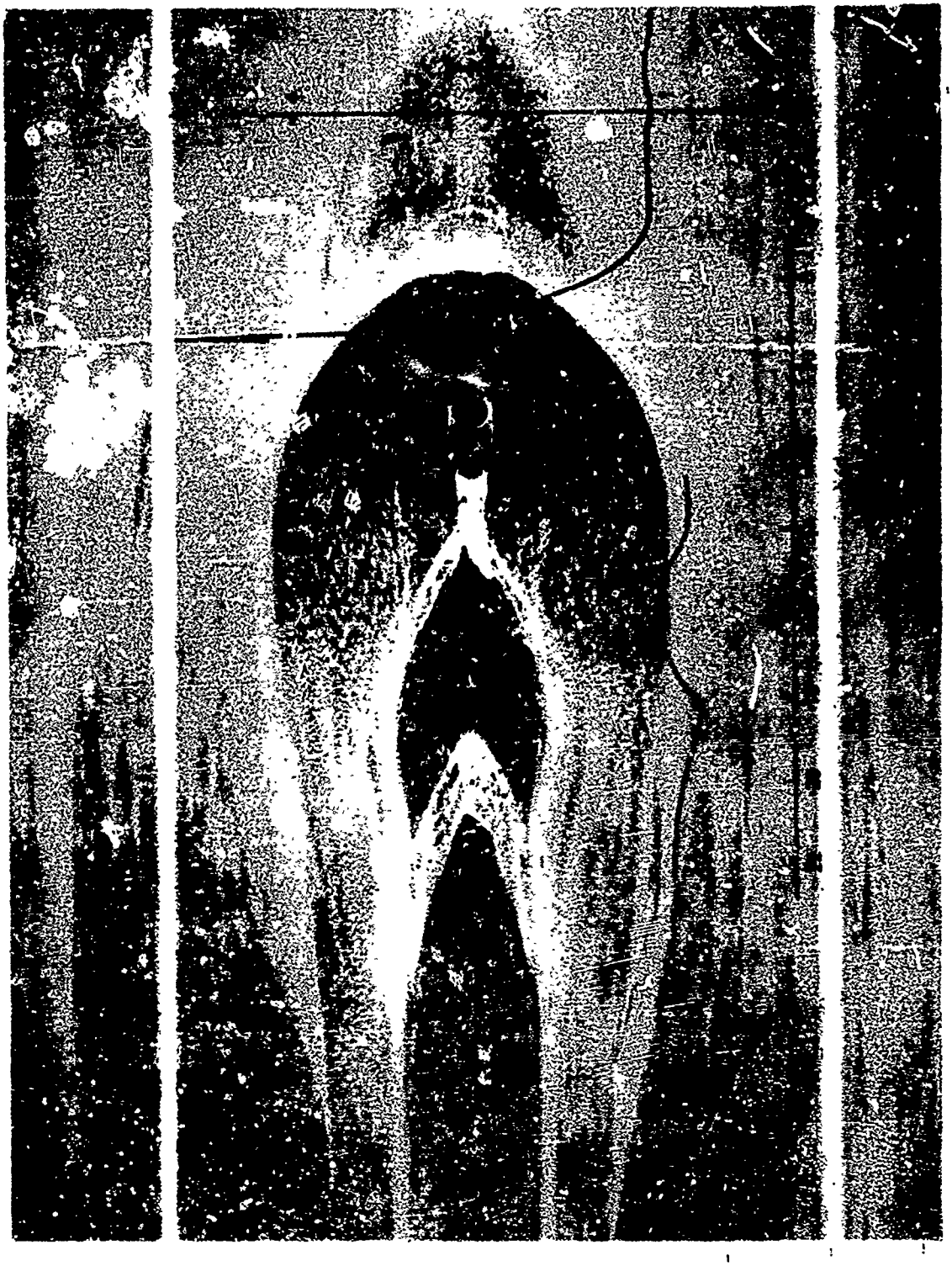

FIG. 29a 60° SWEPT FIN WITH 0.5" CLEARANCE GA

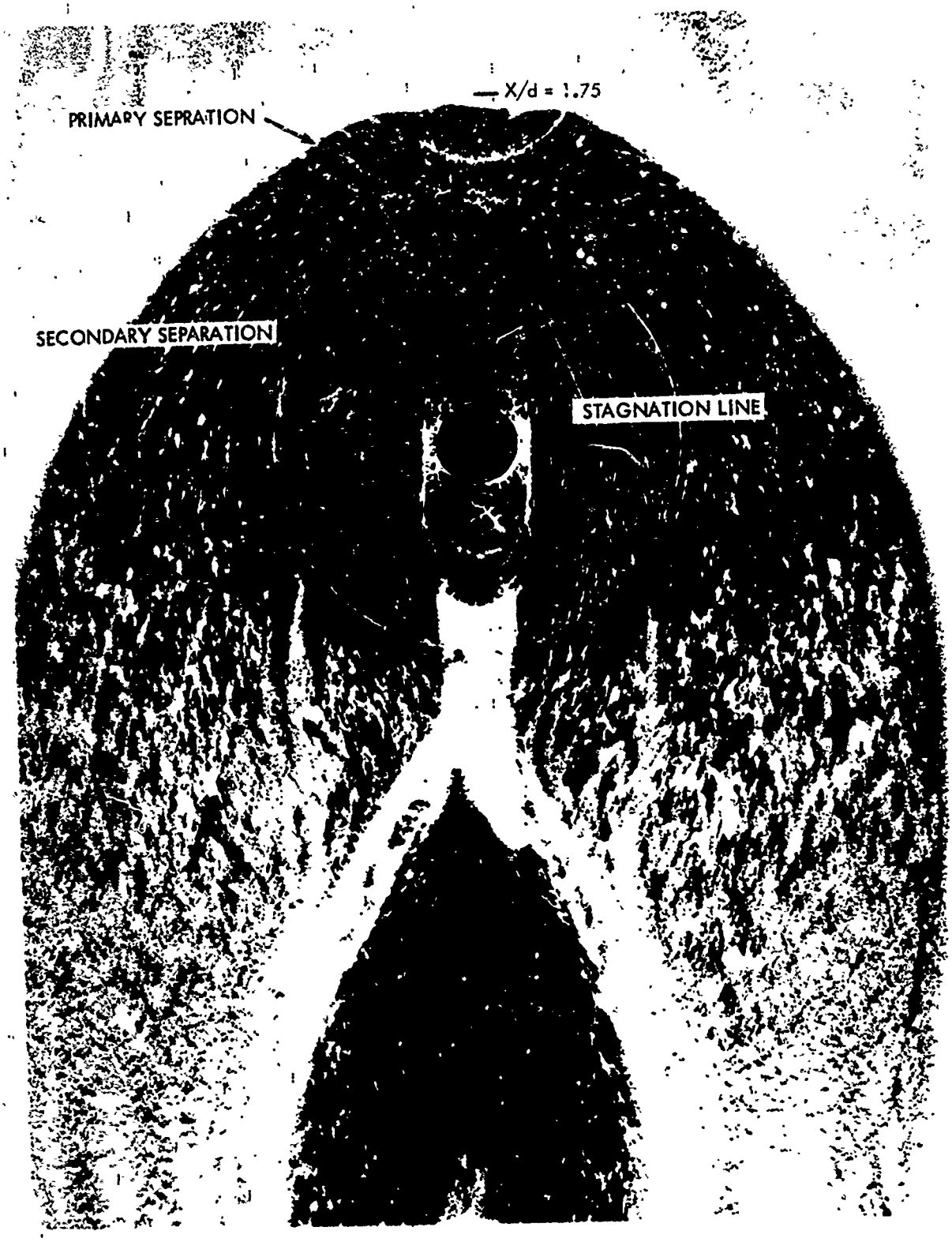

FIG. 29b ENLARGED VIEW-60° SWEPT FIN WITH 0.5" CLEARANCE GAP

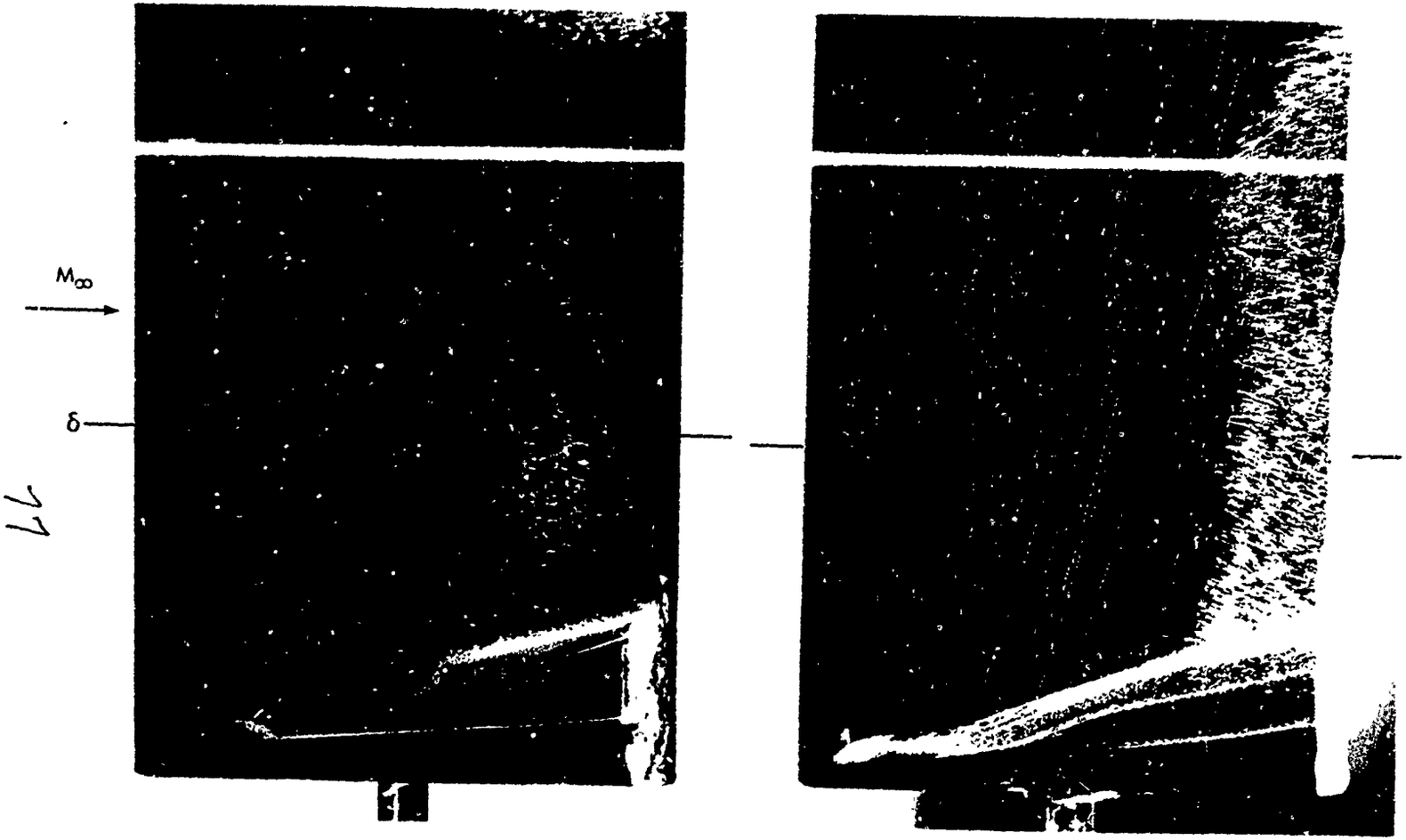

NO CLEARANCE GAP

0.075" CLEARANCE GAP

FIG. 30a OIL PATTERNS ON AN UNSWEPT FIN

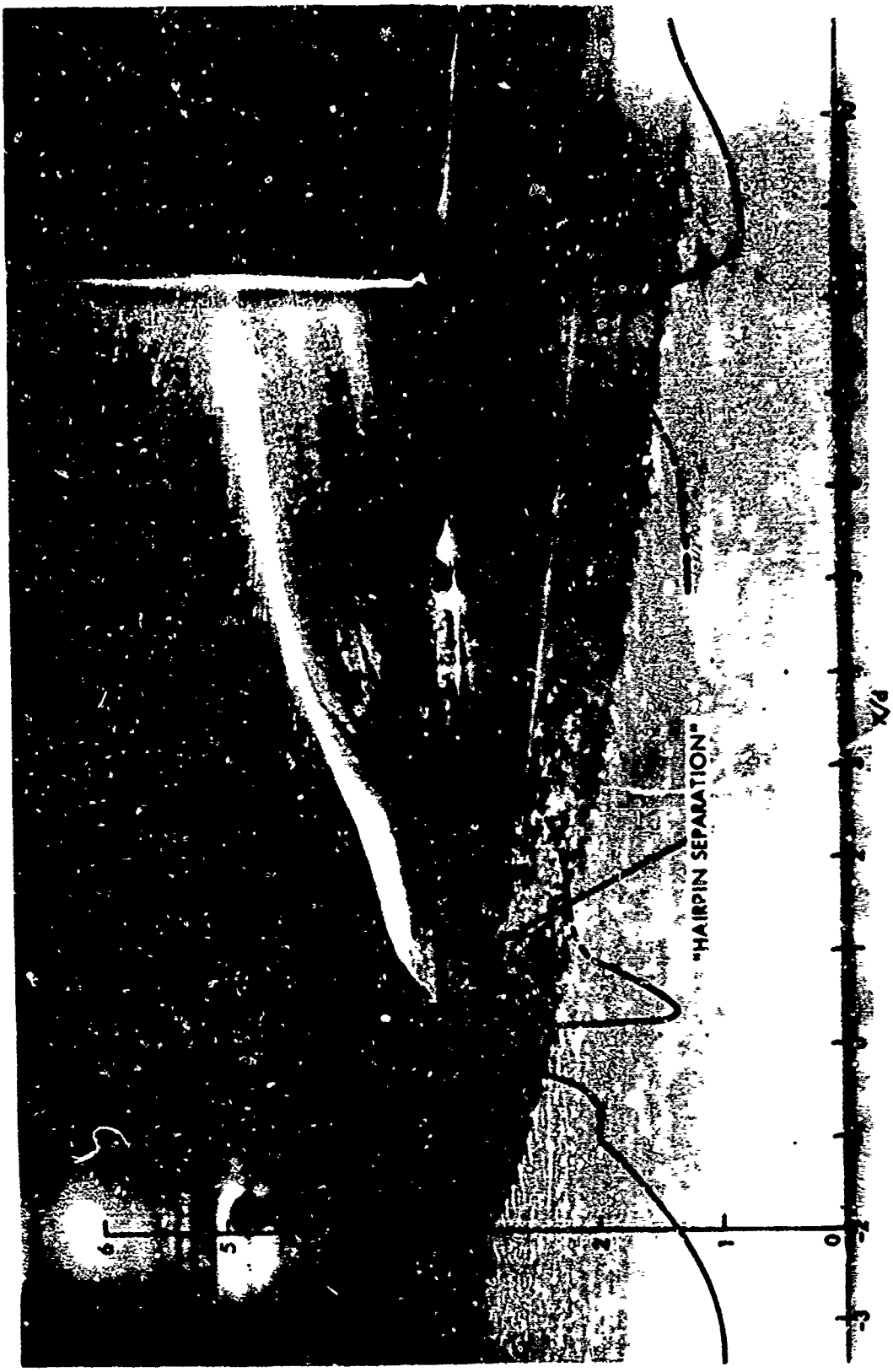

FIG. 30b OIL PATTERN ON AN UNSWEPT FIN WITH AN 0.125" CLEARANCE GAP - OBTAINED DURING TEST

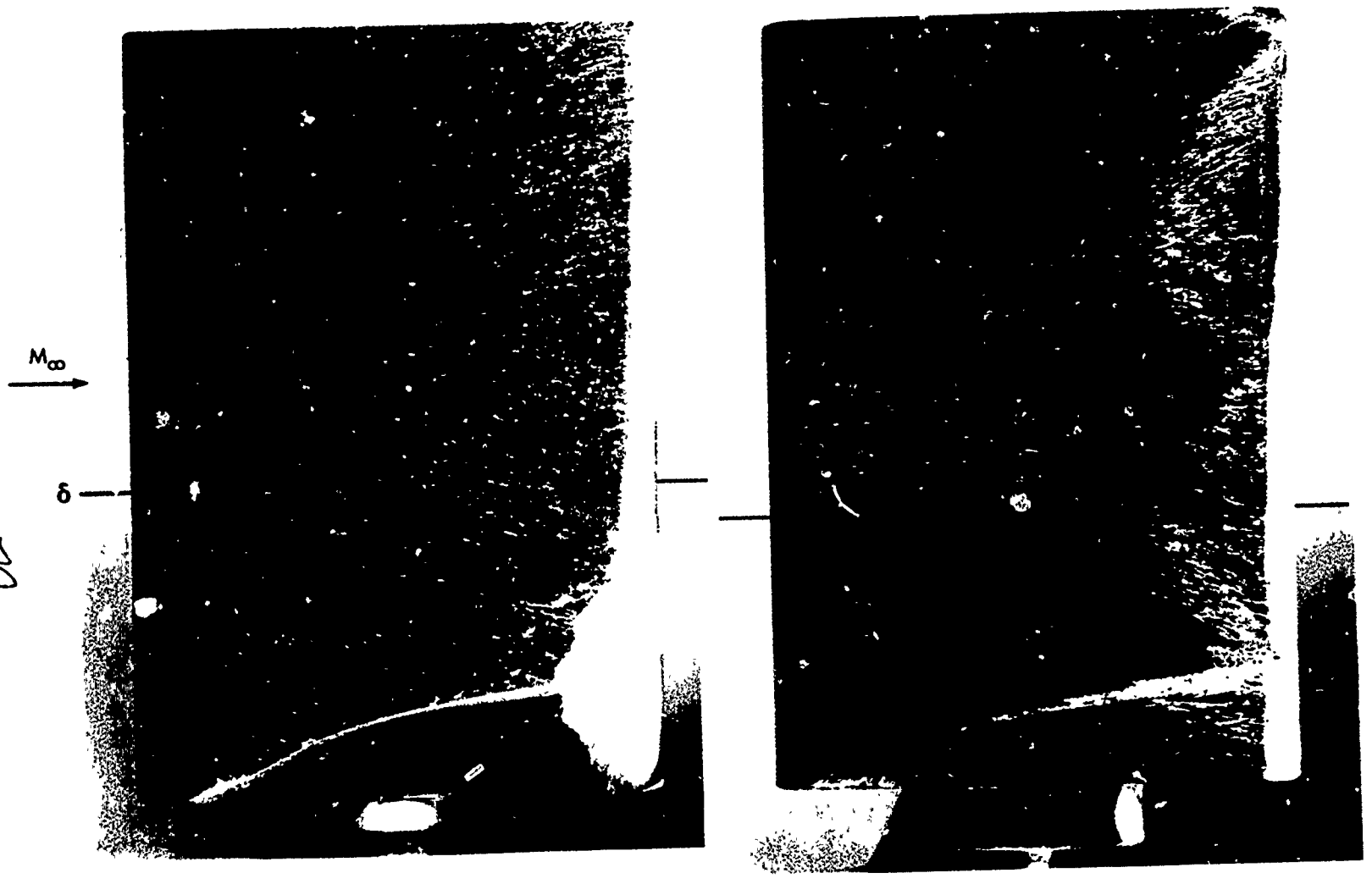

0.25" CLEARANCE GAP

0.5" CLEARANCE GAP

FIG. 30c OIL PATTERNS ON AN UNSWEPT FIN

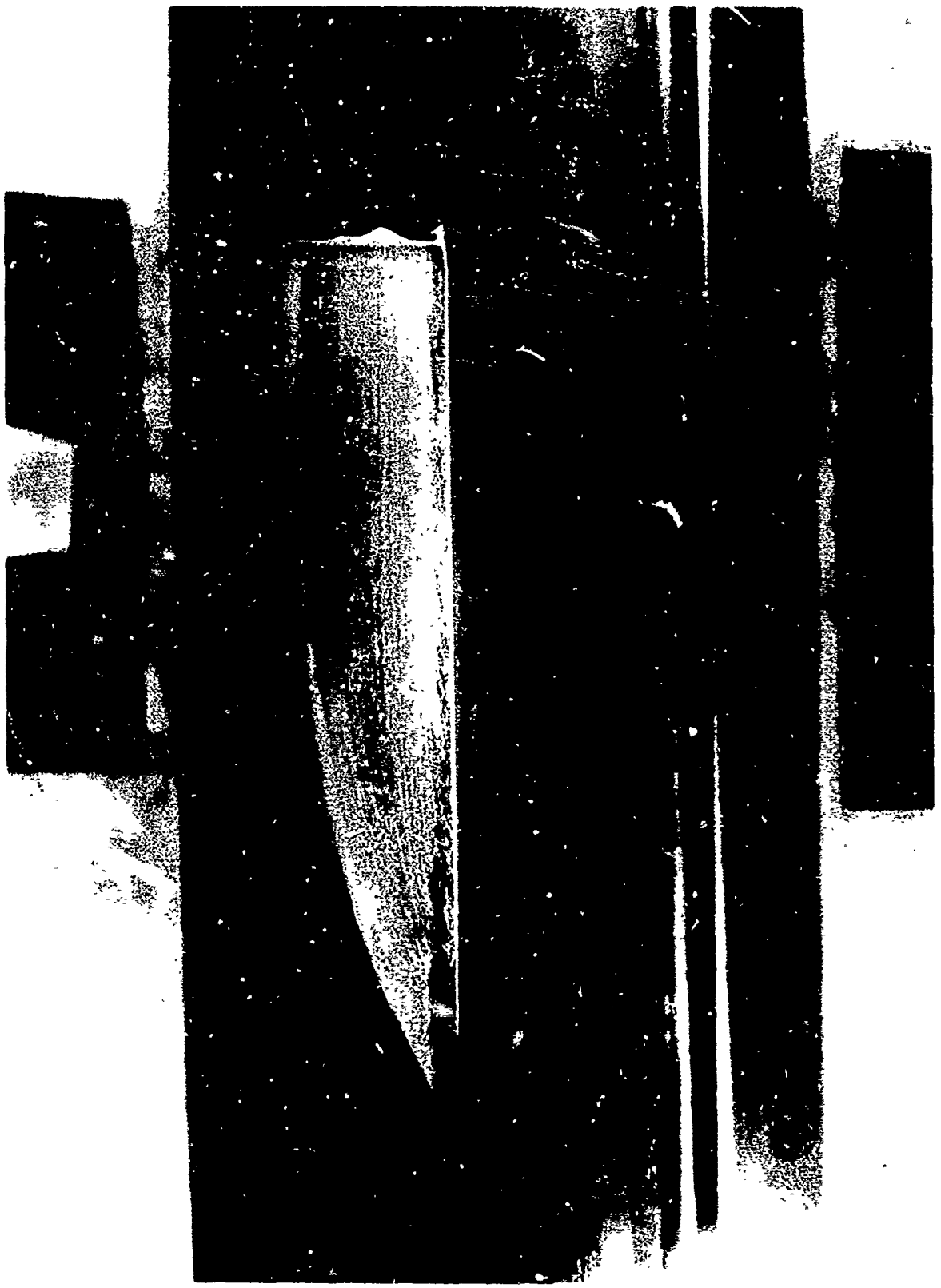

FIG. 31a OIL PATTERN ON A 60° SWEPT FIN-OBTAINED DURING TEST

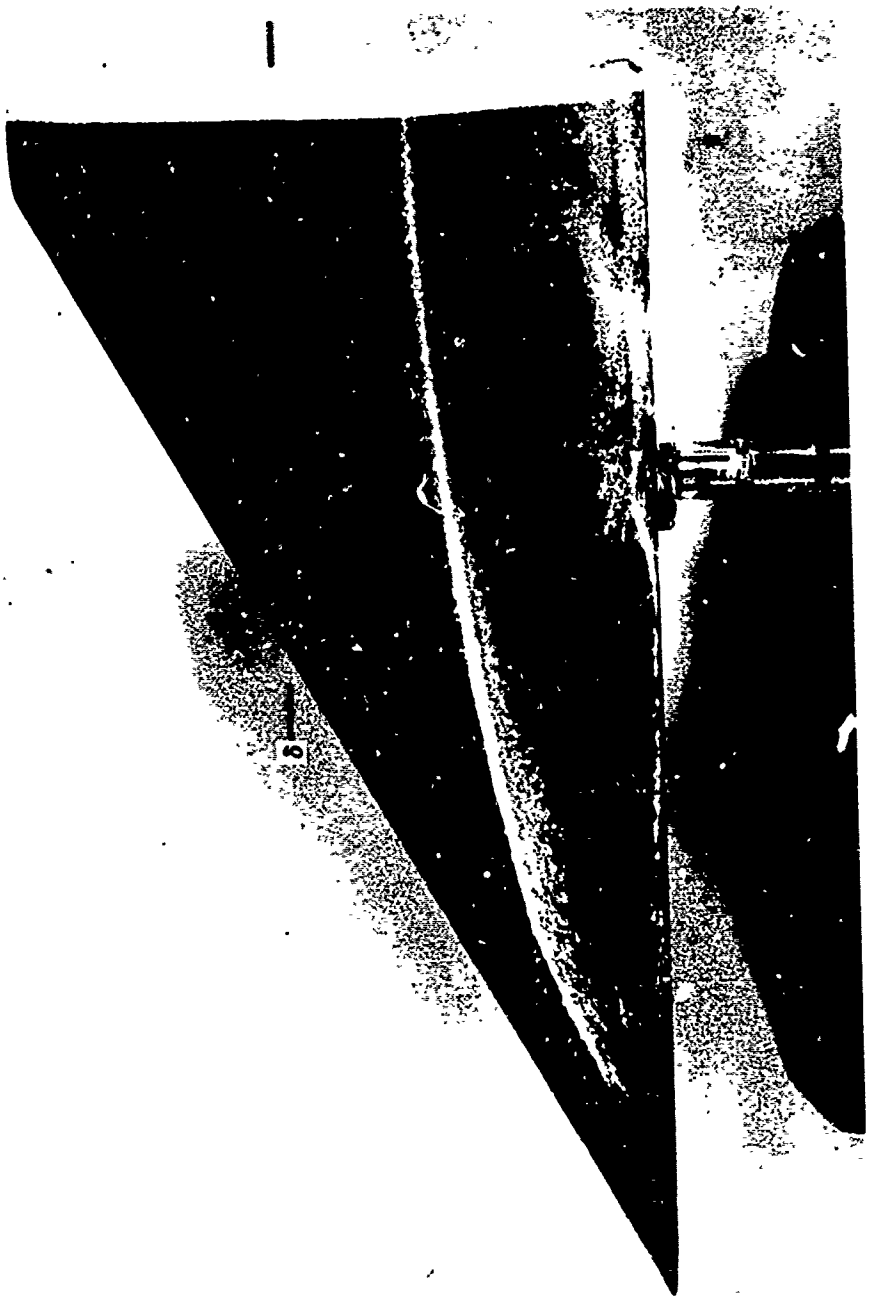

FIG. 31b 60° SWEPT FIN WITH 0.125" CLEARANCE GAP

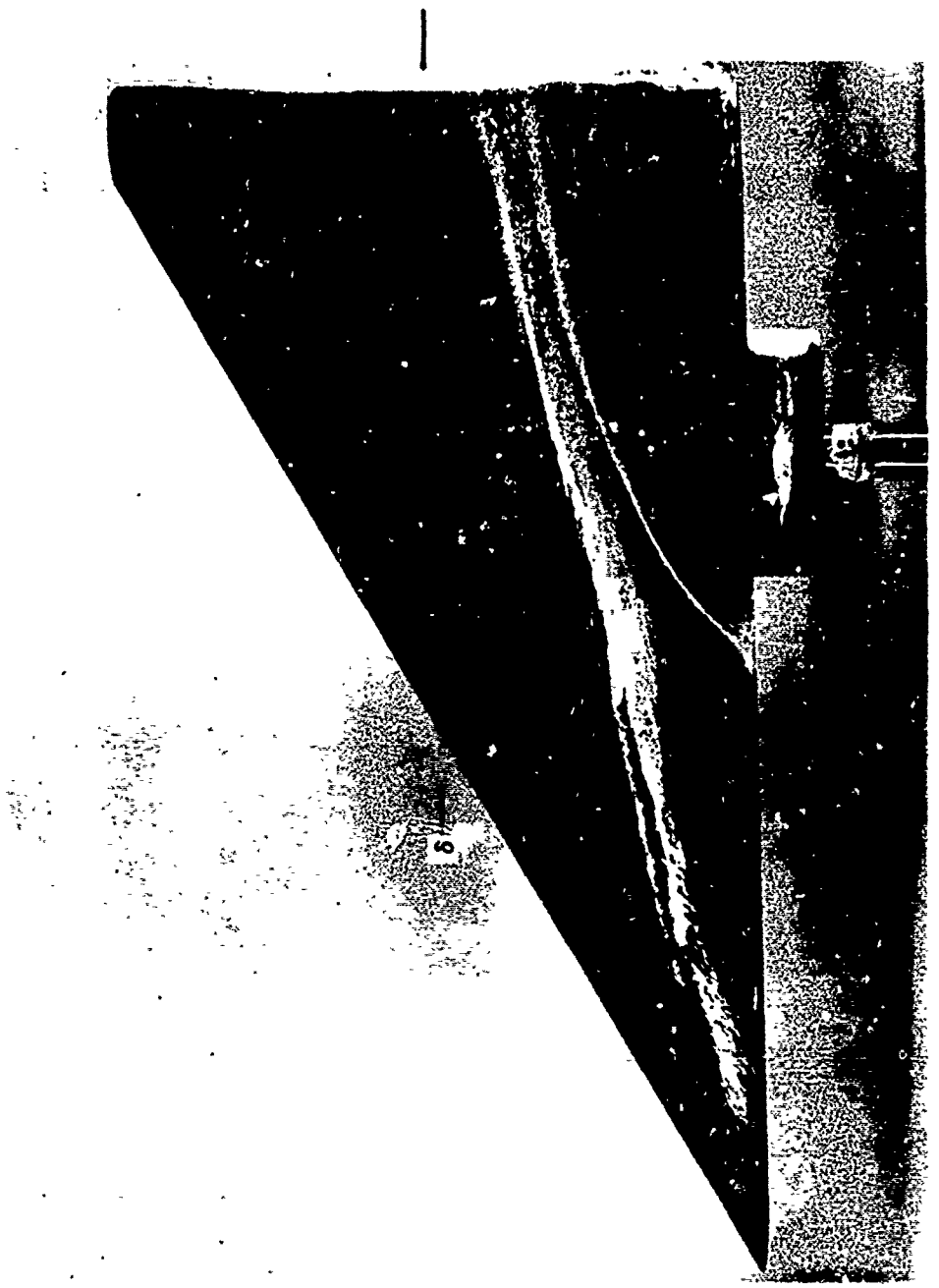

FIG. 31c 60° SWEPT FIN WITH 0.5" CLEARANCE GAP

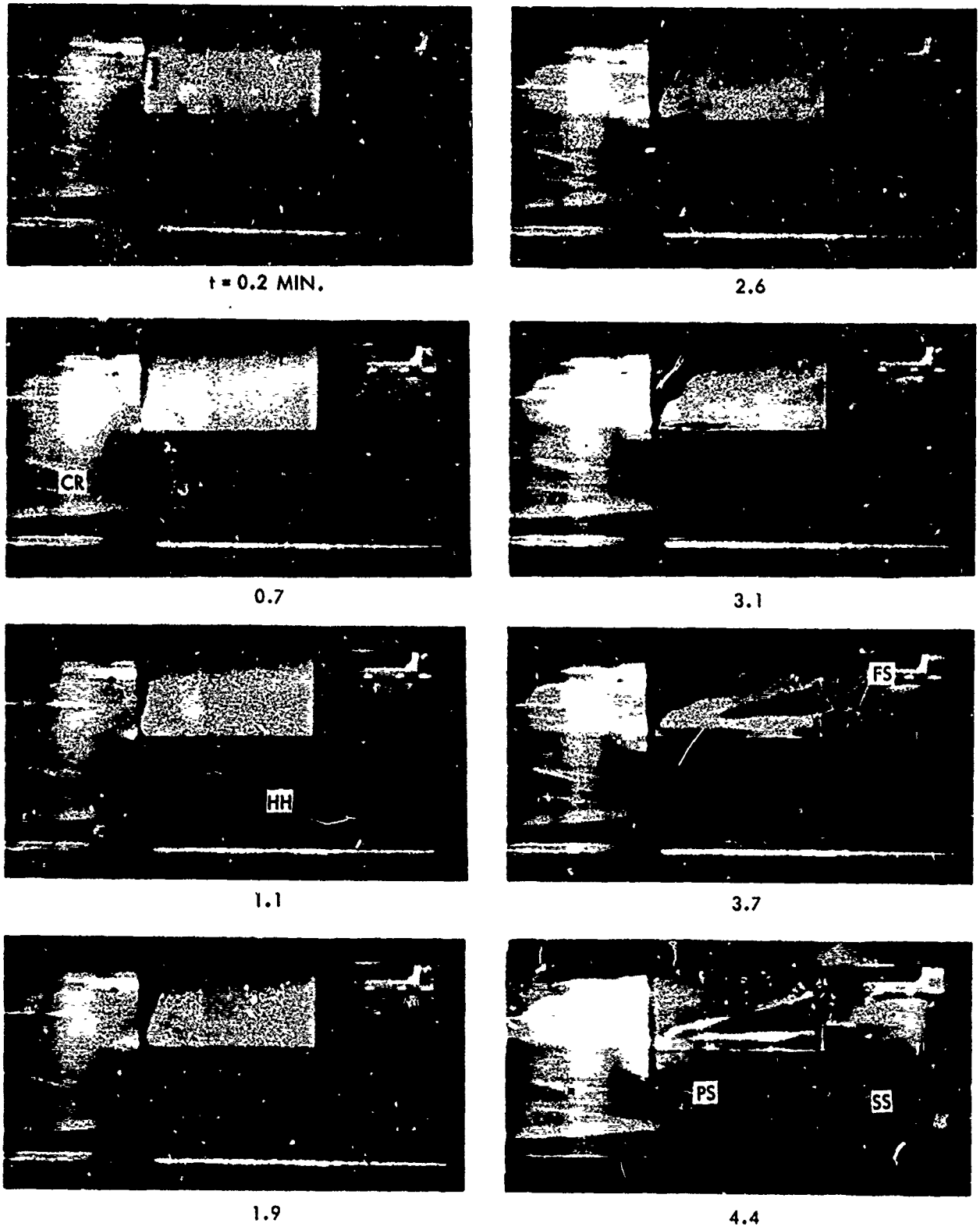

FIG. 32a AZOBENZENE MOVIES OF AN UNSWEPT FIN

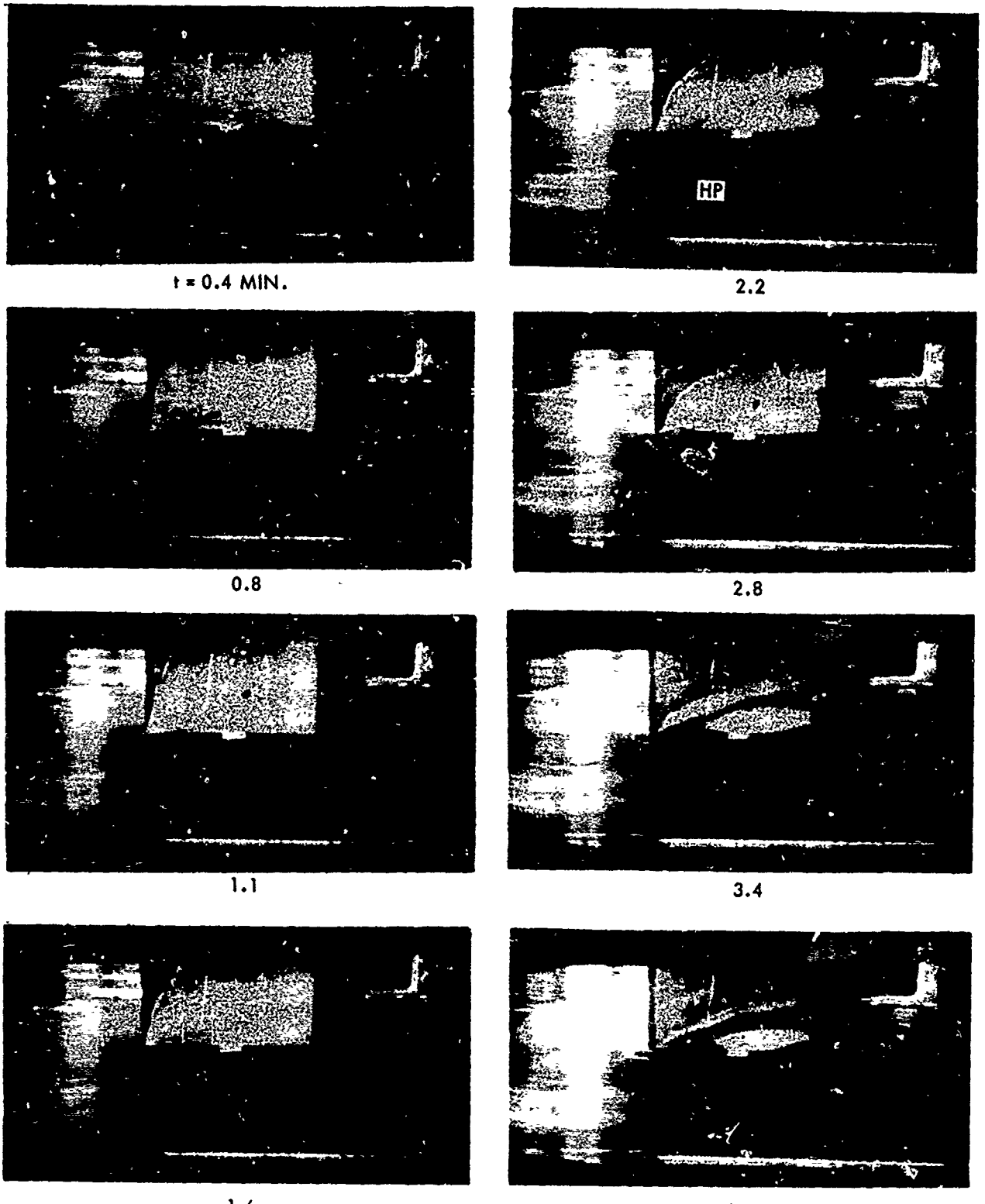

t = 0.4 MIN.

2.2

0.8

2.8

1.1

3.4

1.6

3.7

FIG. 32b AZOBENZENE MOVIES OF AN UNSWEPT FIN WITH A 0.125" CLEARANCE GAP

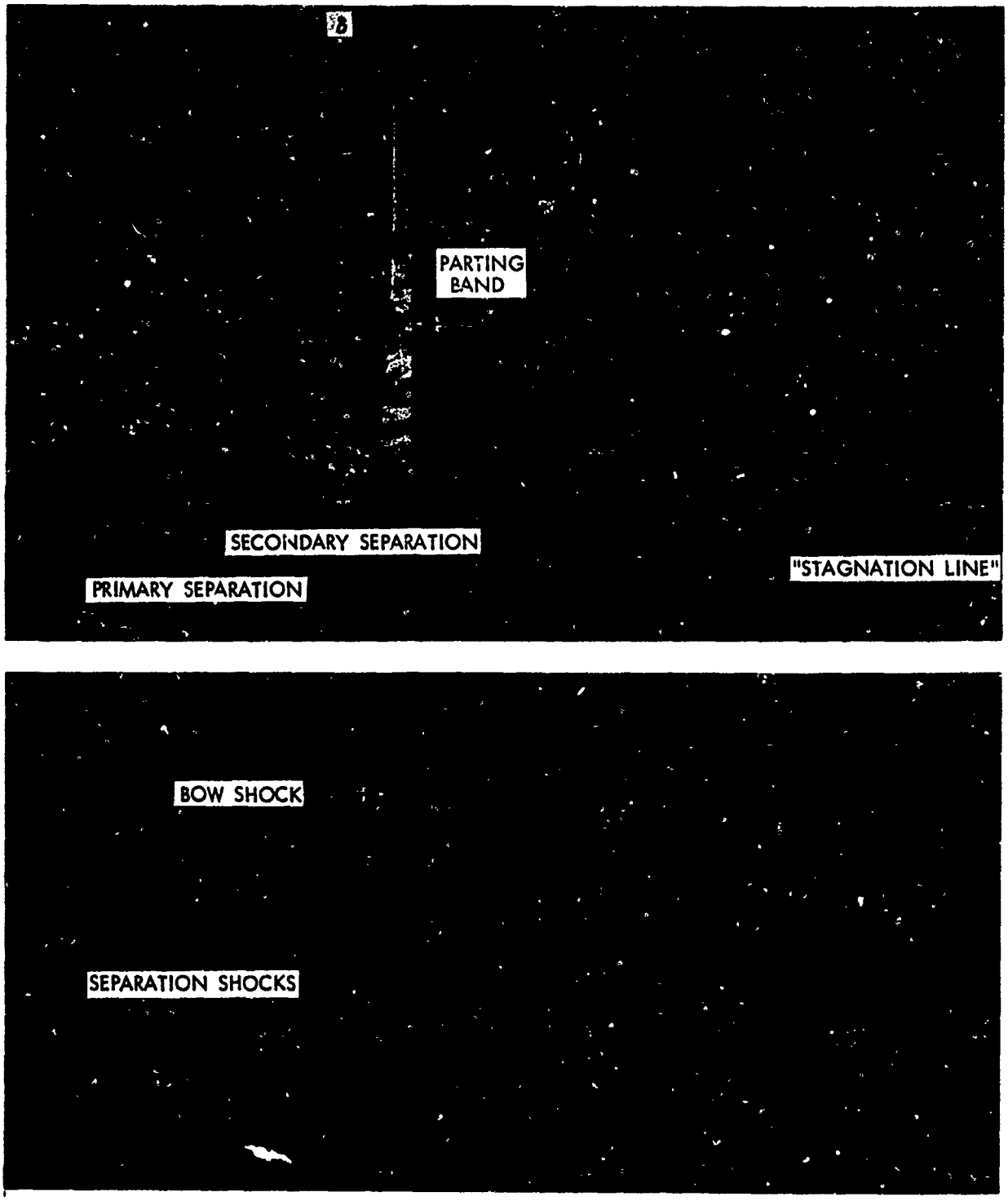

FIG. 33a SCHLIEREN PHOTOGRAPHS OF THE FLOW FIELD UPSTREAM OF AN CYLINDRICALLY BLUNT FIN ($M_\infty = 4.93$ $Re_\infty/FT = 7.4 \times 10^6$)

THIS
PAGE
IS
MISSING
IN
ORIGINAL
DOCUMENT

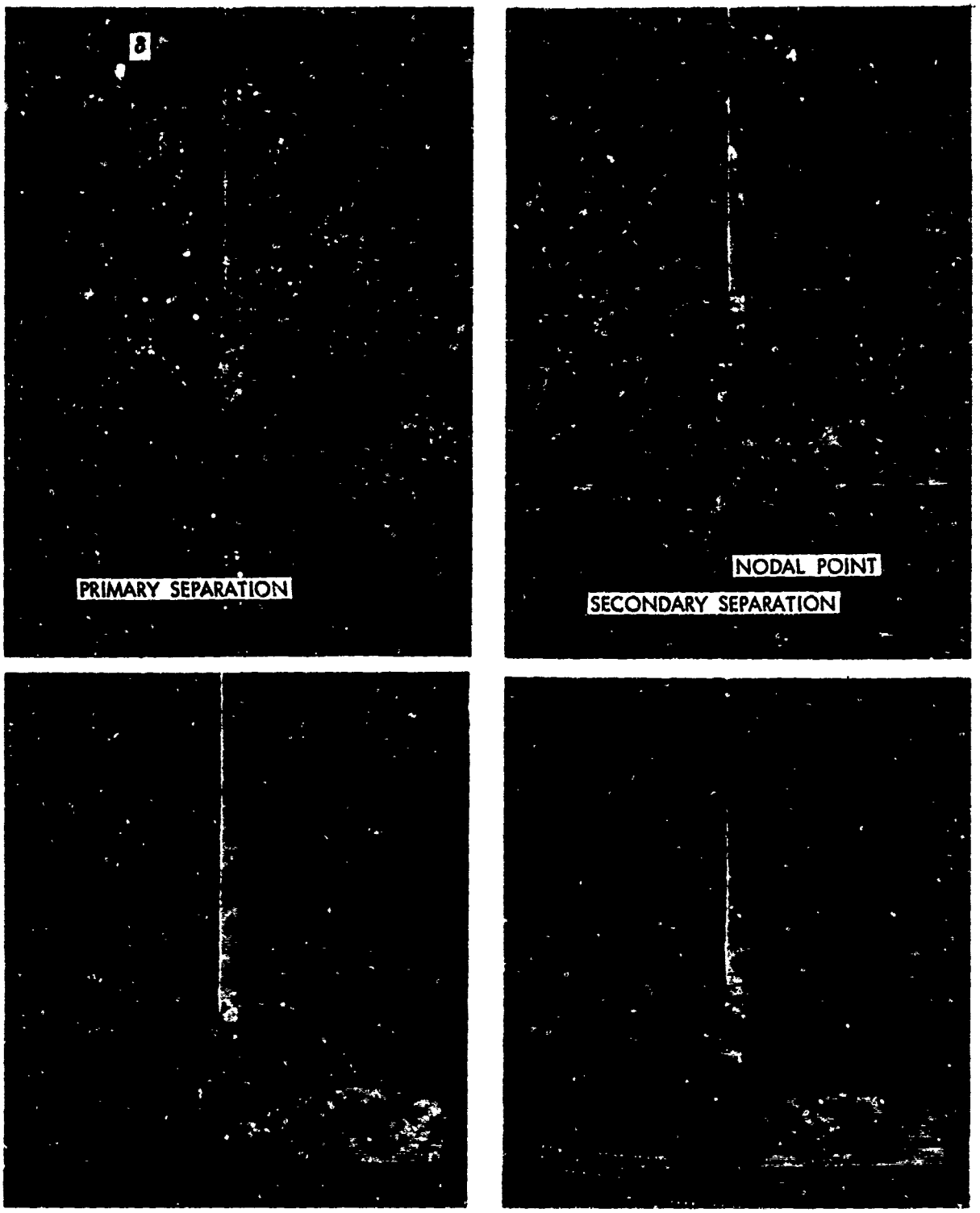

FIG. 33c FIN WITH 0.50 INCH CLEARANCE GAP

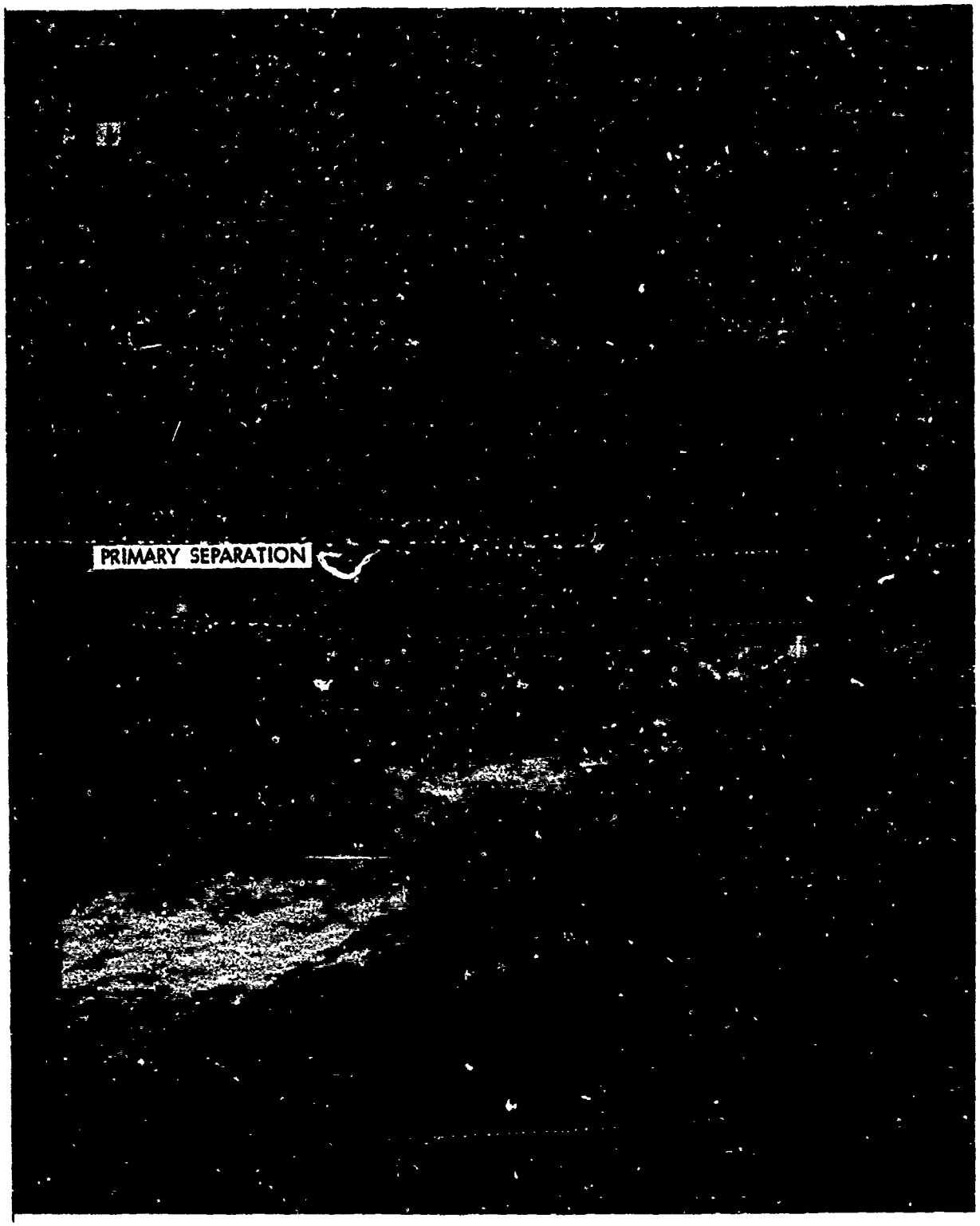

FIG. 34a SCHLIEREN PHOTOGRAPHS OF THE FLOW FIELD UPSTREAM OF A 60° SWEPT, CYLINDRICALLY BLUNT FIN

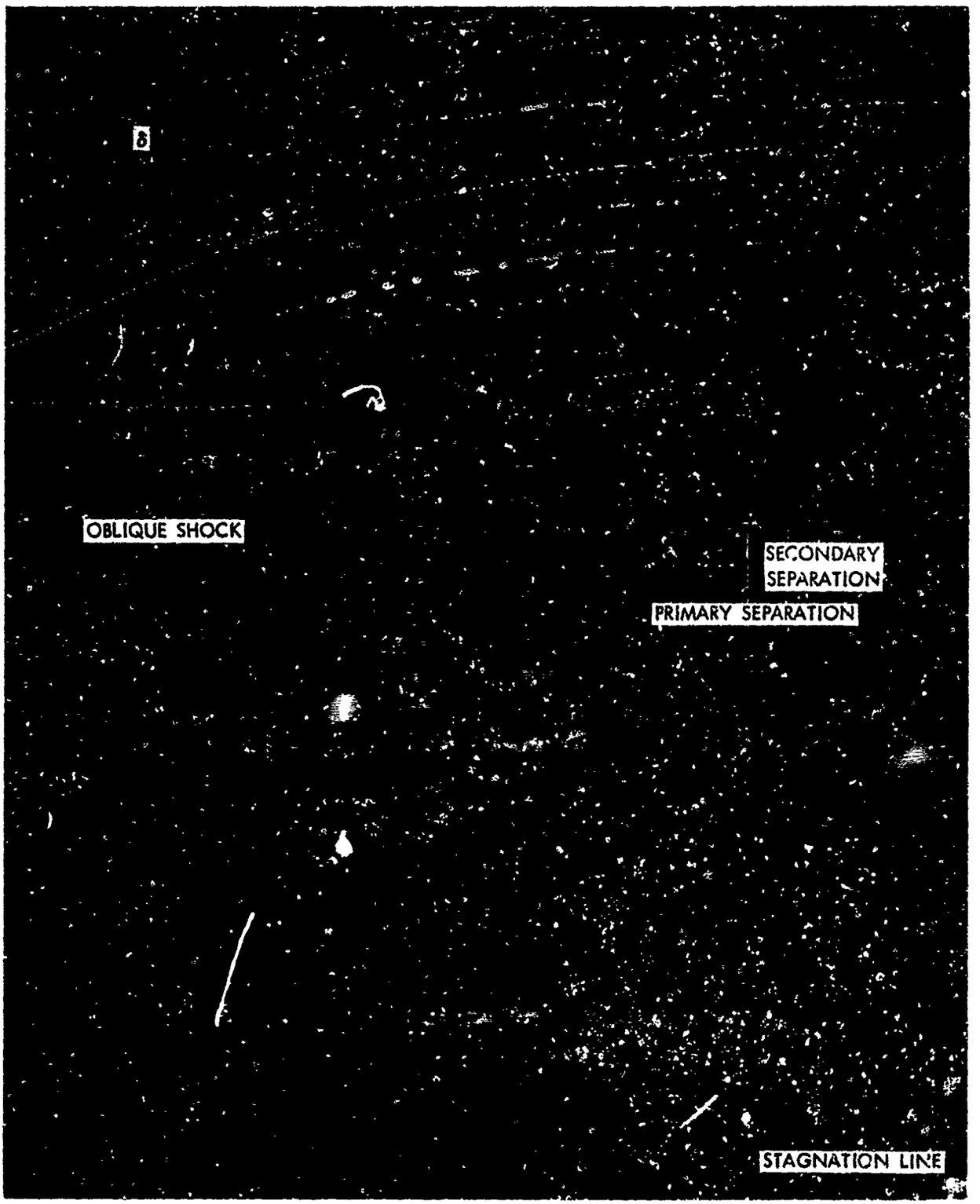

FIG. 34b FIN WITH 0.50 INCH CLEARANCE GAP

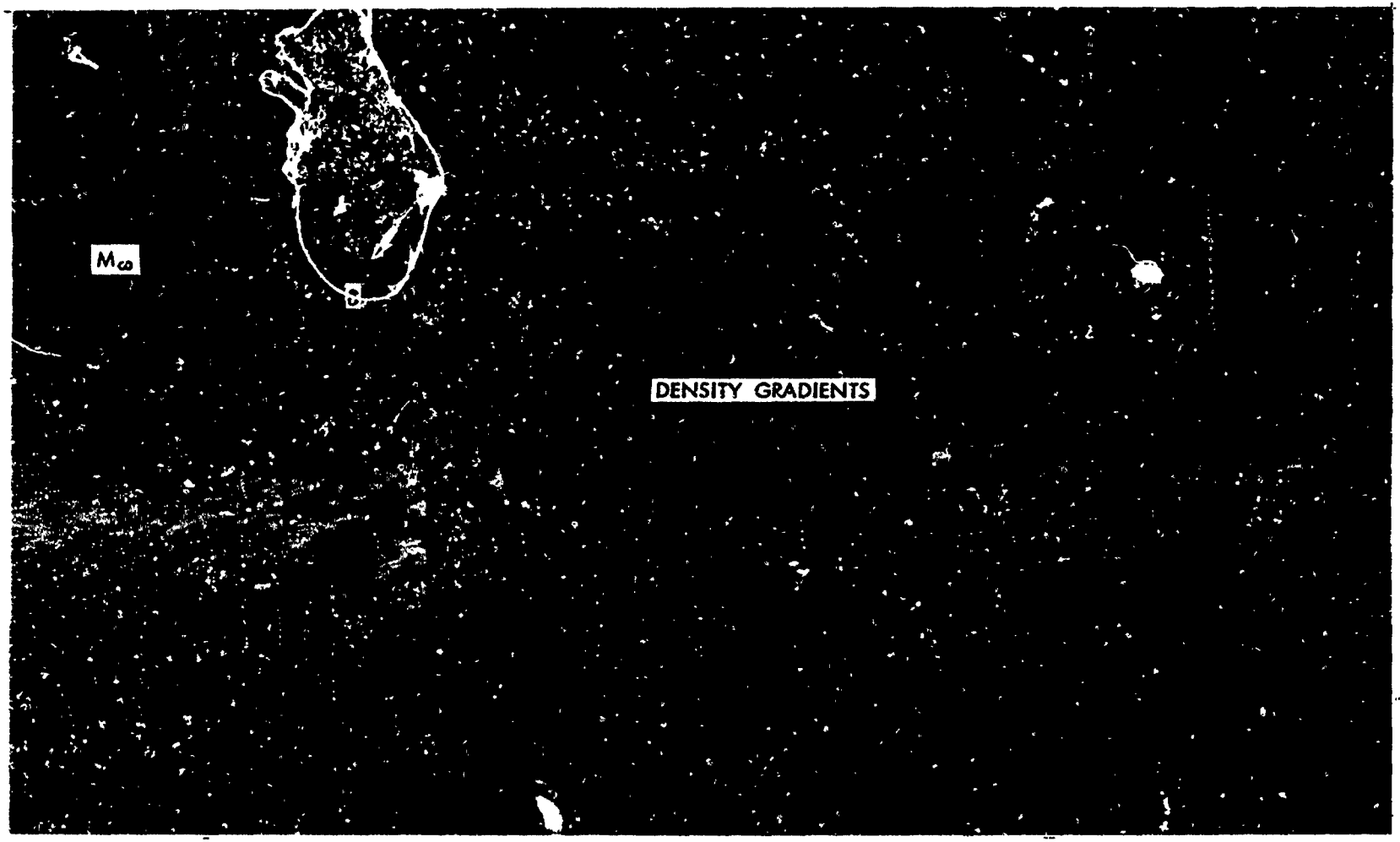

FIG. 35 COMPOSITE OF SCHLIEREN PHOTOGRAPHS OF THE REGIONS UPSTREAM AND DOWNSTREAM OF AN UNSWEPT FIN.

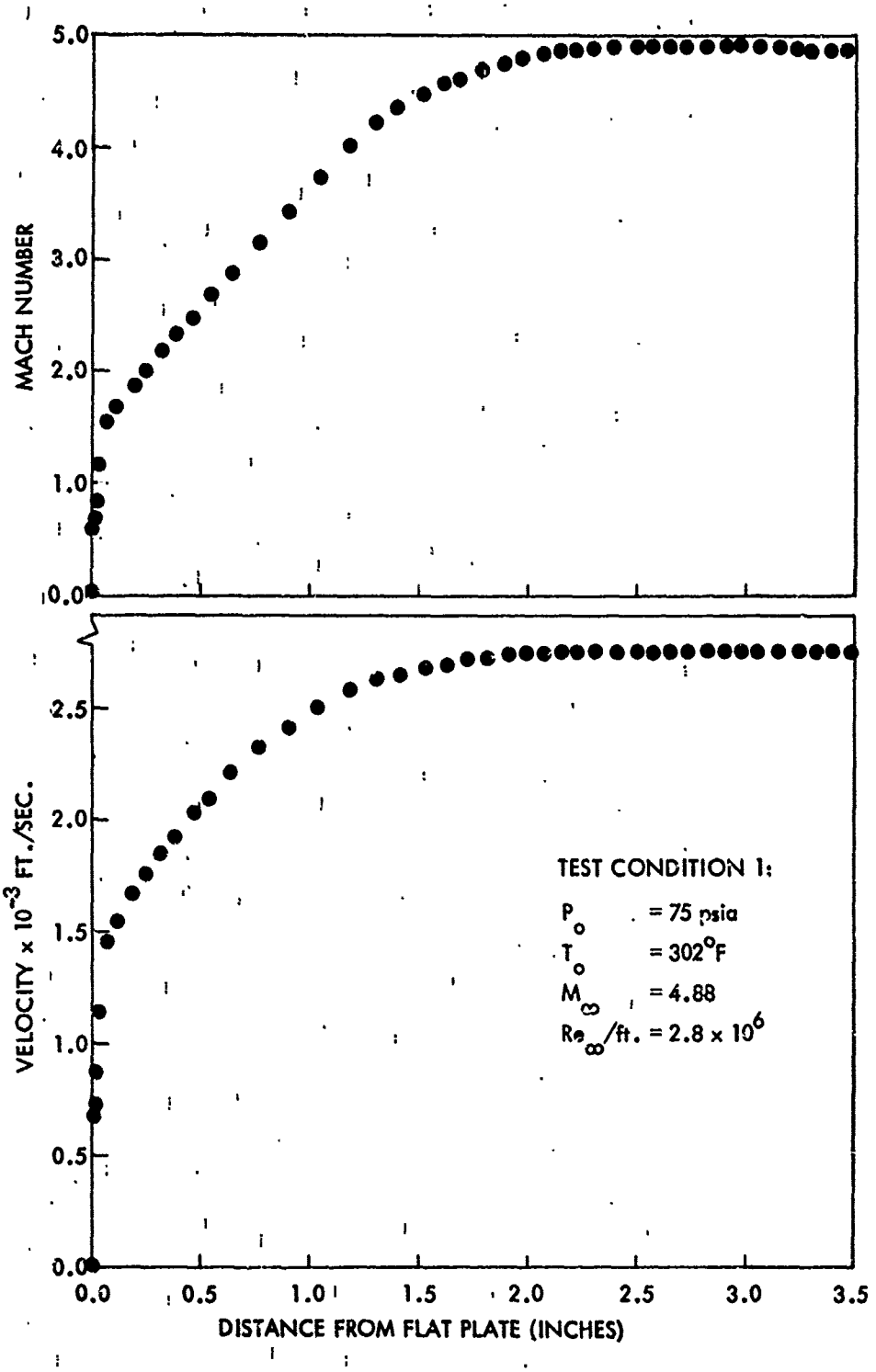

FIG. 36 BOUNDARY LAYER SURVEYS (REFERENCE 5)